INFORMATION TO USERS

This manuscript has been reproduced from the microfilm master. UMI films the text directly from the original or copy submitted. Thus, some thesis and dissertation copies are in typewriter face, while others may be from any type of computer printer.

The quality of this reproduction is dependent upon the quality of the copy submitted. Broken or indistinct print, colored or poor quality illustrations and photographs, print bleedthrough, substandard margins, and improper alignment can adversely affect reproduction.

In the unlikely event that the author did not send UMI a complete manuscript and there are missing pages, these will be noted. Also, if unauthorized copyright material had to be removed, a note will indicate the deletion.

Oversize materials (e.g., maps, drawings, charts) are reproduced by sectioning the original, beginning at the upper left-hand corner and continuing from left to right in equal sections with small overlaps. Each original is also photographed in one exposure and is included in reduced form at the back of the book.

Photographs included in the original manuscript have been reproduced xerographically in this copy. Higher quality 6" x 9" black and white photographic prints are available for any photographs or illustrations appearing in this copy for an additional charge. Contact UMI directly to order.

UMI

A Bell & Howell Information Company
300 North Zeeb Road, Ann Arbor MI 48106-1346 USA
313/761-4700 800/521-0600

RECONSTRUCTION OF THE DAMAGED CENTRAL NERVOUS SYSTEM AND SPINE

A

THESIS

Presented to the Faculty

of the University of Alaska Fairbanks

in Partial Fulfillment of the Requirements

for the Degree of

DOCTOR OF PHILOSOPHY

By

Gregory Anthony Helm, B.S., M.D.

Fairbanks, Alaska

May 1996

RECONSTRUCTION OF THE DAMAGED CENTRAL NERVOUS SYSTEM AND SPINE

By

Gregory Anthony Helm

RECOMMENDED:

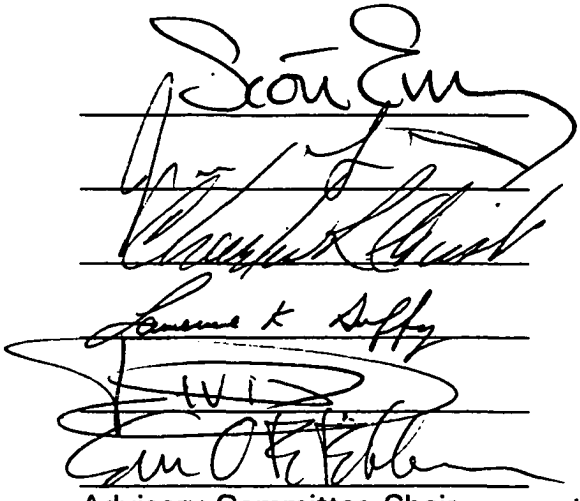

Advisory Committee Chair

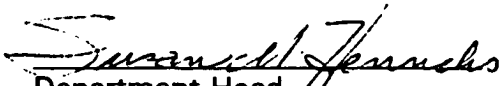

Department Head

APPROVED

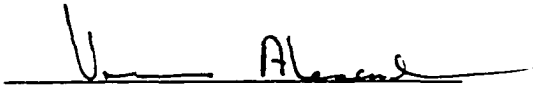

Dean

Dean

4-15-96

Date

Abstract

The field of neuronal transplantation has received a great deal of interest since the 1970's and is currently considered a possible treatment option for both neurodegenerative diseases and spinal cord injury. In this dissertation, fetal neostriatal transplants grafted into the lesioned striatum were studied in both the rat and rhesus monkey. Golgi-impregnation and immunohistochemical techniques were extended to the light and electron microscopic levels to determine the detailed anatomy of the developing striatal implants. Choline acetyltransferase immunoreactive and subtance P-like immunoreactive neurons within the rat striatal transplants were morphologically and ultrastructurally similar to normal striatal neurons. When the striatal grafting studies were extended into the rhesus monkey, normal neuronal maturation was demonstrated three months postoperative, both at the light and electron microscopic levels, using various neuroanatomical techniques. From these studies it can be concluded that fetal striatal grafts may be a useful treatment option for Huntington's disease, although numerous difficulties including neuronal degeneration and transplant rejection need to be addressed before this approach is applied in the clinical setting.

In a second group of experiments, various approaches to improve autologous bone spinal fusions were studied. Specifically, the utilization of

demineralized bone matrix, Type I collagen gel, and recombinant human bone morphogenetic proteins were evaluated for their effects on autologous bone spinal fusions in canines. The study demonstrated that recombinant human bone morphogenetic protein has a strong effect on the amount of bone deposition at the fusion site and, in addition, increases the number of vertebral levels which solidly fuse. The Type I collagen gel appeared to improve the interface between the autologous bone grafts and the host bone, while the demineralized bone matrix had a strong negative effect on the autologous bone graft fusions. Spinal fusion operations in the future will be much more successful if these various methods to improve spinal arthrodesis are utilized to their full potential. It is now clear that reconstruction of the central nervous system and its bony coverings is a real possibility in the very near future, although extensive clinical studies need to be performed before they are widely used in the neurosurgery community.

Dedicated to my parents,

Gunther and Miriam Helm.

Table of Contents

List of Figures

List of Tables

Acknowledgments

The writing of this thesis would have been impossible without the help of numerous people, many of whom have become good friends and comrades in academic neurosurgery. First, I would like to thank Sven O.E. Ebbesson, Ph.D. (University of Alaska Fairbanks) who made my matriculation to the University of Alaska Fairbanks possible. His unending generosity and guidance will always be an inspiration for me. Equally, I would like to thank John A. Jane, M.D., Ph.D. (University of Virginia) for appreciating my rebellious attitude and fully supporting my numerous research endeavors. James P. Bennet, Jr., M.D., Ph.D. (University of Virginia) was also crucial in initiating the neuronal transplantation studies and was always enthusiastic and supportive.

When it comes to cranking out quality scientific data, Patricia Palmer, B.A. (University of Virginia) is unequaled. Her mastery of electron microscopy is evident throughout this thesis and will always be gratefully remembered. Her stubborn and passionate approach to electron microscopy is not unlike Beethoven's approach to symphonic music, and her masterpieces are equally impressive. I would also like to thank Jorn Carlson, M.D., Ph.D. (University of Copenhagen) for being such an outstanding role model as an uncompromising scientist.

I am also grateful to Nathan Simmons, M.D. (University of Virginia) for helping with the rodent, primate, frog, and dog surgery. He was the first of many medical students to help out on these research projects, and his contributions were immense. I would also like to thank Charles diPierro, M.D. (University of Virginia), Jason Sheehan, B.S., M.S. (University of Virginia), Jonas Sheehan, B.A. (University of Virginia), and John Jane, Jr., B.A. (University of Virginia) not only for their strong and consistent laboratory work, but also for their humorous and politically incorrect antics.

I would like to thank David Kallmes, M.D. (University of Virginia) for his radiographic expertise on the spine project, as well as for his long-lasting friendship. Tom Sweeney, M.D., Ph.D. (University of Virginia) was instrumental in getting the spine project off of the ground, as were Roy Ogle, Ph.D. (University of Virginia) and Gary Ballian, Ph.D. (University of Virginia). I would also like to thank George Gilles, Ph.D. (University of Virginia) for his expertise in the biomechanics of the fused spine.

Lastly, I would like to gratefully thank Kim Mann and Lucille Staiger for their help in typing and editing this rather heavy dissertation.

This thesis contains the following manuscripts that have been previously published or are in press:

Helm GA, Palmer PE, Simmons NE, diPierro CG, Ebbesson SOE. A method for utilizing biocytin to study retinofugal pathways at the light and electron microscopic levels. J Neuroscience Methods, 49:97-101, 1993.

Helm GA, diPierro CG, Palmer PE, Simmons NE, Ebbesson SOE. The accessory optic system in the frog, *Rana Pipiens*: an electron microscopic study of the retinal afferents utilizing the anterograde tracer biocytin. Brain Research Bulletin, In press.

Helm GA, Palmer PE, Bennett JP Jr. Fetal neostriatal implants in the rat: a light and electron microscopic Golgi study. Neuroscience 37:735-756, 1991.

Helm GA, Palmer PE, Bennett JP Jr. Choline acetyltransferase and substance P-like immunoreactive elements in fetal striatal grafts in the rat: A correlated light and electron microscopic study. Neuroscience 47:621-639, 1992.

Helm GA, Palmer PE, Simmons NE, diPierro CG, Bennett JP Jr. Descriptive morphology of developing fetal neostriatal allografts in the Rhesus monkey: A correlated light and electron microscopic Golgi study. Neuroscience 50(1):163-179, 1992.

Helm GA, Palmer PE, Simmons NE, diPierro CG, Bennett JP Jr. Degeneration of long-term survival of fetal neostriatal allografts in the Rhesus monkey: an electron microscopic study. Exper Neurol, 123:174-180, 1993.

Helm GA, Sheehan JM, Sheehan JP, Jane JA Jr, diPierro CG, Simmons NE, Gillies GT, Makel D, Kallmes D, Ogle R, Sweeney TM, Jane JA. The utilization of Type I collagen gel, demineralized bone matrix and bone morphogenetic protein-2 (rhBMP-2) to enhance autologous bone lumbar spine fusion. J Neurosurg, To be submitted.

Introduction to Dissertation

The replacement of damaged or diseased tissues in the human has received an inordinate amount of medical research during the last century. It is now possible to surgically extirpate virtually every organ and replace it with human allografts. Every major university hospital has a surgical team capable of successfully transplanting the heart, lungs, liver, pancreas and kidneys. Although most transplant surgeons are either general or cardiothoracic surgeons, the field of transplantation using fetal neuronal tissue is now entering the neurosurgical arena as well. Equally interesting is the utilization of novel growth factors involved in the development of virtually every tissue, including the brain, blood, and bones, to treat diseases ranging from Parkinson's disease to disseminated cancer. The goal of this dissertation is to explore the use of fetal neuronal grafts to reconstruct regions of the central nervous system and to evaluate several novel approaches to reconstruct the diseased or damaged spine.

The first attempt at neuronal transplantation can be traced to W. Gillman Thompson, a professor of physiology at the New York University Medical College.[14] He attempted to transplant mature feline cerebral cortex into cavities in the cortex of adult dogs. Using very crude techniques, he demonstrated no surviving neurons within the xenografts six weeks after transplantation. Unaware of Thompson's previous failures, S. Saltykow,

working at the University of Basel, examined cerebral cortex after it had been excised and reimplanted into the cerebral cortex of young rats.[11] He clearly demonstrated progressive degeneration of the implanted neurons seven days after transplantation and also noted marked gliosis of the neural transplant. A decade later, D'Abundo and Altobelli studied CNS transplants in cats and rabbits, respectively, but because of inadequate neuroanatomical techniques it could not be determined whether healthy neurons survived the transplantation procedure.[1,2]

Elizabeth Dunn, working at the University of Chicago, was the first to clearly demonstrated the survival of transplanted CNS tissue.[3] In 1917, she reported that cerebral cortex from nine and ten day old rats could be successfully transplanted into cortical cavities of other rats. In her break-through studies, she demonstrated that developing neural tissue could consistently survive after transplantation and that the transplants would have improved survival if transplanted onto a rich vascular bed.

Between 1941 and 1970, most of the neural transplantation work was performed by Raoul May.[9] May, using the anterior chamber of the eye as the recipient site, demonstrated that neural grafts can project axons to other neural co-grafts or other normal target tissues. Finally, during the 1970's the neural transplantation field exploded and scores of neuroscientists began to enter this fascinating area.[5] Researchers began to

transplant biochemically and anatomically defined brain regions and to use these neuronal transplants to replace damaged brain regions anatomically, physiologically and functionally.[10]

As the field of neuronal transplantation was exploding, novel techniques to study the anatomical connections, biochemical development and electrophysiologic properties of the brain were also being discovered. In order to determine the neuroanatomical connections of distinct brain regions, techniques were developed to accurately trace axons both anterogradely and retrogradely. These methods included the Fink-Heimer technique,[8] horseradish peroxidase, Phaseolus vulgaris leukoagglutinin,[6,7] and various fluorescent tracers.[12] In addition, modifications of the Golgi impregnation technique have made it relatively easy to examine morphologically distinct cell types in each brain region. With slight modification of the fixatives and staining techniques, tract tracing, immunohistochemistry and Golgi impregnation were subsequently extended to the electron microscopic level.[4] A combination of these techniques give a complete picture of the afferent and efferent connections, as well as the biochemical and morphological characteristics of individual neurons. These approaches, when applied to transplanted neuronal tissue or regenerating fiber tracts, can accurately correlate neuroanatomy with physiological or functional changes or improvements.

The first two chapters of this dissertation involve a novel technique to study the retinal projections to the brain at both the light and electron microscopic levels. This technique can also be used to study the regeneration of the optic nerve after damage or the projection of the retina to neuronal transplants, which could conceivably include the lateral geniculate nucleus or superior colliculus. Since this unique tract tracer can be easily studied at the electron microscopic level, it may be extremely useful in correlating anatomically functioning regenerated synapses with physiological measurements. Following these two "neuroanatomical techniques" chapters, the dissertation focuses on light and electron microscopic analysis of fetal neuronal transplants. More specifically, fetal striatal transplants were injected into the ibotenic acid lesioned striatum, an animal model of Huntington's disease, and the implants were immunohistochemically stained or Golgi-impregnated. The aim of the studies were to determine whether the fetal striatal neurons developed biochemically and morphologically, pre-requisites for successful grafting operations in Huntington's patients.

Although the various approaches for reconstruction of the central nervous system and its pathways is of premiere importance to neurosurgeons and neurologists, the bony coverings of the central nervous system, including the spine and skull, have also been of historical interest to

both neurosurgeons and orthopedic surgeons. The treatment of traumatic injuries, congenital anomalies, and degenerative processes of the spine often require the surgeon to create a bony fusion over several intravertebral segments in order to produce long-term stability and/or halt the progressive pathologic process. Several decades of clinical and research experience have clearly demonstrated that autologous bone grafts are the "gold standard" grafting material for achievement of arthrodesis in the spine. The most common location to obtain a bone autograft is from the iliac crest, but this procedure is not without risk. Significant rates of infection, bleeding, and postoperative pain make this approach far from ideal. Although numerous additives to autologous bone grafts and bone graft substitutes have been studied both experimentally and clinically, none have been shown to be superior to autologous bone alone.

A relatively new approach for improving spinal fusions was initiated in the 1960's when Urist, an orthopedic surgeon, demonstrated that protein extracts from bone can induce cartilage and bone formation.[15] These extracts recapitulate the process of bone formation seen during development, named endochondral ossification. This process is characterized by the formation of cartilage, which subsequently ossifies into mature bone. The proteins involved in this process were termed bone morphogenetic proteins, and were subsequently purified and cloned.[16]

Recombinant human BMP's are currently being tested for a variety of clinical indications, including long bone fractures and periodontal disease.

Another approach for improving bone healing has been the use of Type I collagen gels. The collagen matrix can act as an osteoconductive material onto which osteoblasts can freely migrate and may also bind osteoinductive growth factors, such as TGF-B and the BMP's. Sweeney, et al. demonstrated that the Type I collagen gels can enhance healing of critical sized defects in the rat skull.[13] In chapter 7 of this dissertation, the possible use of demineralized bone matrix, recombinant human bone morphogenetic protein-2 (rhBMP-2), and Type I collagen gel to improve autologous bone spinal fusions is investigated.

References

1. Altobelli, R. (1914) Innesti cerebrali. Gazz Int Med Chir 17:25.
2. D'Abundo, G. (1913) Sulle manifestazioni di vitalita nei trapianti del tessuto nervoso. Riv Ital Neuropat Psichiat Ellettroter 6:145.
3. Dunn, E.H. (1917) Primary and secondary findings in a series of attempts to transplant cerebral cortex in the albino rat. J Comp Neurol 27:565
4. Gabbott, P.L. and Somogyi J. (1984) The "single" section Golgi-impregnation procedure: Methodological description. J Neurosci Methods 11: 221-230.
5. Gash, D., Sladek, J.R., Jr., Sladek, C.D. (1980) Functional development of grafted vasopressin neurons. Science 210:1367.
6. Gerfen, C.R., Sawchenko, P.O. (1984) An anterograde neuroanatomical tracing method that shows the detailed morphology of neurons, their axons and terminals: immunohistological localization of an axonally trasported plant lectin, Phaseolus vulgaris-leucoagglutinin (PHA-L). Brain Res 290:219-238.
7. Gerfen, C.R., Sawchenko. P.O. (1985) A method for anterograde axonal tracing of chemically specified circuits in the central nervous system: Combine Phaseolus vulgaris-leucoagglutinin (PHA-L) tract tracing and immunohistochemistry. Brain Res 343: 144-150.
8. Heimer, L. (1970) Bridging the gap between light and electron microscopy in the experimental tracing of fiber connections, in: Contemporary Research Methods in Neuroanatomy (W.J.H. Nauta and S.O.E. Ebbeson, eds) Springer-Verlag, Berlin, pp162-172.

9. May, R.M. (1930) La greffe dans l'oeil de rat blanc adulte du tissu cerebral de rat nouveau-ne. Arch Anat Microsc Morphol Exp 26:433

10. Perlow, M.J., Freed, W.J., Hoffer, B.J., et al (1979) Brain grafts reduce motor abnormalities produced by destruction of nigrostriatal dopamine system. Science 204:643.

11. Saltykow, S. (1905) Versuche uber gehirnreplantation, zugleich ein beitrag sur kenntniss reactiver vorgange an den zelligen gehirnelementen, Arch Psychiatr 40:329.

12. Schmued, L.C., Fallon, J.H. (1986) Fluoro-gold: A new fluorescent retrograde axonal tracer with numerous unique properties. Brain Res 377:147-154.

13. Sweeney T.M., Chabra A., Brook B., et al (1994) Type I collagen gels mediate total repair of critical size bone defects through intramembranous ossification. Orthop Trans 582.

14. Thompson, W.G. (1890) Successful brain grafting. NY Med J, June28, 701.

15. Urist M.R., Huo Y.K., et al (1984) Purification of bovine bone morphogenetic protein by hydroxylapatite chromatography. Proc Nat Acad Sci 371-375.

16. Wozney J.M., Rosen V., Celeste A.J., et al (1988) Novel regulators of bone formation: Molecular clones and activities. Science 242:1528-1534.

Chapter 1

A METHOD FOR UTILIZING BIOCYTIN TO STUDY RETINOFUGAL PATHWAYS AT THE LIGHT AND ELECTRON MICROSCOPIC LEVELS

(Published, Journal of Neuroscience Methods, 49 (1993) 97-101)

INTRODUCTION

Neuroanatomists have successfully utilized numerous methods to study the connections of the optic pathway at the light microscopic level, including the Nauta-Laidlaw method, the Fink-Heimer method, anterogradely transported horseradish peroxidase and anterogradely transported cobaltous lysine[8,9]. Evaluation of retinal projections at the electron microscopic level has been more problematic. Anterograde degeneration is limited by the lack of a light microscopic correlate, a wide range of degeneration times for various axonal populations within a given tract, and aberrant ultrastructural morphology. Cobaltous lysine is somewhat difficult to use and requires that the tissue is treated with ammonium sulfide to stabilize transported cobalt, which distorts the ultrastructure of synaptic junctions[2]. Although horseradish peroxidase has been widely used to study the retinal pathways at the electron microscopic level, several studies suggest that many of the smaller axons are not adequately stained by this method[3,9]. In the present paper, we present a method for utilizing biocytin as an anterograde tracer for retinofugal fibers at both the light and electron microscopic levels. Biocytin has not previously been used for defining retinal projections, but has been used for studying other neural pathways at both the light and electron microscopic levels[4,5].

MATERIALS AND METHODS

Twenty frogs (Rana pipiens) were used in this study. The frogs were anesthetized by immersion in 0.1% tricaine (Sigma, St. Louis, MO). Both intraocular and transoral approaches were utilized in this study. In five frogs, the optic nerve was surgically exposed through the oral mucosa and sectioned close to the optic canal. A slurry of biocytin (50 mg/ml in 0.1 Tris buffer, pH 7.4) was placed over the cut optic nerve and the oral mucosa was closed. In 15 frogs, the frogs were anesthetized as above and the posterior chamber of the eye was entered. The lens and vitreous humor were removed, 0.25 ml of the biocytin slurry was placed over the retina, and the eye was closed with 6-0 prolene suture. The animals were allowed to survive one to three days prior to perfusion fixation.

Perfusion and Fixation. The animals were anesthetized by immersion in 0.1% tricaine and perfused transcardially with 25 ml of 0.12 mol/l phosphate buffer (pH 7.4) containing 0.25% procaine and 3% sucrose followed by 600 ml of a fixative containing 4% paraformaldehyde, 1% glutaraldehyde, 15% saturated picric acid, and 3% sucrose in 0.12 mol/l phosphate buffer (pH 7.4). This was followed by 800 ml of a second fixative containing 4% paraformaldehyde, 1% glutaraldehyde and 3% sucrose in 0.12 mol/l phosphate buffer (pH 7.4). The heads were removed

four hours later and immersed in the second fixative overnight. The brains were then removed and cut coronally at 75 mm on a vibrating microtome.

Biocytin Histochemistry. The sections were immersed in 20% sucrose in phosphate buffer and frozen in liquid nitrogen in order to improve penetration of the avidin-biotin complex (ABC) complex. The sections were washed three times in phosphate buffer and placed in streptavidin-biotinylated horseradish peroxidase (ABC elite, Vector) for two hours with constant agitation at 4°C. The sections were washed three times in phosphate buffer and placed in a nickel diaminobenzidine solution for 35 - 45 minutes before rinsing in buffer and further processing. The DAB solution contained 50 mg diaminobenzidine, 40 mg ammonium chloride, 200 mg B-D-glucose, 0.4 mg glucose oxidase, and 0.05 mg of nickel, in 100 cc of 0.1 phosphate buffer.

Processing for Electron Microscopy. For light microscopy the sections were photographed with a Zeiss Axiophot research microscope. Vibratome sections processed as above were placed in 1% osmium for one hour, followed by two changes of 3.6% sodium chloride for 30 minutes, and dehydrated in increasing concentrations of Quetol 523m (Ted Pella, Inc.) in distilled water: 35, 50, and 70% for 10 min each; 80 and 90% for 15 min each; followed by 100% Quetol for 20 min. Sections were then floated in a

50% Quetol-50% maraglas solution (Ted Pella, Inc.) for 12 h followed by pure maraglas for 6 h. The sections were flat-embedded on siliconized microscope slides and cured for two days at 60°C. Tissue was then cut from the area of interest and fixed to epon blocks. Following serial thin-sectioning on a Reichert ultramicrotome, the sections were placed on formvar-coated grids, double-stained with uranyl acetate and lead citrate, and examined with a JEOL electron microscope.

RESULTS

The animals in which biocytin slurry was placed directly on the optic nerve demonstrated no anterograde transport of biocytin into the usual optic nerve targets. However, many of the animals receiving biocytin injections into the posterior chamber demonstrated variable amounts of transport into all of the usual retinal targets, including the tectum, basal optic nucleus, and nucleus Bellonci[3,7,8,9].

Light Microscopy. The nickel-enhanced DAB reaction product completely filled labeled axons and boutons (Figs. 1.1A, B). Many of the labeled axons were more fine and delicate compared to the coarser axons which were labeled with horseradish peroxidase (HRP) in previous studies in our laboratory. The entire retinal projection was not always labeled when biocytin was placed in the posterior chamber, although the reason for this is

unclear. It is possible that small areas of retinal damage occurred during the initial surgery, allowing only limited diffusion of biocytin into the surrounding extracellular space and subsequent transport into nearby ganglion cells. Using the methods described above, the penetration of the ABC complex was fairly complete throughout the entire section, although regions deep within the section had reactive elements that were more lightly stained than in regions close to the surface of the section.

Electron Microscopy. At the electron microscopy level, axospinous and axodendritic contacts were clearly demonstrated in the nucleus Bellonci (Fig. 1.2A), tectum (Fig. 1.2B), and basal optic nucleus. The DAB reaction product completely filled axons and axon terminals, but left the synaptic cleft intact enabling accurate identification of axosomatic, axodendritic and axospinous synapses. The preservation of the surrounding neuropil using this method was excellent. The microtubules in the axons and dendrites and neuronal membranes were left intact throughout the entire section and demonstrated no obvious adverse effect from the freeze thaw method (Figs. 1.2A,B).

DISCUSSION

Biocytin as an anterograde tracer of the retinal projection neurons seems to be comparable to the HRP method, which has been used

extensively[3,9]. With the addition of this method, numerous double labeling neuroanatomical studies can now be performed at the electron microscopic level. For example, DAB can be utilized to label anterogradely transported biocytin from one eye and various other chromogens, such as BDHC or TMB, can be used to label anterogradely transported HRP from the other eye. This method would be particularly useful in ontogenetic or comparative studies of primitive vertebrate species in order to study incomplete parcellation[1]. In addition, visual circuits could be studied in detail by using biocytin to label retinofugal axons in a given nucleus, and using HRP to retrogradely label the nucleus' projection neurons.

Biocytin also seems to have several other advantages over many other anterograde tracing methods. Biocytin clearly labels very small axons and boutons, a characteristic not shared with the cobaltous lysine and some HRP techniques. In addition, the retinal axons are not severed, eliminating degeneration artifacts, and the ABC-DAB staining technique is extremely clean and relatively easy to use.

The major drawbacks of the technique are that apparently only a small portion of the retinal ganglion cells transport biocytin after intraocular injections and possibly inadequate penetration of ABC and DAB during the staining procedure, leading to incomplete staining of biocytin filled axons and terminals deep within the section. However, biocytin is an extremely useful

anterograde tracer for electron microscopic studies designed to qualitatively demonstrate neuroanatomical circuits of the optic system.

Figures and Tables

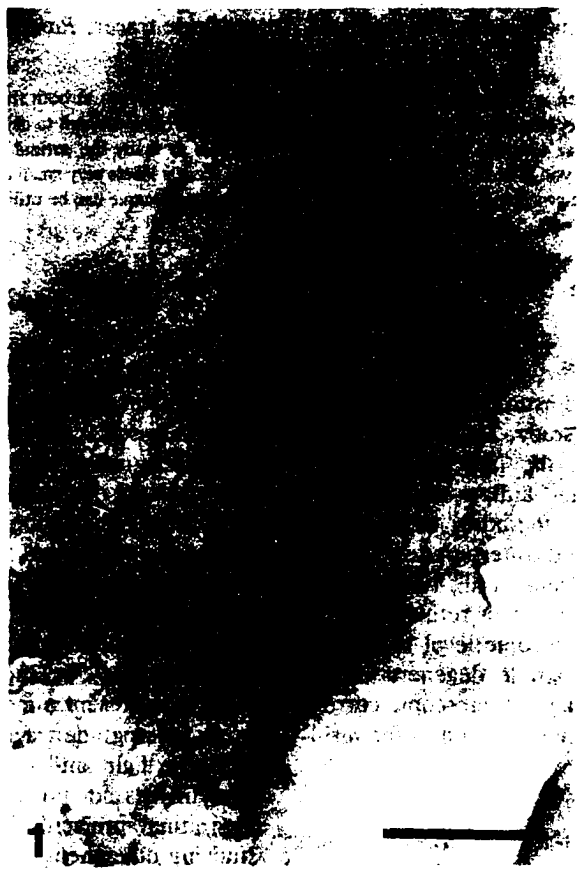

Figure 1.1: Photomicrograph of ipsilateral nucleus Bellonci following biocytin injection into the posterior chamber of the eye demonstrating numerous labeled incoming axons (arrowheads) and axon terminals. Scale bar = 50 μm.

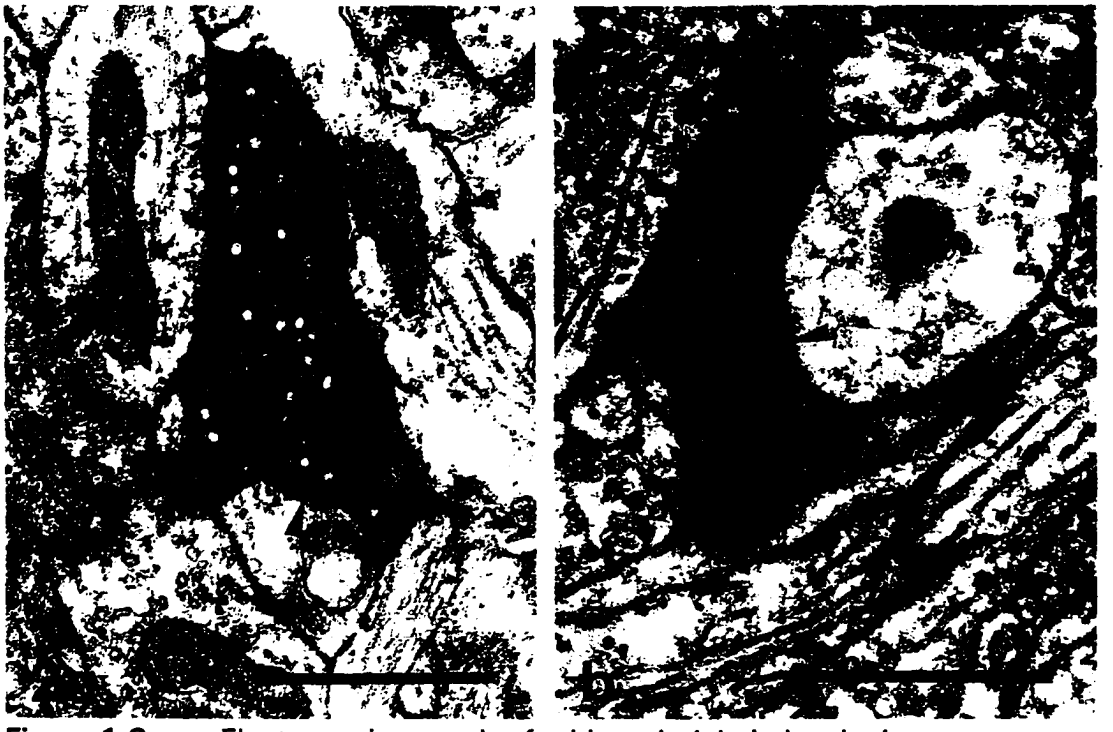

Figure 1.2: a. Electron micrograph of a biocytin labeled retinal axon terminals in the nucleus Bellonci demonstrating a symmetric axodendritic synapse (arrowhead). b. Electron micrograph of a biocytin labeled bouton in the optic tectum making a symmetric axodendritic synapse (arrowhead). Scale bars = 0.75μm.

REFERENCES

1. Ebbesson, S.O.E. (1984) Evolution and ontogeny of neuronal circuits. Behav. Brain Sci., 7: 321-366.
2. Ebbesson, S.O.E. and Bazer, G.T. (1987) Double labeling of neural circuits using horseradish peroxidase and cobalt. J. Neurosci. Methods, 20: 1-5.
3. Hughes, T.E. (1990) A light- and electron-microscopic investigation of the optic tectum of the frog, *Rana pipiens*, I: The retinal axons. Visual Neurosci., 4: 499-518.
4. Izzo, P.N. (1991) A note on the use of biocytin in anterograde tracing studies in the central nervous system: application at both light and electron microscopic level. J. Neurosci. Methods, 36: 155-166.
5. King, M.A., Louis, P.M., Hunter, B.E. and Walker, D.W. (1989) Biocytin: a versatile anterograde neuroanatomical tract-tracing alternative. Brain Res., 497: 361-367.
6. Lazar, G. (1978) Application of cobalt-filling techniques to show retinal projections in the frog. Neuroscience, 3: 725-736.
7. Montgomery, N., Fite, K.V. and Bengston, L. (1981) The accessory optic system of *Rana pipiens*: Neuroanatomical connections and intrinsic organization. J. Comp. Neurol., 203: 595-612.

8. Scalia, F., Knapp, H., Halpern, M. and Riss W. (1968) New observations on the retinal projection in the frog. Brain. Behav. Evol., 1: 324-353.

9. Scalia, F. and Colman, D.R. (1974) Aspects of the central projection of the optic nerve in the frog as revealed by anterograde migration of horseradish peroxidase. Brain Res., 79: 496-504.

Chapter 2

THE ACCESSORY OPTIC SYSTEM IN THE FROG, *RANA PIPIENS*: AN ELECTRON MICROSCOPIC STUDY OF THE RETINAL AFFERENTS UTILIZING THE ANTEROGRADE TRACER BIOCYTIN*

*(Published, Brain Research Bulletin, 39 (1995) 83-87)

INTRODUCTION

The accessory optic system (AOS) is now generally recognized as a primary visual system in vertebrates. Comparative neuroanatomical studies have demonstrated a broad range of species variation in the AOS, although a basic underlying neural circuit seems to be conserved in both mammalian and non-mammalian vertebrates.[1,6] Numerous functional studies have demonstrated that the AOS is principally involved in optokinetic nystagmus and retinal image stabilization.[5] Detailed neuroanatomical studies of the circuit in mammals have demonstrated that the AOS consists of the inferior and superior accessory optic fasciculi, which terminate in three target nuclei in the anterior midbrain, the medial, lateral, and dorsal terminal nuclei. The AOS is some mammals is missing one or several major components, leading to marked interspecies variation in the typical projection pattern.[6]

The neuronal circuits of the AOS in non-mammalian species is much more simplistic. The basal optic root (BOR) leaves the main optic tract immediately after crossing the optic chiasm and projects to the basal optic root nucleus (nBOR) which is located at the ventral margin of the midbrain tegmentum. In frogs, the basal optic root can be separated into a lateral fasciculus and a smaller, diffuse, medial fasciculus, both of which innervate the nBOR.[2] These two fasciculi have different innervation patterns within the nBOR, suggesting that the anuran AOS may have more components of

the classical AOS than previously recognized. A previous retrograde horseradish peroxidase study demonstrated that at least six types of retinal ganglion cells project to the nBOR and also determined, using the Golgi-Cox method, that there are at least four cell types present in the pterional field of the nBOR.[4] Despite numerous neuroanatomical studies in various species, there have been no electron microscopic studies of the AOS to determine the ultrastructural details of the circuit. The main objective of this study was to determine the ultrastructure of the pre- and post-synaptic elements of the retinal projection to the nBOR.

METHODS

Twenty frogs (*Rana pipiens*) were used in this study. The frogs were anesthetized by immersion in 0.1% tricaine (Sigma, St. Louis, MO) and a slurry of biocytin (50 mg/ml in 0.1 Tris buffer, pH 7.4) was placed over the retina as described previously.[3] The eye was then closed with 6-0 prolene suture. The animals were allowed to survive one to three days prior to perfusion fixation.

Perfusion and Fixation. The animals were anesthetized by immersion in 0.1% tricane methanesulfonate and perfused transcardially with 25 ml of 0.12 mol/l phosphate buffer (pH 7.4) containing 0.25% procaine and 3% sucrose followed by 600 ml of a fixative containing 4% paraformaldehyde,

1% glutaraldehyde, 15% saturated picric acid, and 3% sucrose in 0.12 mol/l phosphate buffer (pH 7.4). This was followed by 800 ml of a second fixative containing 4% paraformaldehyde, 1% glutaraldehyde and 3% sucrose in 0.12 mol/l phosphate buffer (pH 7.4). The heads were removed four hours later and immersed in the second fixative overnight. The brains were then removed and cut coronally or sagittally at 75 μm on a Vibratome.

Biocytin Histochemistry. The sections were immersed in 20% sucrose in phosphate buffer and frozen in liquid nitrogen in order to improve penetration of the avidin-biotin complex (ABC elite, Vector). The sections were washed three times in phosphate buffer and placed in ABC elite at the standard dilution for two hours with constant agitation at 4°C. The sections were washed three times in phosphate buffer and placed in a nickel-diaminobenzidine solution for 35 - 45 minutes. The DAB solution contained 50 mg diaminobenzidine, 40 mg ammonium chloride, 200 mg β-D-glucose, 0.4 mg glucose oxidase, and 0.05 nickel ammonium sulfate, in 100 cc of 0.1M phosphate buffer.

Processing for Electron Microscopy. Vibratome sections were placed in 1% osmium for one hour, followed by two changes of 3.6% sodium chloride for 30 minutes, and dehydrated in increasing concentrations of Quetol 523m

(Ted Pella, Inc.) in distilled water: 35, 50, and 70% for 10 min each; 80 and 90% for 15 min each; followed by 100% Quetol for 20 min. Sections were then floated in a 50% Quetol-50% maraglas solution (Ted Pella, Inc.) for 12 h followed by pure maraglas for 6 h. The sections were flat-embedded on siliconized microscope slides and cured for two days at 60°C. Tissue was then cut from the area of interest and fixed to epon blocks. Following serial thin-sectioning on a Reichert ultramicrotome, the sections were placed on formvar-coated grids, double-stained with uranyl acetate and lead citrate, and examined with a JEOL electron microscope.

RESULTS

Light Microscopy. Biocytin-labeled axons clearly labeled the optic tracts and medial and lateral basal optic fasciculi. As demonstrated in previous studies, the nBOR was situated between the caudal edge of the hypothalamus and the nucleus of cranial nerve III (Fig. 2.1). Both large and small axons were clearly labeled, although a detailed study of individual axons within the nBOR could not be determined at the light microscopic level secondary to the dense staining of the terminal field.

Electron Microscopy. At the electron microscopic level, the axon terminals labeled with biocytin in the nBOR appeared quite dense, but did not fill the synaptic vesicles. Many of the axons followed in serial sections terminated

in numerous large axon terminals, although some of the axons made *en passant* synaptic contacts. The synaptic terminals varied in size from 0.5 μm to 2.0 μm in diameter (Figs. 2.2,2.3). Most of the labeled axon terminals made symmetric axodendritic synapses, but there were very rare axosomatic and axospinous contacts as well. The axodendritic synapses were more numerous on the smaller dendrites (Figs. 2.2a, 2.3a, b,c,d), although there were synapses on the large proximal dendrites (Fig. 2.2c). Interestingly, a moderate number of small dendrites or spines were completely surrounded by and received synaptic contacts from two labeled boutons (Fig. 2.2b). In addition, unlabeled boutons adjacent to labeled axon terminals were seen on many of the dendritic segments (Figs. 2.2a,2.3a).

DISCUSSION

Previous investigators have demonstrated that the basal optic root is composed of numerous small, myelinated fibers and occasional large, myelinated fibers, which display four different types of axon terminal arborizations within the nBOR.[2] The large diameter axons appeared to contact neuronal perikarya and also terminated in the cell-free regions of the nBOR. In the present study, the presence of axosomatic and axospinous synapses were rare, and most of the large diameter axons made axodendritic synapses. These investigators also demonstrated small diameter axons ending diffusely in small boutons or which made *en passant* synapses. The

smallest diameter axons terminated in fine terminal arborization creating a very dense plexus within the nBOR. This type of arborization was clearly seen in our material and certainly comprised the majority of axon terminals in the nBOR.

Using the Golgi technique, other investigators demonstrated that there are six major cell types present in the nBOR, of which the stellate type is most numerous.[2,4] In addition, in the peri-nBOR region and nucleus of the medial longitudinal fasciculus, neurons extend their dendrites into the nBOR, where they presumably receive direct optic input. The present study demonstrates that neurons in the nBOR, in general, receive mainly axodendritic and little axospinous synaptic input. The rare axospinous input to the nBOR could have been predicted from the previous Golgi studies, which demonstrated most dendrites within the nBOR are spineless. Since direct axosomatic synapses were only rarely seen, it is impossible to determine the ultrastructure of the retinal input to specific cell types in the nBOR without a combined anterograde tracer-Golgi impregnation electron microscopic study.

Figures and Tables

Figure 2.1: Light photomicrograph of the biocytin filled retinal input to the basal optic nucleus. Labeled retinal axons are seen streaming into the nucleus from its rostral surface (right), forming a dense fiber network within the nucleus. Arrows mark the ventral surface of the brain. Scale bar = 200 μm.

Figure 2.2: Electron micrographs of biocytin filled retinal axon terminals in the basal optic nucleus. **a.** Biocytin labeled (arrowhead) and unlabeled (arrow) axon terminals making symmetric synaptic contacts with a medium-sized dendrite. **b.** Two biocytin labeled axon terminals completely surrounding and making symmetric synapses (arrowheads) with a small dendrite or spine. c. A large proximal dendrite (d) receiving an *en passant* symmetric synaptic contact (arrowhead) from a labeled axon. Scale bars = 1.0 μm.

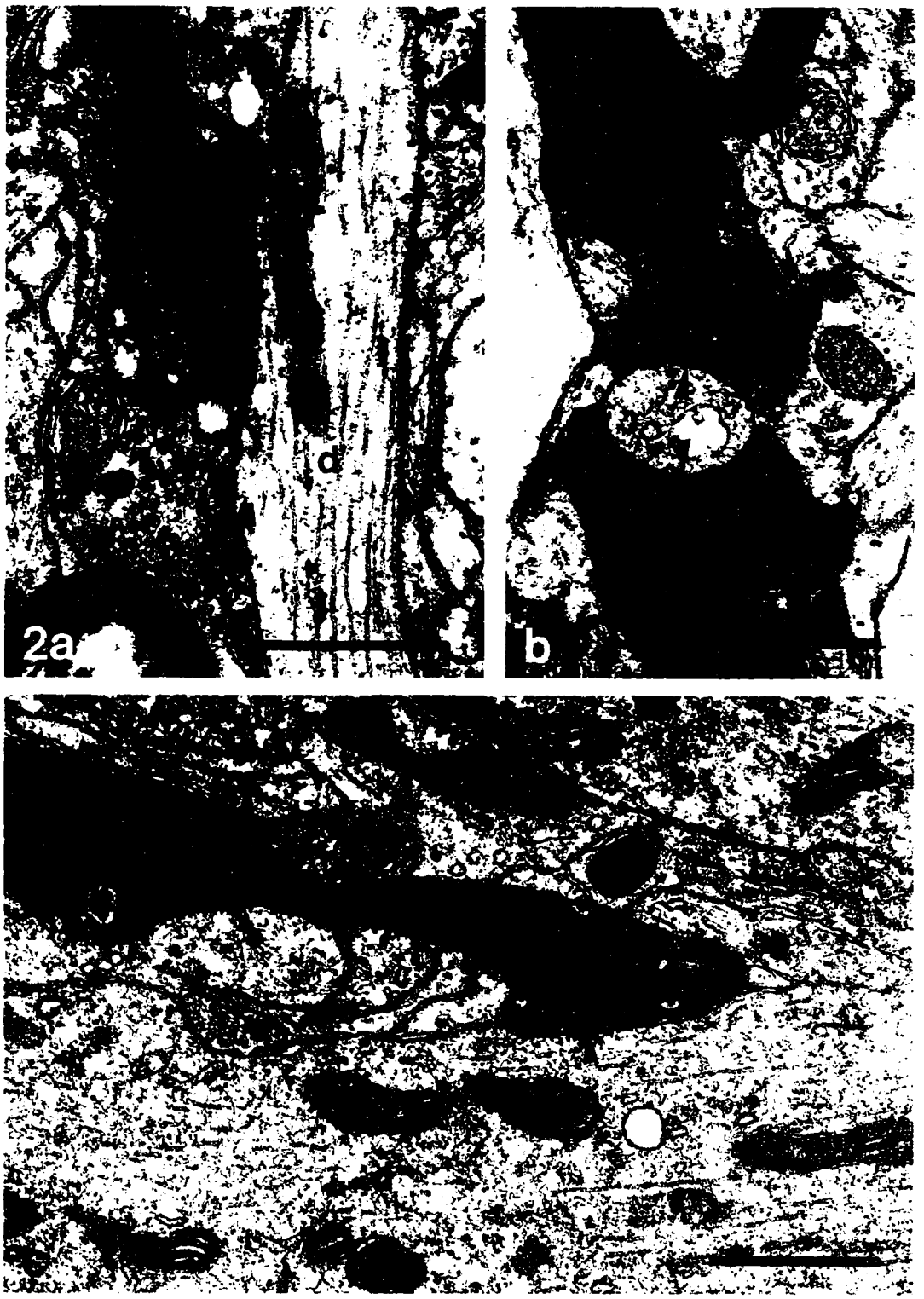

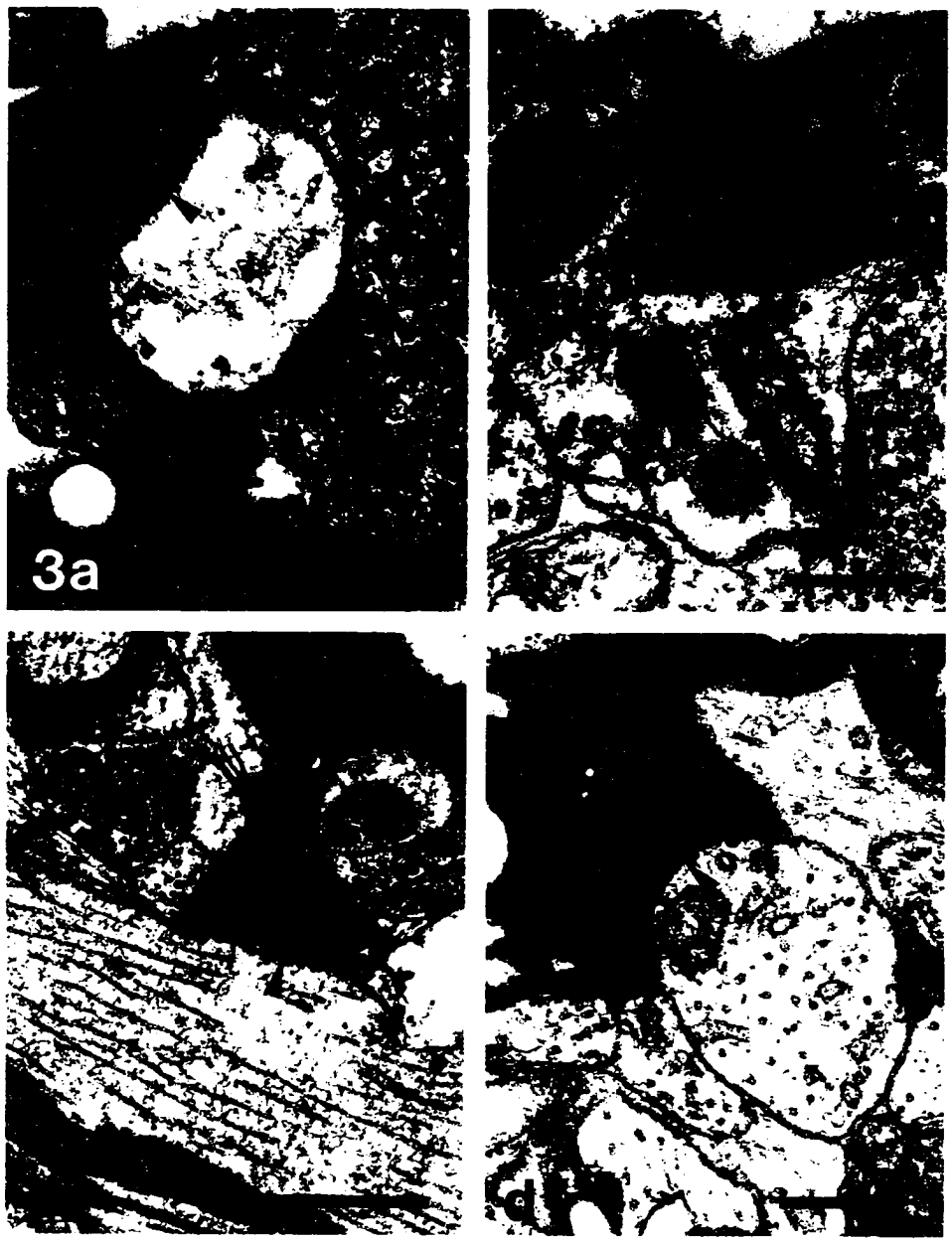

Figure 2.3: Electron micrographs of biocytin labelled retinal axon terminals in the basal optic nucleus. **a,b,c,d.** Biocytin labeled axon terminals making symmetric synaptic contact with small and medium-sized dendrites (arrowheads). Note unlabeled terminal synapsing on opposite side of dendrite in **a** and the area of "fallen out" vesicles in the labeled bouton in **d.** **a,b,d.** Scale bars = 0.5 μm. c. Scale bar = 1.0 μm.

REFERENCES

1. Fite, K.V. (1985) Pretectal and Accessory Optic Visual Nuclei of Fish, Amphibia and Reptiles: Theme and Variations, Brain Behav. Evol. 26:71-90.

2. Fite, K.V., Bengston L.C. and Montgomery N.M. (1988) Anuran Accessory Optic System: Evidence for a Dual Organization, J. Comp. Neurol. 273:377-384.

3. Helm, G.A., Palmer, P.E., Simmons, N.E., diPierro, C.G. and Ebbesson, S.O.E. (1993) A Method for Utilizing Biocytin to Study Retinofugal Pathways at the Light and Electron Microscopic Levels. J. Neurosci. Methods 49:97-101.

4. Montgomery, N., Fite, K.V. and Bengston, L. (1981) The Accessory Optic System of *Rana Pipiens*: Neuroanatomical Connections and Intrinsic Organization, J. Comp. Neurol. 203:595-612.

5. Montgomery, N., Fite, K.V., Taylor, M. and Bengston, L. (1982) Neural Correlates of Optokinetic Nystagmus in the Mesencephalon of *Rana Pipiens*: A Functional Analysis, Brain Behav. Evol. 21:137-151.

6. Simpson, J.I. (1984) The Accessory Optic System, Ann. Rev. Neurosci. 7:13-41.

Chapter 3

FETAL NEOSTRIATAL TRANSPLANTS IN THE RAT:

A LIGHT AND ELECTRON MICROSCOPIC GOLGI STUDY*

*(Published, Neuroscience 37 (1990) 735-756)

INTRODUCTION

The feasibility of using fetal neuronal transplants for the treatment of neurodegenerative diseases is gaining acceptance in the neuroscience community.[2,48] Not only do transplanted neurons establish sparse afferent and efferent connections with the host brain[9,23,40,41,52-54], but they also differentiate into morphologically[35] and biochemically[1,42,50] distinct cell types typical of the brain region transplanted.

The functional effects neuronal transplants have on the host brain may be the direct result of the reproduction of normal neuroanatomical features in the lesioned areas.[13-15,28-30] Anatomical development of neuronal grafts has been most heavily characterized in fetal striatal grafts in the lesioned rat striatum, an animal model of Huntington's disease.[10,33,36] Initial tract-tracing studies of connections formed by striatal grafts, utilizing WGA-HRP as a combined retrograde and anterograde tracer, were largely inconclusive.[40,51] A recent series of papers[9,52-54] on the other hand, which relied primarily on the use of fluorescent tracers, Phaseolus vulgaris-leucoagglutinin, and EM-immunohistrochemistry provide considerable evidence that intrastriatal striatal grafts are capable of establishing significant and appropriate afferent and efferent connections with the host brain.

Grafted fetal striatal neurons also differentiate neurochemically into several different cell types, including GABA-ergic and enkephalinergic medium-sized neurons and cholinergic large neurons.[42,51] A previous light microscopic Golgi study of striatal transplants demonstrated that the grafted neurons differentiate into several morphologically different striatal cell types;

however, not all of the normal striatal cell types were demonstrated.[35] In addition, an ultrastructural study of striatal transplants revealed that the grafts differentiate into several different cell types based on somatic size and nuclear morphology and have a neuropil resembling that of the normal striatum, but this study was limited by the fact that striatal cells and their processes cannot be identified by ultrastructural characteristics alone.[17]

It may be hypothesized that all of the striatal cell types must be present for the grafts to establish normal function with the host brain. The present project was undertaken in order to determine whether the grafted neurons differentiate into all of the normal striatal cell types and to characterize each of the Golgi identified cell types at the ultrastructural level.

MATERIALS AND METHODS

A total of 25 adult female Sprague-Dawley rats weighing 250-300 gms and 8 pregnant female rats 14-16 days of gestation were used in this study.

Striatal lesioning and transplantation. The transplantation of fetal brain tissue into lesioned adult host brain has been previously described[2] and was only slightly modified in this study. The animals were anesthetized with chloropent (3.0 ml/kg) and received unilateral striatal injections of 0.25 μl of ibotenic acid (Sigma, 20 mg/μl in phosphate buffer, pH=7.0) with a 2.0 μl Hamilton microsyringe at the following stereotaxic coordinates from bregma: A=0.7 mm, L=3.0 mm, and V=4.5 mm.[39] Striatal implantation was performed two weeks after the lesioning. Female rats 14-16 days post-gestation were anesthetized with chloropent (3.0 ml/kg) and the fetuses

were removed by cesarian section. The fetuses were kept in cold Hank's solution without calcium or magnesium (modified Hank's solution, Sigma) containing 10 g/l of glucose and 10 U/ml of insulin. Striatal tissue was dissected from the dorsal ventricular ridge, suspended in modified Hank's solution by repeated suctioning through a fire-polished glass micropipette, and injected (2.5-3.0 µl) at the same stereotaxic coordinates into the lesioned striatum. Three months following transplantation the rats were anesthetized and perfused transcardially with 20 ml of 0.1 phosphate buffer (pH 7.4) followed by 500 ml of a fixative containing 4% paraformaldehyde, 0.1% glutaraldehyde, and 15% saturated picric acid in 0.1 M phosphate buffer (pH 7.4).[47] This was followed by 800 ml of a second fixative containing 4% paraformaldehyde and 0.1% glutaraldehyde in 0.1 M phosphate buffer. The brains were removed, placed in the second fixative for 12-16 hours at 4°C, sectioned coronally at 75 µm in 0.1 M phosphate buffer on a Lancer vibratome, and rinsed for 2 hours in several changes of 0.1 M phosphate buffer.

Golgi impregnation. The vibratome sections were Golgi impregnated by the "single section technique" previously described.[24,31] Briefly, the sections were postfixed in 1% osmium tetroxide in 0.1 M phosphate buffer for 30 minutes and free-floated in 3.5% potassium dichromate for 6 hours. The sections were mounted between two microscope slides which were then taped together at the ends and immersed in 1.5% silver nitrate for 8-10 hours. The sections were then mounted in glycerol and examined at the light microscopic level. Since Golgi impregnated neurons lose much of their detail during gold toning, neurons well within the margins of the graft were

then photographed. The sections were floated off into 0.1 phosphate buffer and gold-toned according to the method described by Fairen et al.[18] The tissue was placed in cold 0.04% gold chloride for 10-12 minutes, rinsed in cold distilled water for 20 minutes, and placed in 1% thiosulfate for 45 minutes. The sections were then reosmicated in 1% osmium tetroxide for 30 minutes.

The single section Golgi method consistently impregnates the entire dendritic tree in a given section. However, some impregnated dendrites may be cut at the surface of the section, making their apparent dendritic lengths significantly shorter than the actual dendritic lengths. Because of this limitation with the technique, only dendrites completely within the section were measured.

A considerable amount of effort was made to preserve tissue ultrastructure and to minimize the amount of gold left in the impregnated neurons during tissue processing. In previous EM-Golgi studies the cellular membranes and synaptic detail were obscured by the large amounts of gold present after gold-toning.[7,46] In the present study the gold particles were minimized by decreasing the silver nitrate treatment time, which seems to decrease the amount of silver deposition during Golgi-impregnation. This made it possible to clearly observe the synaptic specializations and cellular detail of the neurons, even after Golgi-impregnation and gold-toning. Although the neuronal somata and their appendages were more difficult to locate at the electron microscopic level, they were still clearly labeled with gold.

Processing for electron microscopy. The sections were dehydrated in increasing concentrations of Quetol 523M (Ted Pella, Inc.) in distilled water: 35%, 50%, and 70% for 10 minutes each; 80% and 90% for 15 minutes each followed by 100% Quetol for 20 minutes. The sections were then floated in a 50% Quetol, 50% Maraglas solution (Ted Pella, Inc.) for 12 hours followed by pure Maraglas for 6 hours. Sections were flat embedded on siliconized microscope slides and cured for 2 days at 60°C. Gold-toned transplant neurons previously identified and photographed at the light microscopic level were then cut from the sections and affixed to Epon blocks. Following serial thin sectioning on a Reichert Ultramicrotome with a Diatome diamond knife, the sections were placed on Formvar coated slot grids, double stained with uranyl acetate and lead citrate, and examined with a JEOL electron microscope.

RESULTS

Because of the capriciousness of the Golgi impregnation method and the rarity of several striatal neuron types, the classification of normal rat striatal cell types has remained a controversial area.[6] The most comprehensive Golgi study of the normal rat neostriatum[6] utilized a classification scheme based on somatic size and cellular morphology. Using this scheme, neurons are initially grouped by somatic size,with large neurons having a somatic diameter larger that 20 μm, medium neurons having a somatic diameter between 10 and 20 μm, and small neurons having a somatic diameter less than 10 μm. These groups are then subdivided by somatic and dendritic morphology. Type I large neurons have aspinous

somata and smooth or sparsely spined dendrites, while Type II large neurons have somatic spines and sparsely spined dendrites. Type I medium neurons have aspinous somata and proximal dendrites, but densely spined distal dendrites, whereas Type II medium neurons have somatic spines and sparsely spined dendrites. Type III medium neurons have aspinous somata and poorly branched, sparsely spined dendrites. Type IV medium cells have aspinous somata and highly branched, sparsely spined dendrites and Type V medium cells have aspinous somata and sparsely spined varicose dendrites. The rare small cells have various somatic and dendritic morphologies. Since our own light microscopic observations of Golgi-impregnated neurons in the normal rat neostriatum are consistent with this classification scheme, the identical scheme has been used in the present study to classify Golgi-impregnated transplanted neurons at the light microscopic level.

All neurons studied were located in the core of the transplants (see Fig. 3.1). In this way, any ambiguity about the source of the cells examined (transplant versus host) was avoided.

Large Neurons

Type I large neurons. At the light microscopic level these neurons were either fusiform (Figs. 3.2a and 3.4a) or polygonal in shape and did not display somatic spines. The dendrites were non-varicose, very sparsely spined, and sparsely branched. The longest dendrite observed was approximately 175 μm.

At the electron microscopic level the somata of Type I large neurons were characterized by an oval, highly invaginated nucleus surrounded by abundant, pale cytoplasm rich in organelles, including rough endoplasmic

reticulum, mitochondria, free ribosomes, polyribosomes, Golgi complexes, lysosomes and microtubules (Fig. 3.4b). A moderate number of symmetric axosomatic synapses with axon terminals with loosely packed vesicles were observed (Fig. 3.4c). The proximal dendrites also had multiple symmetric synapses with axon terminals loosely packed with vesicles (Fig. 3.4d). The axon of the neuron shown in Figure 3.4 arose from the soma, was unmyelinated and rich in neurofilaments, and had multiple synapses on the its hillock (Fig. 3.5a). The large dendrites exhibited numerous mitochondria, microtubules, and symmetric axodendritic synapses (Fig. 3.5b). The axodendritic terminals were loosely packed with vesicles.

Type II large neurons. At the light microscopic level the somata of this second type of large neuron was polygonal or fusiform (Fig. 3.2b) and displayed multiple somatic spines. Due to the refractiveness of the glycerol it was difficult to photograph these spines; however, they were clearly demonstrated at the electron microscopic level. The dendrites were moderately branched and sparsely spined throughout their lengths.

At the ultrastructural level the somata of these neurons had deeply invaginated nuclei and a large amount of pale cytoplasm rich in organelles similar to the Type I large cell. Multiple somatic spines exhibiting various morphologies protruded from the soma (Fig. 3.7a,b). Axon terminals both loosely and densely packed with vesicles made symmetrical and asymmetrical synapses with these spines. Often, both types of boutons contacted the same spine (Fig. 3.7a,b). A moderate number of axosomatic synapses were observed whose axon terminals were similar to those occurring on the somatic spines, i.e. both loosely (Fig. 3.7a) and densely

(Fig. 3.7b) packed with vesicles. The proximal dendrites displayed numerous spines, which received symmetric synaptic input from boutons loosely packed with vesicles (Figs. 3.6c and 3.7c), and axodendritic synapses with boutons loosely packed with vesicles (Figs. 3.6c and 3.7c). Several boutons synapsed with both the dendritic surface and a dendritic spine (Fig. 3.6c). The majority of somatic and dendritic spines contained a spine apparatus (Fig. 3.7a,b,c). The distal dendrites displayed both symmetric (Fig. 3.7d) and asymmetric synaptic input.

Medium Neurons

Type I medium neurons. At the light microscopic level these cells were characterized by aspinous somata and proximal dendrites, but densely spiny distal dendrites (Figs. 3.3c and 3.8a). The dendrites were moderately branched and unusually long, with the longest dendrite measuring 200 μm. Occasional distal dendrites were only sparsely spined or totally without spines.

At the electron microscopic level the somata of Type I medium neurons were characterized by unindented nuclei surrounded by a thin rim of dense cytoplasm containing a large number of free ribosomes and polyribsomes, but only a moderate number of mitochondria and lysosomes (Fig. 3.8b). The rough endoplasmic reticulum and Golgi complexes were quite sparse. Several large axon terminals containing numerous mitochondria and loosely packed vesicles made symmetric contacts with the somata (Fig. 3.8c). Sparse axodendritic synapses were present on aspinous proximal dendrites, which contained occasional mitochondria and numerous microtubules (Fig. 3.9c). The distal dendrites had many spines with varying

morphologies which were asymmetrically contacted by axon terminals loosely packed with vesicles (Fig. 3.9a,b). These spines consistently displayed a spine apparatus (Fig. 3.9a,b).

Type II medium neurons. At the light microscopic level these neurons were characterized by spiny somata and moderately spined proximal and distal dendrites (Fig. 3.10a). Unlike the Type I medium neurons, the dendrites displayed spines which were evenly distributed over the entire dendritic length, not just on the distal dendrites.

At the electron microscopic level these neurons were characterized by highly invaginated nuclei surrounded by a moderate amount of cytoplasm packed with rough endoplasmic reticulum forming nissl bodies (Fig. 3.10b). Mitochondria, lysosomes, perinuclear Golgi complexes, free ribosomes, and polyribosomes were also observed. Axon terminals loosely (Figs. 3.10c and 3.11a) and tightly (Fig. 3.10d) packed with vesicles made symmetric synapses with the somata. Multiple axodendritic and axospinous synapses were present on the dendrites (Fig. 3.11b).

Type III medium neurons. At the light microscopic level Type III medium neurons were characterized by aspiny somata with sparsely branched, very sparsely spined dendrites (Figs. 3.3a and 3.12a). The primary dendrites branched into several short secondary dendrites, with the longest dendrite observed being 100 μm in length.

At the electron microscopic level these cells were characterized by somata with invaginated nuclei in a moderate amount of cytoplasm containing mitochondria,lysosomes, free ribosomes, and polyribosomes, but very sparse rough endoplasmic reticulum and Golgi complexes (Fig. 3.12b).

Although the neuron in Figure 3.12b appears to have only an irregular nuclear outline, an invaginated nuclear envelope was demonstrated through the examination of serial sections. Relatively few symmetric axosomatic synapses with boutons densely packed with vesicles were observed (Fig. 3.13a). The dendrites had very few axodendritic synapses and only one dendritic spine with an asymmetric axospinous contact was observed (Fig. 3.13b).

Type IV medium neurons. At the light microscopic level Type IV medium neurons were characterized by aspinous somata with highly branched dendrites (Figs. 3.3b and 3.14a). The dendrites were non-varicose and were either sparsely spined or totally smooth, with both types occurring on the same cell.

At the electron microscopic level these cells were characterized by somata with slightly invaginated nuclei surrounded by a rim of cytoplasm containing relatively few organelles, which included mitochondria, lysosomes, ribosomes, Golgi complexes, and rough endoplasmic reticulum (Fig. 3.14b). The somata received symmetric synaptic input from large axon terminals moderately packed with vesicles (Fig. 3.14c). Dendrites rich in microtubules and with sparse mitochondria received sparse symmetrical axodendritic synapses from large axon terminals loosely packed with vesicles (Fig. 3.15a,b).

Type V medium neurons. At the light microscopic level these neurons displayed aspinous somata and markedly varicose dendrites (Fig. 3.16a). These dendrites were very sparsely branched and were completely devoid of spines. The dendritic lengths varied greatly with each cell, some with

relatively short dendrites (Fig. 3.16a) and others with dendrites extending up to 150 μm.

At the electron microscopic level Type V medium neurons were characterized by somata containing a highly invaginated nucleus and a moderate amount of dense cytoplasm rich in mitochondria, free ribosomes, polyribosomes, Golgi complexes, and microtubules (Fig. 3.16b). Lysosomes and rough endoplasmic reticulum were relatively scarse in this cell type. Axon terminals loosely packed with vesicles made rare symmetric axosomatic contacts (Fig. 3.16a). Varicosities in the dendrites could also be seen at the electron microscopic level (Fig. 3.17). These dendrites received numerous symmetric synaptic input from boutons loosely packed with vesicles (Fig. 3.15).

Small Neurons

No small neurons were observed in this study. However, some of the medium neurons did have somatic sizes on the borderline between medium and small cells, i.e. 10 μm.

DISCUSSION

The present study has employed the "single section Golgi" technique to demonstrate unequivocally that fetal neostriatal transplants differentiate within three months of implantation into all seven major striatal cell types. Gold-toned, Golgi-impregnated neurons were subsequently examined at the electron microscopic level in order to evaluate the ultrastructural characteristics of each cell type. The results suggest that both similarities and differences exist between normal adult and transplanted fetal striatal neurons at the light and electron microscopic levels. Other investigators

have suggested that at least some of the differences seen betwen the striatal transplants and the normal striatumm could be accounted for by the contamination of the transplants by non-striatal tissue.[17,54] Therefore, the differences seen between Golgi-impregnated transplant neurons and normal striatal neurons may be due to the inclusion of non-striatal cells in the study.

Large Neurons

Light microscopic analysis. In the normal rat neostriatum, most previous studies have demonstrated only Type I large neurons, which are characterized by smooth somata, sparsely spined or smooth proximal dendrites, and sparsely spined and occasionally varicose distal dendrites.[6,7,11,12,18,34,37] Type II large neurons, which are characterized by somata bearing spines and sparsely spined dendrites, have been demonstrated only by two group of investigators in the rat[4,6,7], but have also been demonstrated in the monkey.[16,38]

In the present study both Type I and Type II large neurons are present. At the light microscopic level these neurons are very similar to those described by Chang et al.[6], except that the dendrites of both of these large neurons were noticeably shorter in the transplant than those described in the normal rat striatum.[6,7] This may well be due to the limitations of the single-section Golgi method used in this study.

Large neurons have also been observed in neostriatal grafts by several other investigators. McAllister et al.[35] demonstrated large neurons with somatic diameters between 40-50 μm with cresyl violet staining. Because no large neurons were found in their Golgi-impregnated material, they could not comment on the somatic and dendritic morphologies of these cells.

Large acetylcholinesterase-reactive neurons presumed to be Type I or Type II large neurons have been identified in striatal transplants at the light microscopic level.[50] In an ultrastructural study of striatal grafts[17], two types of large neurons were observed: one with a "globular" soma and the other with an "elongated" soma. No spines were observed on these cells; therefore, these two cell types probably represent the two somatic morphologies, polygonal and fusiform, of the Type I large neurons described in the present study.

Electron microscopic analysis. Type I large cells have been studied at the electron microscopic level in the primate[16,21,22,38], cat[32], and rat.[7,18] Type II large neurons have been examined at the electron microscopic level in the primate[16] and rat.[4,7] In general, both types of large neurons are characterized by invaginated nuclei surrounded by copious, pale cytoplasm rich in organelles, including rough endoplasmic reticulum. Chang and Kitai[7] also observed that Type II large neurons not only had somatic spines, but also had qualitatively more axosomatic synapses than Type I large neurons. These investigators postulated that the presence of somatic spines and numerous somatic synapses may account for any functional differences between the two large cell types.[7]

The present Golgi study demonstrates that both Type I and Type II large neurons are ultrastructurally similar to those in the normal rat neostriatum. Both normal and transplanted large neurons have highly invaginated nuclei and large amounts of organelle rich cytoplasm. In addition, somatic spines can be demonstrated on Type II cells at the electron microscopic level. However, the difference in the number of somatic

synapses seen on normal Type I and Type II large cells are not characteristic of the transplanted cells. Chang and Kitai[7] frequently observed more than one axon terminal synapsing with one somatic or proximal dendritic spine. In our transplants this is also seen; however, in striatal transplants two types of axon terminals, one moderately filled and the other tightly packed with vesicles, synapse on one somatic spine. This suggests that there are two distinct afferent fibers projecting to these somatic spines.

In rat striatal transplants large cells have been previously demonstrated at the electron microscopic level by DiFiglia et al.[17] In their electron microscopic analysis of neostriatal grafts, these investigators described large cells with indented nuclei, but did not classify these cells as Type I or Type II based on the presence or absence of somatic spines or discuss any differences in the number of somatic synapses.

Medium Neurons

Type I medium neurons. The Type I medium neuron is by far the most common cell type in the neostriatum, accounting for 95% and 94% of the striatal neurons in the cat[32] and rat[43], respectively. Numerous Golgi studies have described these neurons at the light microscopic level in the primate[16,21,22], cat[32], dog[49], and rat.[7,11,12,34,37] These studies have shown that these medium-sized neurons have smooth somata and proximal dendrites, but densely spiny distal dendrites.

Transplanted Type I medium neurons morphologically similar to normal Type I medium neurons have been identified in Golgi-impregnated striatal grafts.[35] The only differences observed were that some dendrites displayed slightly fewer spines than normal Type I medium neurons. This was also

demonstrated in the present study, with some dendrites of these cells only sparsely spined, while others were heavily spined. McAllister et al.[35] suggests that these differences are due to the presence of immature forms of the Type I medium neuron in the grafts. It has been demonstrated that much of the afferent input into the striatum terminates on the spines of these medium neurons.[8,25,26,32,38,45] The decreased spine density may therefore be due to insufficient input from regions extrinsic to the graft. These neurons may also represent a variant of the Type I medium neuron that has a decreased spine density which has been observed in a previous study (medium spindle cells of Lu and Brown).[34]

At the electron microscopic level Type I medium neurons have been described as having unindented nuclei, sparse, moderately dense cytoplasm containing no Nissl bodies, and smooth primary dendrites which are rich in microtubules but poor in mitochondria.[7,18,43,45,46] The transplanted Type I medium cells in the present study displayed each of these ultrastructural characteristics. A previous study[17] reported that the percentage of neurons with unindented nuclei was dramatically decreased in the graft, suggesting that their are either fewer Type I medium neurons present or that transplanted Type I medium neurons also have indented nuclei. This was not observed in the present study.

Numerous asymmetric axospinous synapses are characteristically seen on the distal dendrites of Type I medium neurons in both the normal striatum[38,46] and transplanted striatum. DiFiglia et al.[17] quantitatively studied these axospinous synapses in striatal graft neuropil and found that a

normal percentage (approximately 92%) were asymmetric, although these spines could not be identified as belonging to Type I medium neurons.

Type II medium neurons. Type II medium neurons were first identified as a medium-sized striatal cell exhibiting somatic spines by Chang et al.[6] These investigators recognized the similarities between Type II medium neurons and Type II large neurons, but chose to classify them as two different cell types for clarity and consistency. In reality, however, these two types may represent one cell type with a continuous distribution of somatic size in both the medium and large cell ranges. In the present study transplanted Type II medium neurons, identified at the light microscopic level, were identical to normal Type II medium neurons[6], displaying numerous somatic spines and sparsely to moderately spined dendrites, with these spines evenly distributed along the entire dendrite. Medium sized neurons having somatic spines were not mentioned in the previous Golgi study of transplanted striatal neurons, although they may have been classified as another cell type (Spiny II neuron of McAllister et al.).[35]

Type II medium neurons in the normal rat striatum have never been demonstrated at the electron microscopic level. This study has demonstrated that these neurons are characterized by an invaginated nucleus and contain the largest amount of Nissl substance of any cell type. The invaginated nuclei are consistent with the indented nuclei usually seen in normal "aspiny" striatal cells.[18] The cytoplasm tightly packed with Nissl substance is characteristic of this cell type and differentiates it from the Type II large cell. Therefore, the separation of neurons having somatic spines into Type II large and Type II medium neurons may well be justified.

Type III medium neurons. At the light microscopic level there have been many inconsistencies in the classification of this striatal cell type.[6,11,12,18,34,37] The normal Type III medium neuron has an aspinous somata and long, sparsely spined dendrites that are sparsely branched. Transplanted Type III medium neurons demonstrate all of these features, but their dendritic lengths are significantly shorter than normal. This cell type was also demonstrated in the previous Golgi study of transplanted striatuM.[35]

At the electron microscopic level this neuron is characterized by somata with invaginated nuclei, minimal cytoplasm, few organelles, and numerous dense bodies (the Type IV neuron of DiMova et al.).[18] In the present study the characteristics of this cell type are quite similar, except that the large number of dense bodies seen in normal striatum are not seen in the transplant.

Type IV medium neurons. Type IV medium neurons have been inconsistently identified and classified in the normal striatum.[6,11,12,18,34,37] The transplanted Type IV medium neurons found in the present study were identical to the Type IV medium neurons found in the normal striatum[6], with highly branched, non-varicose, sparsely spined dendrites. This cell type was not seen in the previous Golgi study of transplanted striatum.[35] At the electron microscopic level the transplanted Type IV medium neurons are similar to those observed in the normal striatum, with indented nuclei and moderate amounts of cytoplasm, but the transplanted cells had a significantly lower number of mitochondria than normal Type IV neurons (Type II neuron of DiMova et al.).[18]

Type V medium neurons. Type V medium neurons have been consistently and easily identified in the normal rat striatum, and are characterized by varicose dendrites radiating outwardly up to 250 μm away from the soma.[6,11,12,18,34,37] In the present study neurons with varicose dendrites were identified, but the dendrites of these cells were not as long or as branched as those seen in the normal striatum. These neurons were also previously observed in striatal transplants by McAllister et al.[35]

At the electron microscopic level normal Type V medium neurons exhibit indented nuclei surrounded by a considerable amount of cytoplasm, mitochondria, and Nissl granulations.[18] Transplanted Type V medium neurons have indented nuclei and abundant mitochondria, but only sparse cytoplasm and no Nissl bodies.

The origins of afferent terminals and their ultrastructural characteristics in the normal striatum have been summarized by Bolam.[3] Afferent terminals from the cerebral cortex, thalamus, and dorsal raphe nucleus make asymmetric contacts within the striatum. Dopaminergic terminals from the substantia nigra and acetylcholine, substance P- and GABA-containing terminals from intrinsic striatal neurons all form symmetric synapses within the striatum. The presence of both symmetric and asymmetric synapses within the grafts, suggests that both intrinsic and extrinsic striatal circuits are formed within the graft. The existence of a nigrostriatal projection into the graft and intrinsic GABAergic connections within the graft has been demonstrated in several studies[42,53], but the presence of other intrinsic striatal graft circuits is only speculative.

The present study demonstrates that transplanted fetal neurons have the capacity to differentiate and develop into morphologically and ultrastructurally mature brain tissue. All of the major neuronal components present in the normal striatum have also been demonstrated in striatal grafts. Other studies have demonstrated that transplanted and normal striatum contain identical neurochemical markers, including GABA, leucine-enkephalin, NADPH-diaphorase, and acetylcholinesterase.[42,50] It is therefore likely that normal intrinsic striatal circuits are also present in striatal grafts. Chang et al.[6] demonstrated that all of the normal striatal cell types, except Type II large neurons, have local axon collaterals, indicating that they function, at least partially, as interneurons; however, the presence of local axon collaterals could not be demonstrated in our Golgi preparations since axons were only rarely impregnated. Although striatal transplants exhibit many morphologic and ultrastructural similarities with normal rat striatum, it is still unclear how the tissue implants effect behavioral recovery in lesioned rats.

Figures and Tables

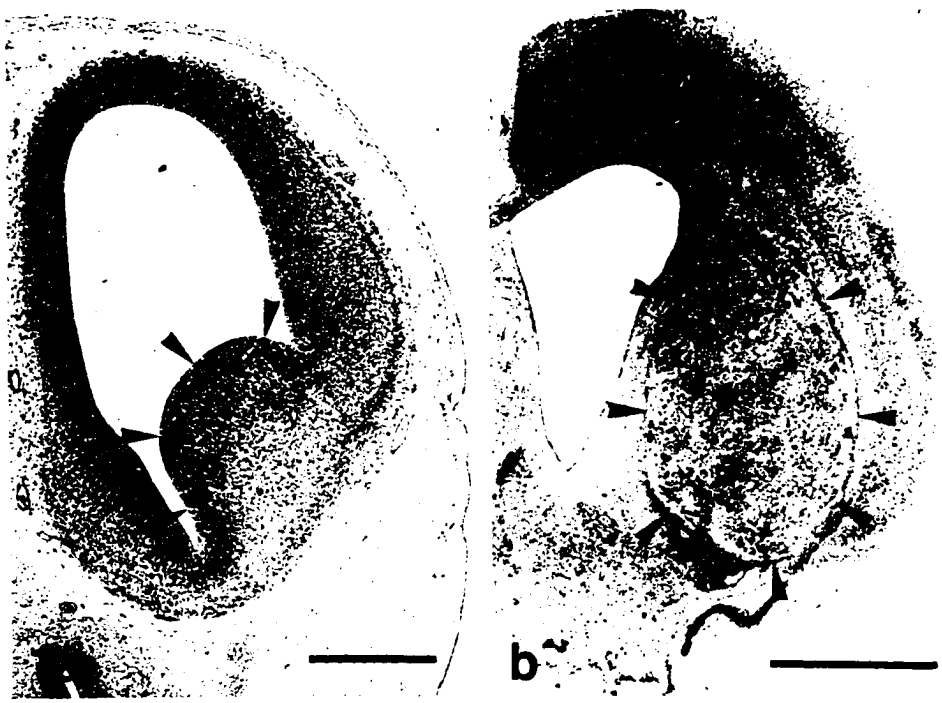

Figure 3.1: Fetal neostriatal transplants. a. Light micrograph of a Nissl-stained coronal section of a fetal rat brain 15 days post-gestation. The dorsal ventricular ridge is outlined by arrowheads. Scale bar 0.5 mm. (Courtesy of Dr. Peter Brunjes, Department of Psychology, University of Virginia). **b:** Light micrograph of fetal striatal transplant in an ibotenic-acid lesioned striatum five months after implantation (outlined by arrowheads). Scale bar 2.0 mm.

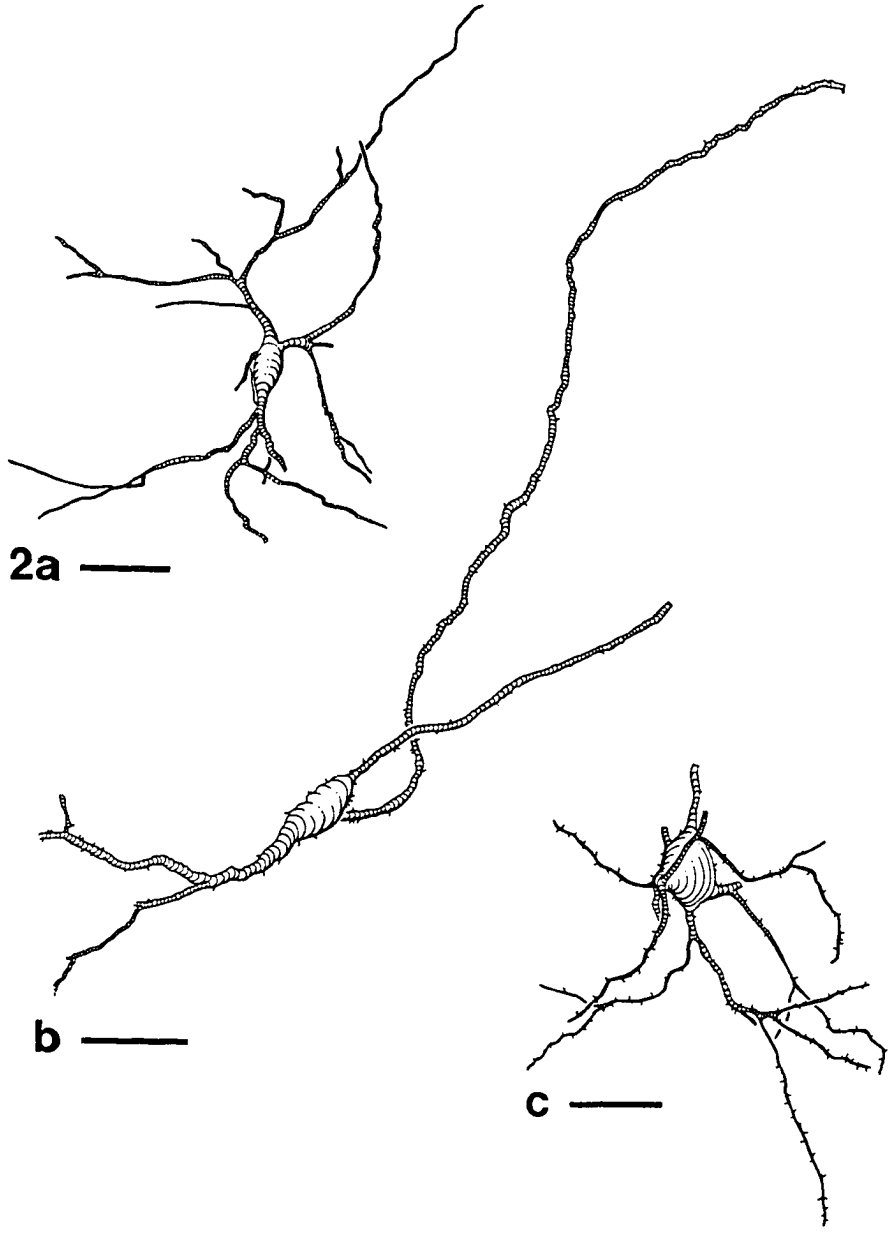

Figure 3.2: Drawings of Golgi-impregnated neurons in fetal striatal grafts. **a:** Type I large neuron. Scale bar 40 μm. **b:** Type II large neuron. Scale bar 35 μm. **c:** Type II medium neuron. Scale bar 20 μm.

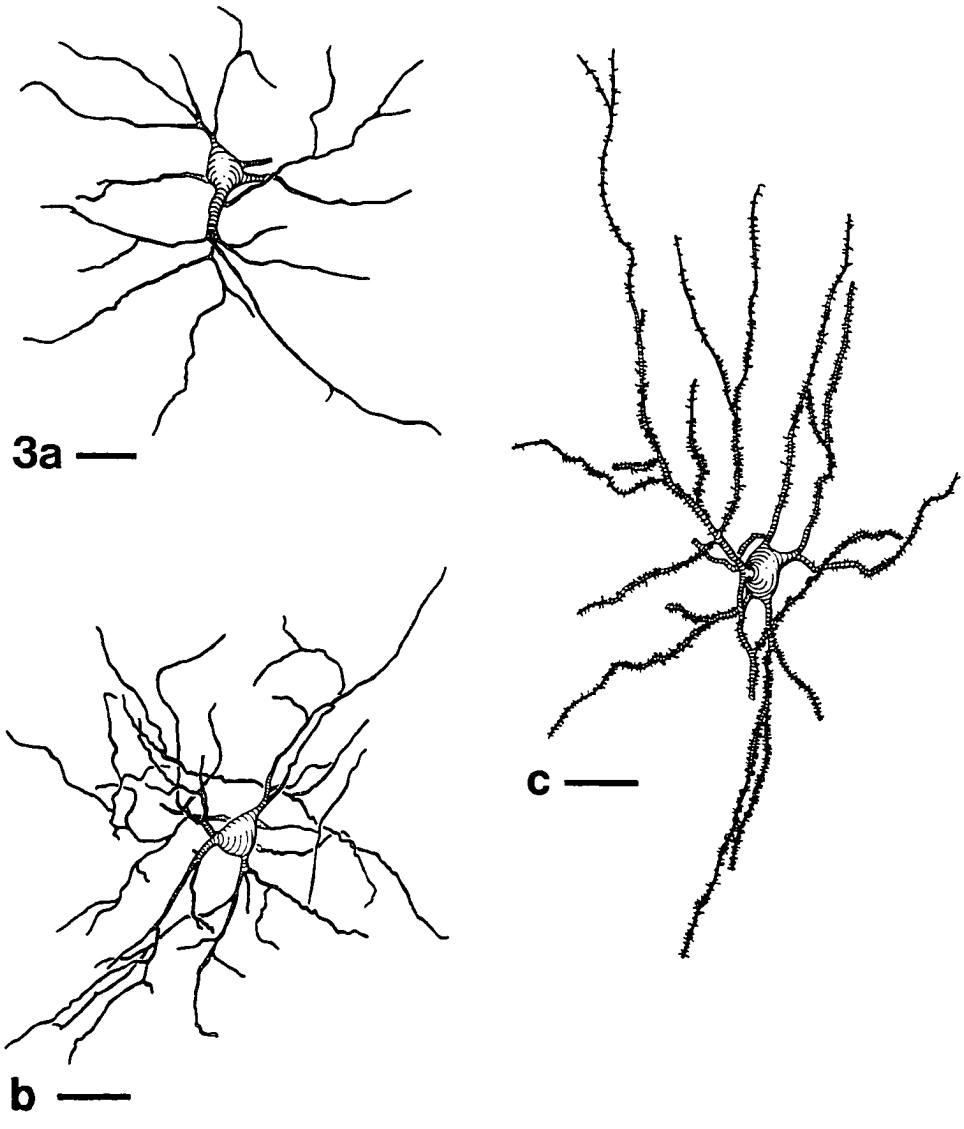

Figure 3.3: Drawings of Golgi-impregnated neurons in neostriatal grafts. **a:** Type III medium neuron. Scale bar 20 μm. **b:** Type IV medium neuron. Scale bar 20 μm. **c:** Type I medium neuron. Scale bar 20 μm.

Figure 3.4: Golgi-impregnated Type I large neuron in fetal striatal transplant. **a:** Light micrograph of Golgi-impregnated Type I large neuron prior to gold-toning. Scale bar 30 μm. **b:** Electron micrograph of the cell after gold-toning. Scale bar 5.0 μm. **c:** Perikaryon of the cell receiving symmetric synaptic input (arrowhead) from an axon terminal loosely packed with vesicles. Scale bar 1.0 μm. **d:** Proximal dendrite of the cell receiving symmetric synaptic input (arrowhead) from an axon terminal loosely packed with vesicles. Scale bar 0.75 μm.

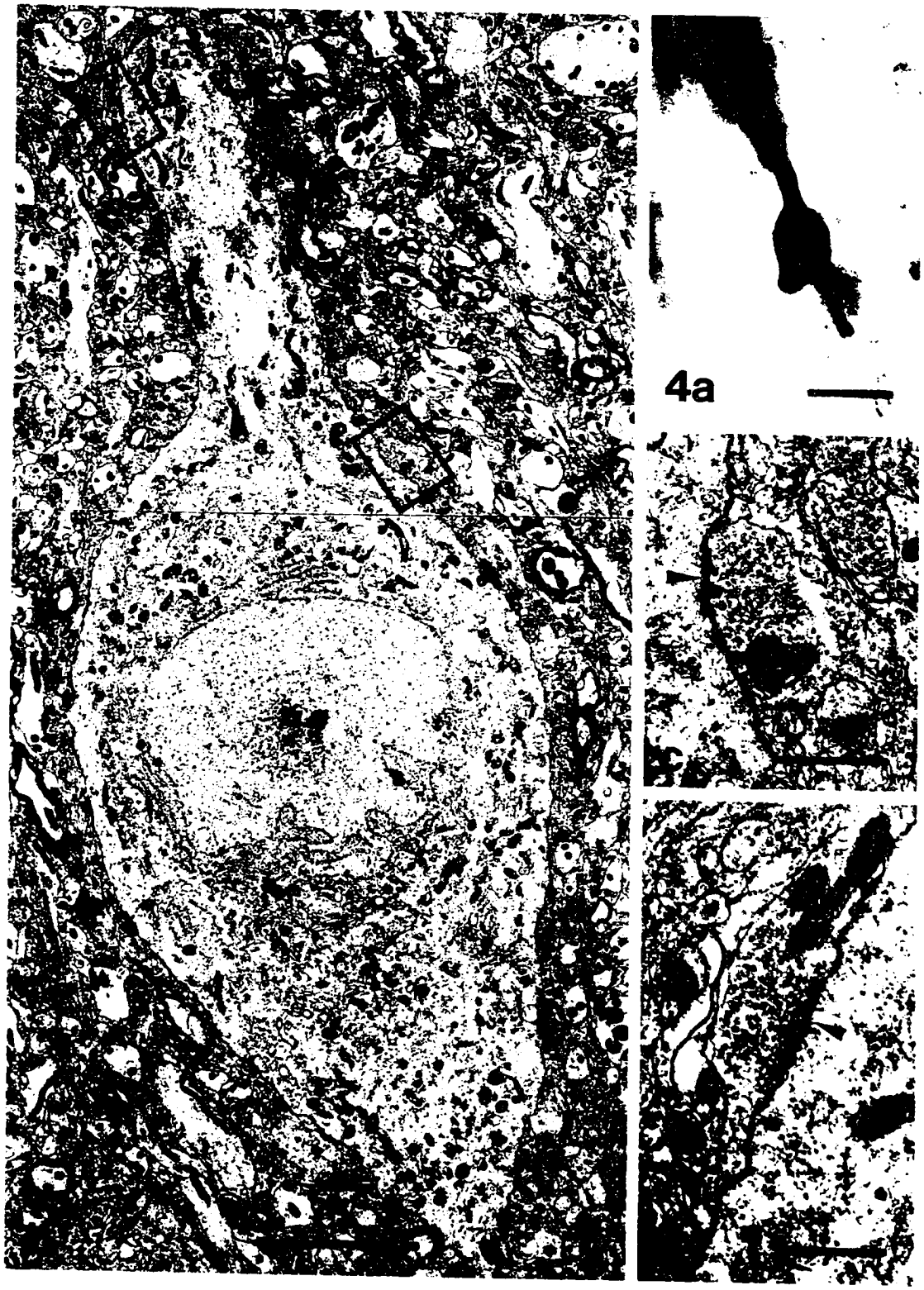

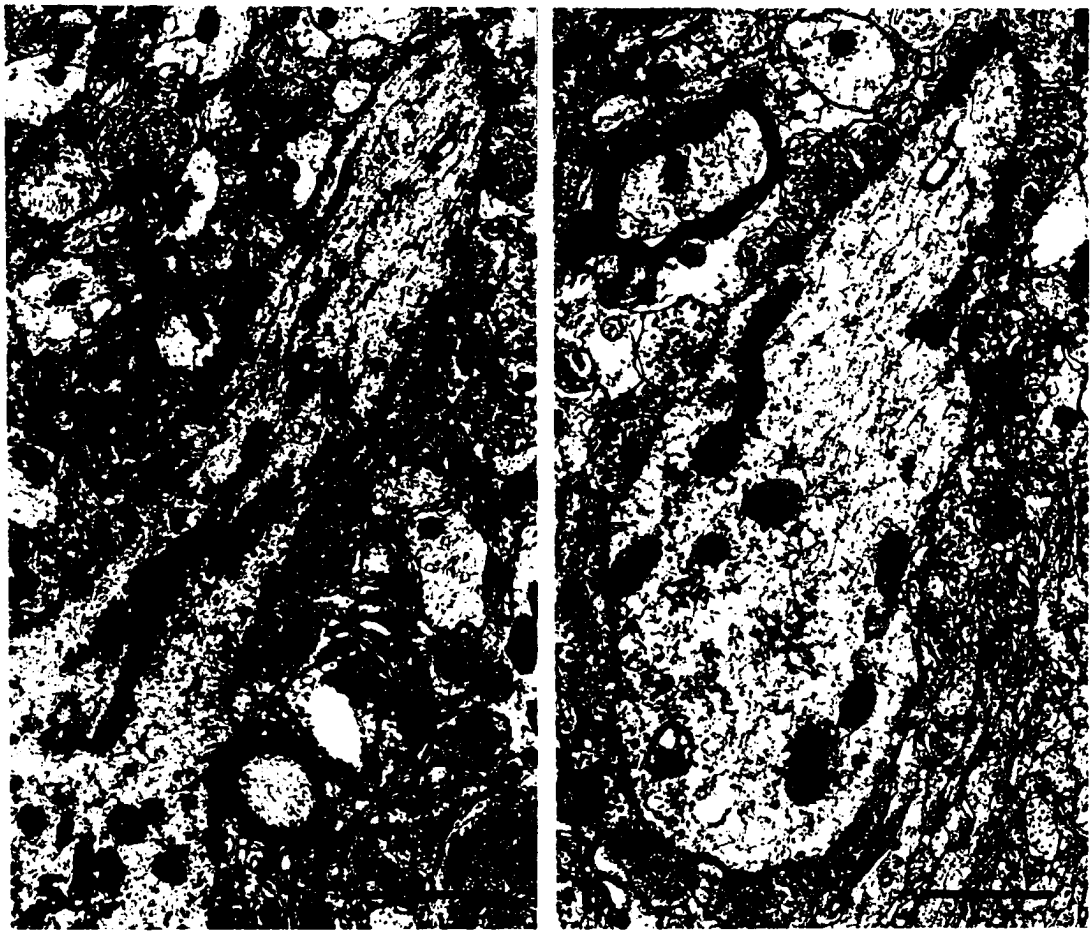

Figure 3.5: Ultrastructural details of Type I large neuron. a: Axon hillock of the Type I large neuron in Figure 2 receiving symmetric synaptic input from an axon terminal loosely packed with vesicles (arrowhead). Scale bar 2.0 μm. b: Mid-portion dendrite of the cell receiving symmetric axodendritic contacts from boutons loosely packed with vesicles (arrowheads). Scale bar 1.0 μm.

Figure 3.6: Golgi-impregnated Type II large neuron in fetal striatal transplant. **a:** Light micrograph of Golgi-impregnated Type II large neuron prior to gold-toning. Scale bar 50 μm. **b:** Electron micrograph of the cell after gold-toning. Scale bar 5.0 μm. **c:** Axon terminals loosely packed with vesicles making axodendritic and axospinous contacts with the neuron (arrowheads). Scale bar 1.0 μm.

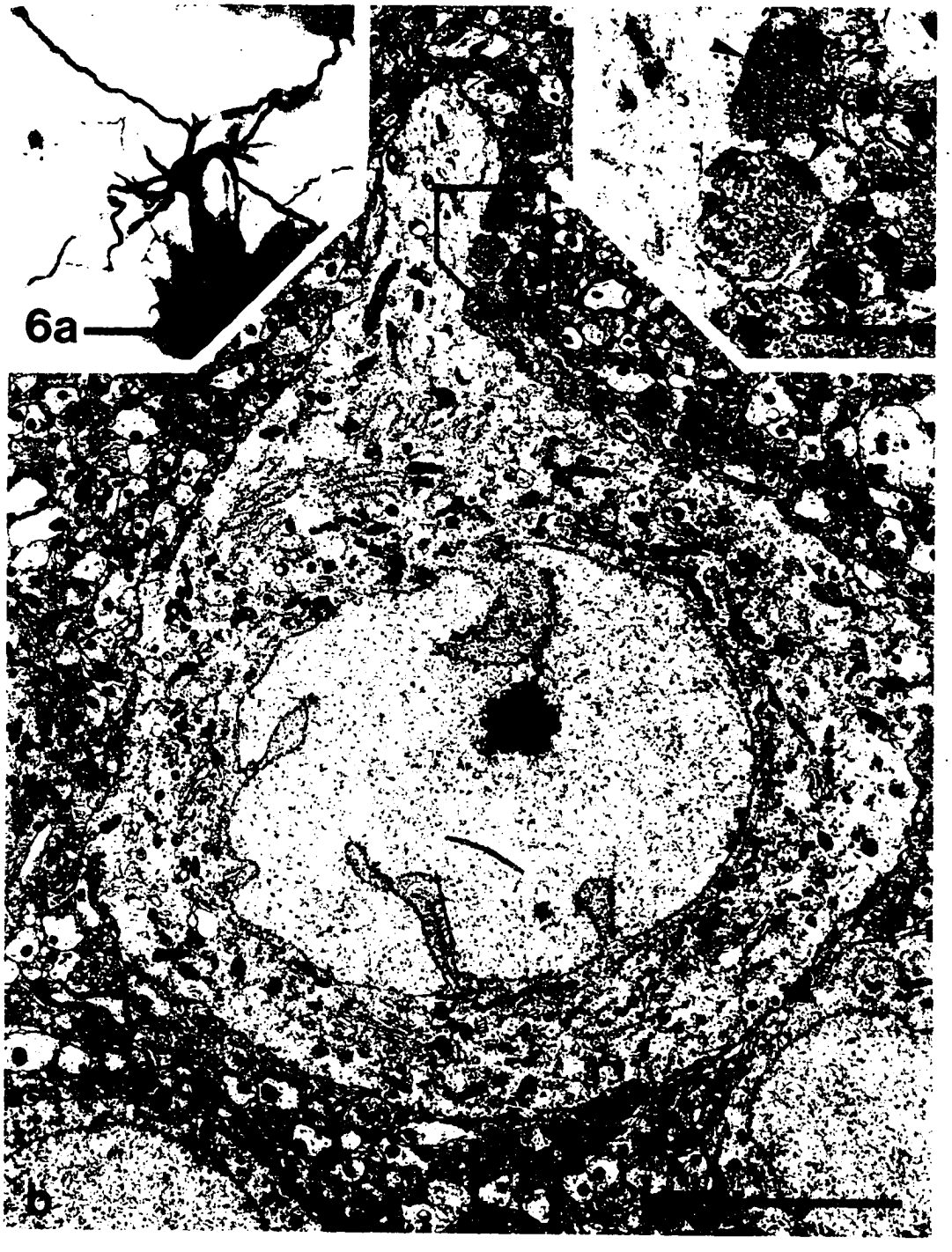

Figure 3.7: Ultrastructural details of Type II large neuron. **a:** Somatic spine of the Type II large neuron's perikaryon (P) shown in Figure 3.4 receiving symmetric synaptic input from axon terminals both loosely and densely packed with vesicles. Scale bar 1.0 μm. **b:** Electron micrograph of the perikaryon (P) showing axon terminals both loosely and densely packed with vesicles making asymmetric contacts (arrowheads) with a somatic spine. Scale bar 0.5 μm. **c:** Proximal dendrite exhibiting dendritic spine receiving symmetric input (arrowhead) from axon terminals loosely packed with round vesicles. Scale bar 1.0 μm. **d:** Distal dendrite receiving symmetric synaptic input (arrowhead) from an axon terminal loosely packed with vesicles. Scale bar 1.0 μm.

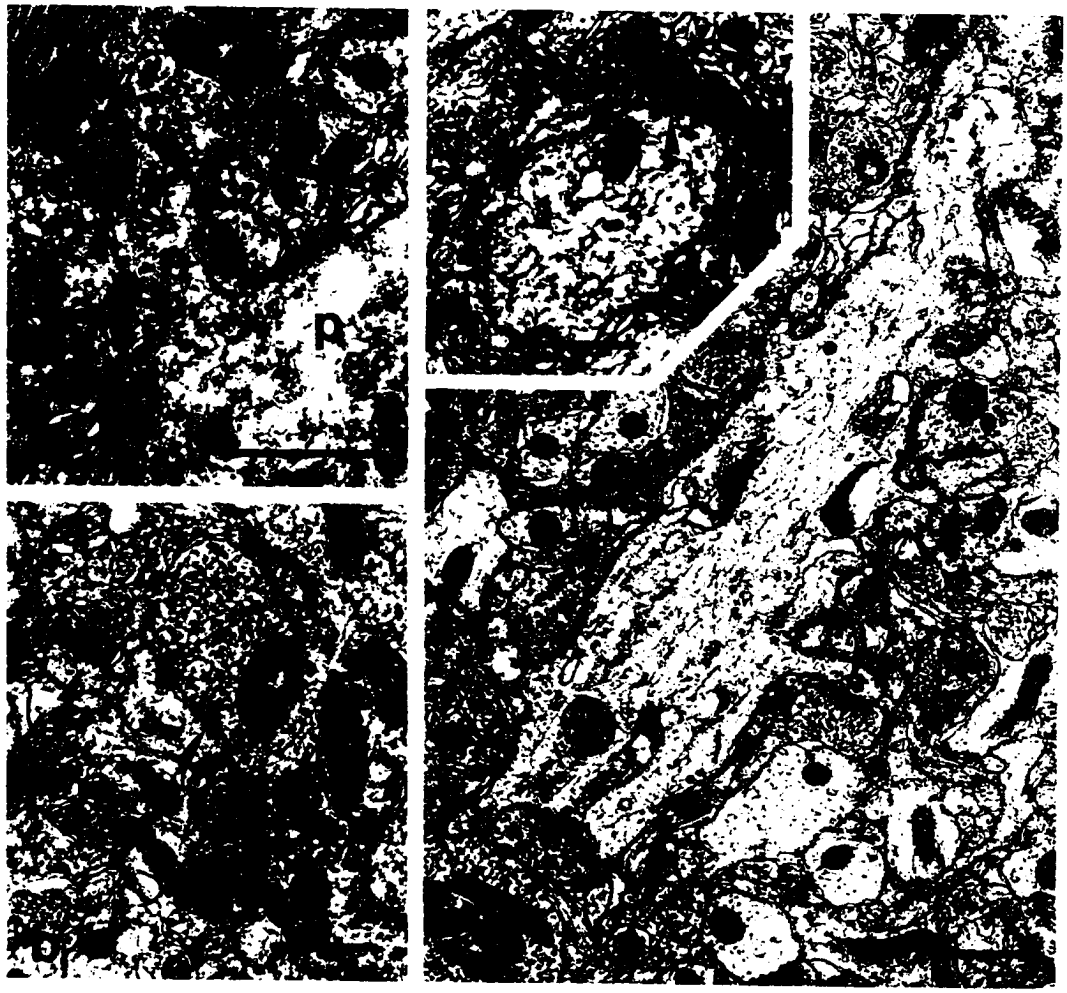

Figure 3.8: Golgi-impregnated Type I medium neuron in fetal striatal transplant. **a:** Light micrograph of Golgi-impregnated Type I medium neuron prior to gold-toning. Scale bar 50 μm. **b:** Electron micrograph of the cell in **a** after gold-toning. Scale bar 2.5 μm. **c:** Perikaron receiving symmetric synaptic input (arrowhead) from an axon terminal loosely packed with vesicles. Scale bar 1.0 μm.

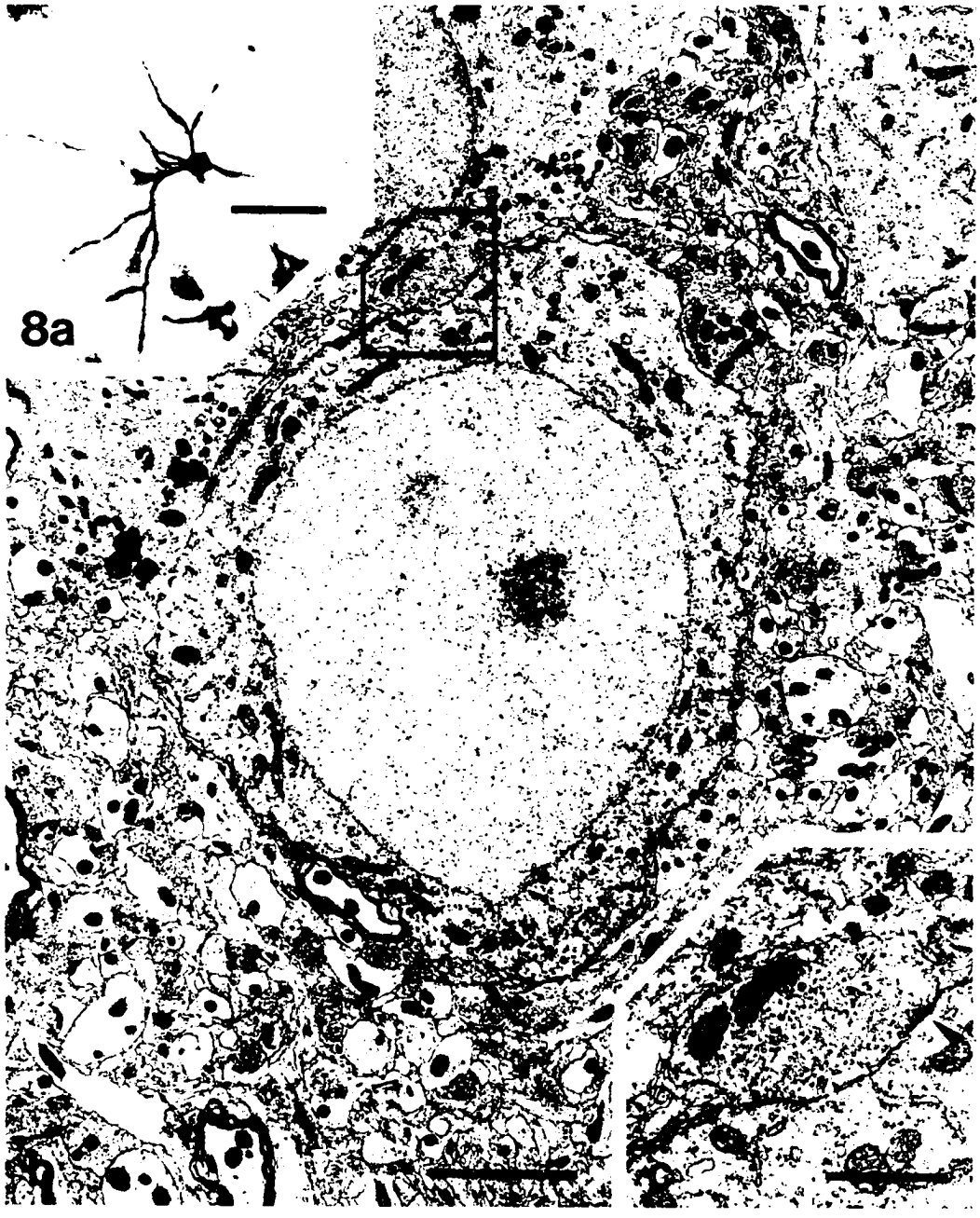

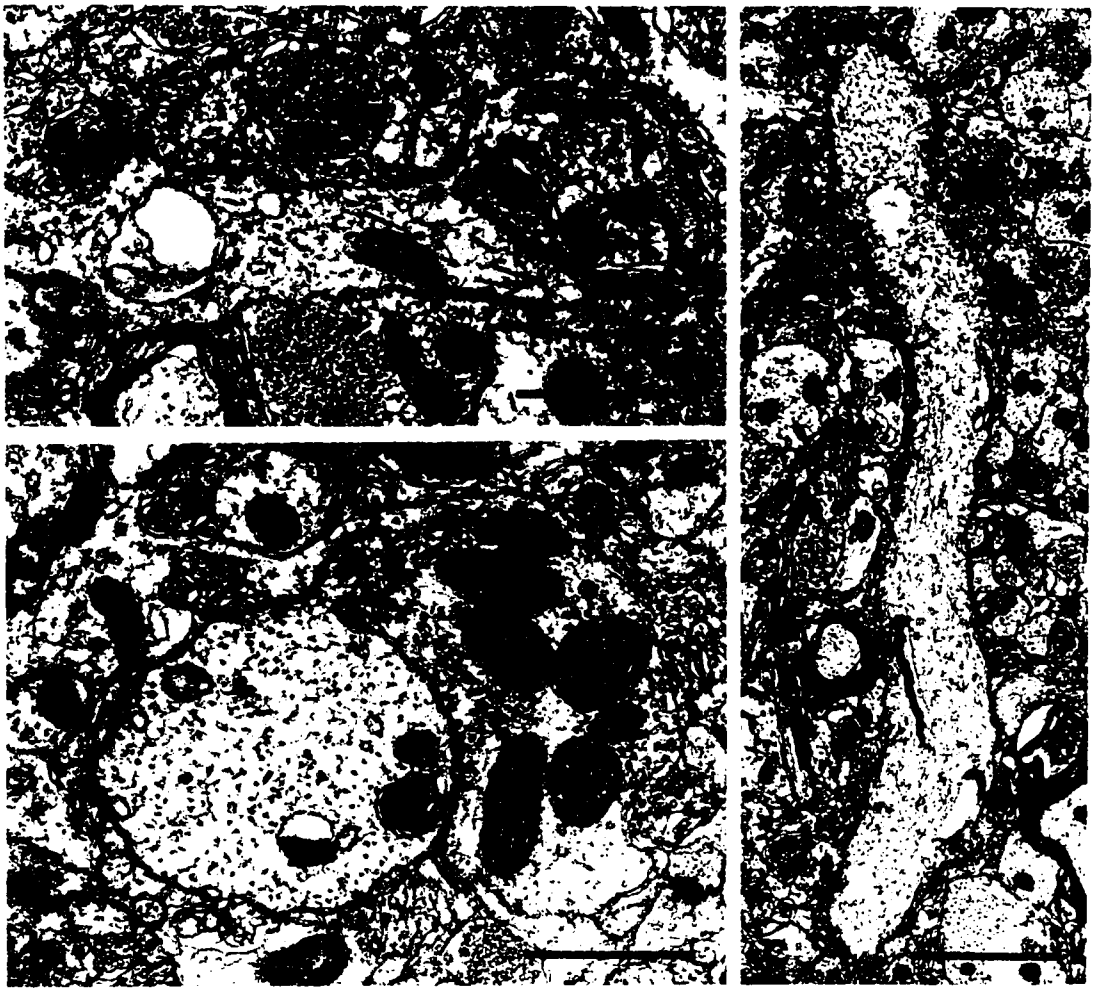

Figure 3.9: Ultrastructural detail of Type I medium neuron. **a:** Dendritic spine of the Type I medium neuron shown in Figure 6 receiving an asymmetrical synapse from a bouton loosely packed with vesicles. Scale bar 1.0 μm. **b:** Distal dendrite and dendritic spine of the cell receiving synaptic input from an axon terminal loosely packed with vesicles. Scale bar 2.0 μm. **c:** Proximal dendrite of the neuron exhibiting no spines. Scale bar 2.0 μm.

Figure 3.10: Golgi-impregnated Type II medium neuron in fetal striatal transplant. a: Light micrograph of Golgi-impregnated Type II medium neuron prior to gold-toning. Scale bar 40 μm. b: Electron micrograph of the cell after gold-toning. Scale bar 2.5 μm. c: High-magnification micrograph of the perikaryon receiving symmetric synaptic input (arrowhead) from an axon terminal loosely packed with vesicles (lower boxed area in b). Scale bar 0.5 μm. d: High-magnification micrograph of the perikaryon receiving symmetric synaptic input (arrowhead) from an axon terminal densely packed with vesicles (upper boxed area in b). Scale bar 0.5 μm.

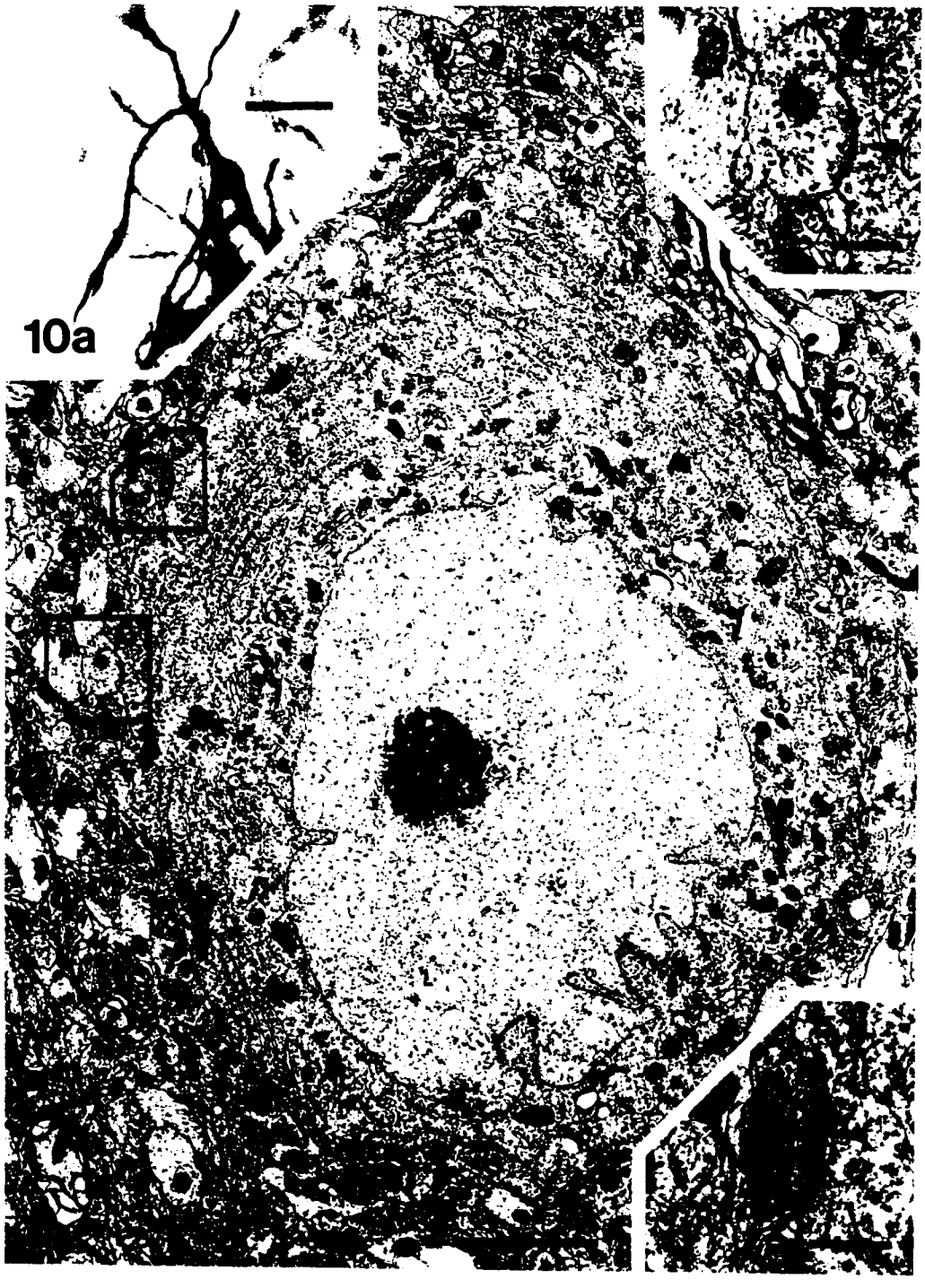

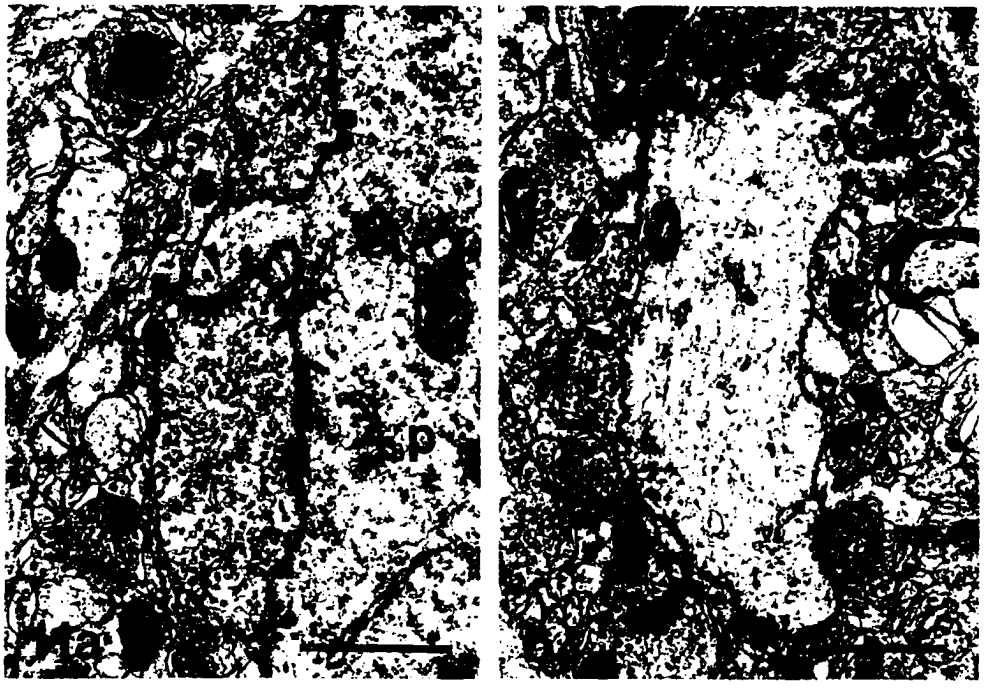

Figure 3.11: Ultrastructural detail of Type II medium neuron. **a:** Somatic spine of the Type II medium neuron in Figure 8 receiving symmetric synaptic input (arrowhead) from an axon terminal loosely packed with vesicles. The same bouton also makes a contact with the perikaryon (P). Scale bar 1.0 μm. **b:** A spine on a dendrite of the cell receiving symmetric synaptic input (arrowhead). Scale bar 1.0 μm.

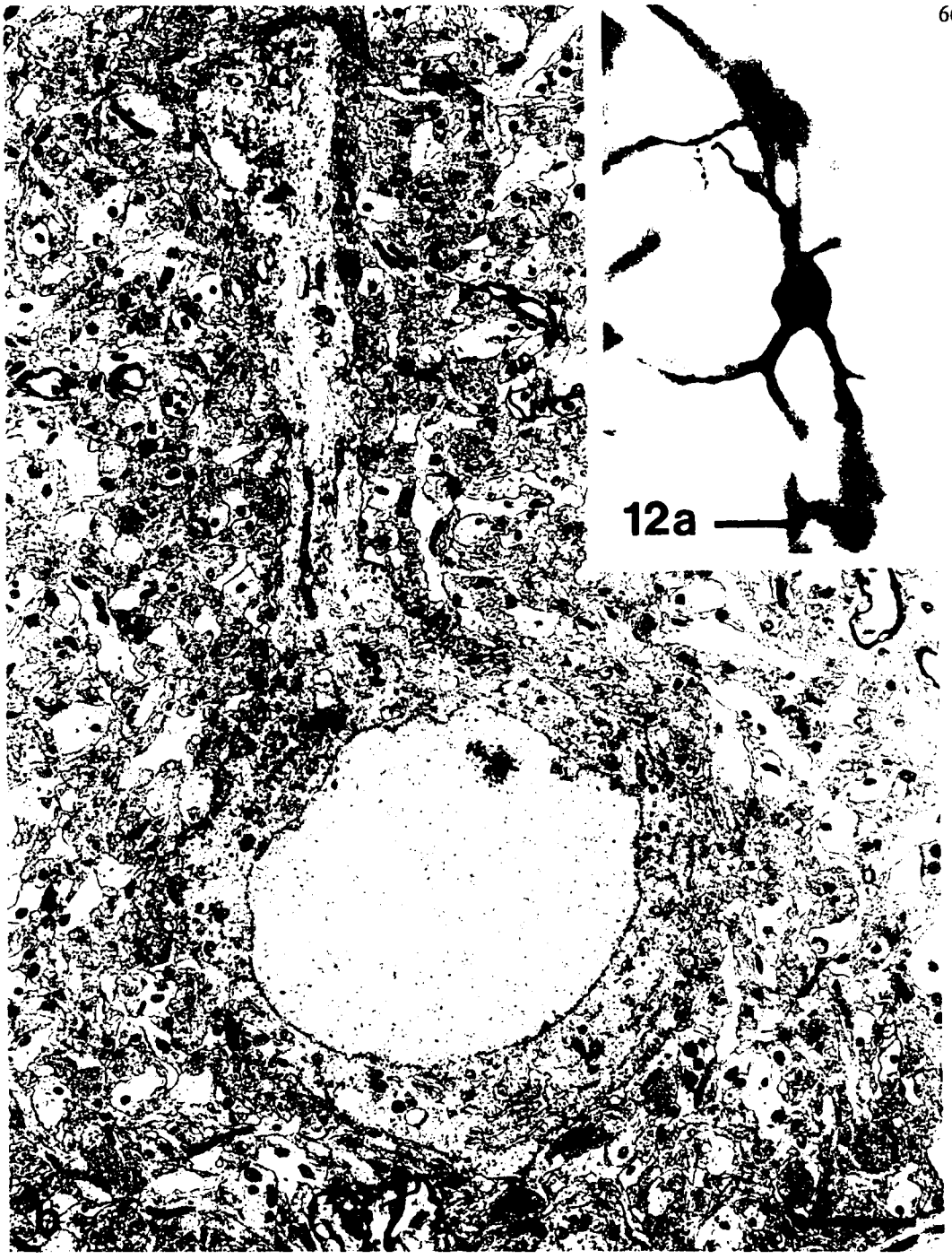

Figure 3.12: Golgi-impregnated Type III medium neuron in fetal striatal transplant. **a:** Light micrograph of Golgi-impregnated Type III medium neuron prior to gold toning. Scale bar 20 μm. **b:** Electron micrograph of the cell after gold-toning. Scale bar 2.5 μm.

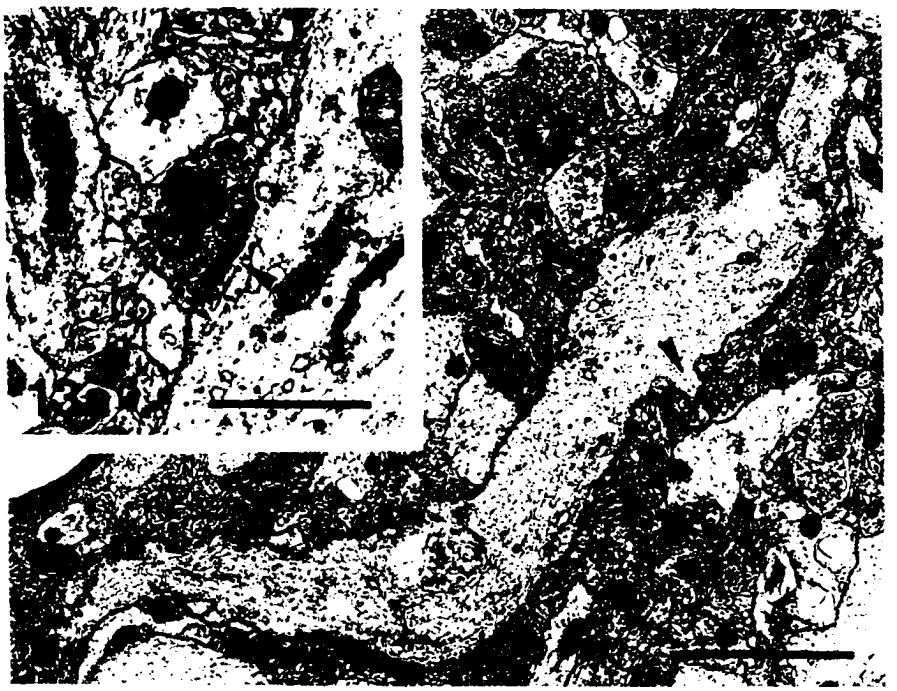

Figure 3.13: Ultrastructural detail of Type III medium neuron. **a:** The perikaryon of the Type III medium neuron shown in Figure 10 receiving symmetric synaptic input (arrowhead) from an axon terminal densely packed with vesicles. Scale bar 1.0 μm. **b:** A dendrite of the neuron followed by serial section exhibiting a small spine (arrowhead). Scale bar 2.0 μm.

Figure 3.14: Golgi-impregnated Type IV medium neuron in fetal striatal transplant. **a:** Light micrograph of Golgi-impregnated Type IV medium neuron prior to gold-toning. Scale bar 20 μm. **b:** Electron micrograph of the neuron after gold-toning. Scale bar 2.5 μm.

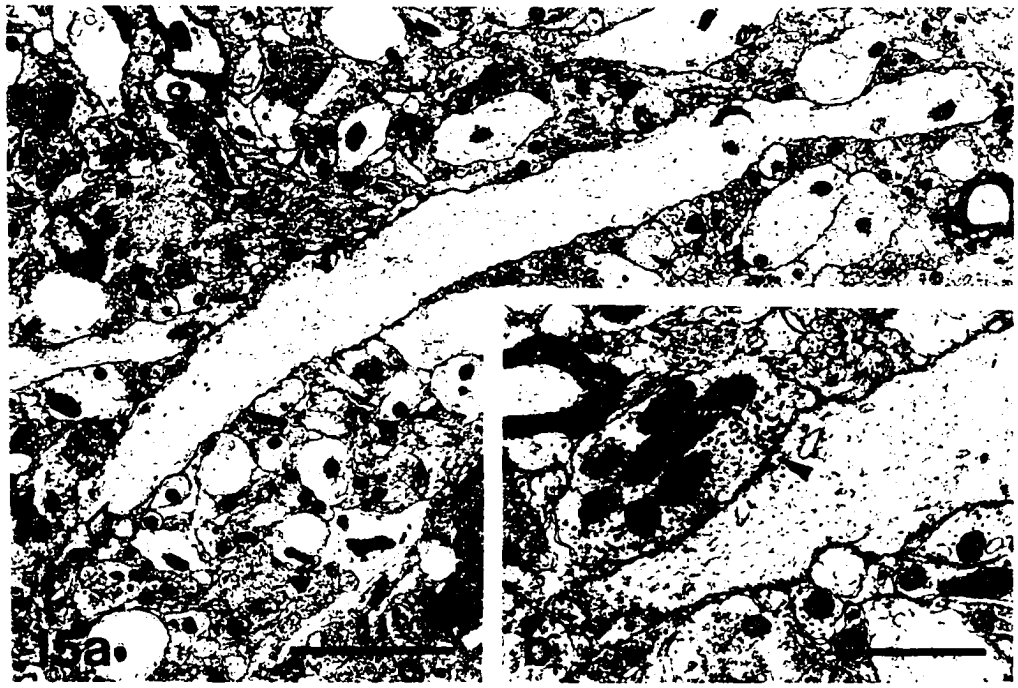

Figure 3.15: Ultrastructural detail of Type IV medium neuron. **a:** Dendrite of the Type IV medium neuron shown in Figure 14 receiving symmetric synaptic input (arrow) from an axon terminal loosely packed with vesicles. Scale bar 3.0 μm. **b:** High magnification micrograph of the symmetric synapse (arrowhead) shown in **a.** Scale bar 1.0 μm.

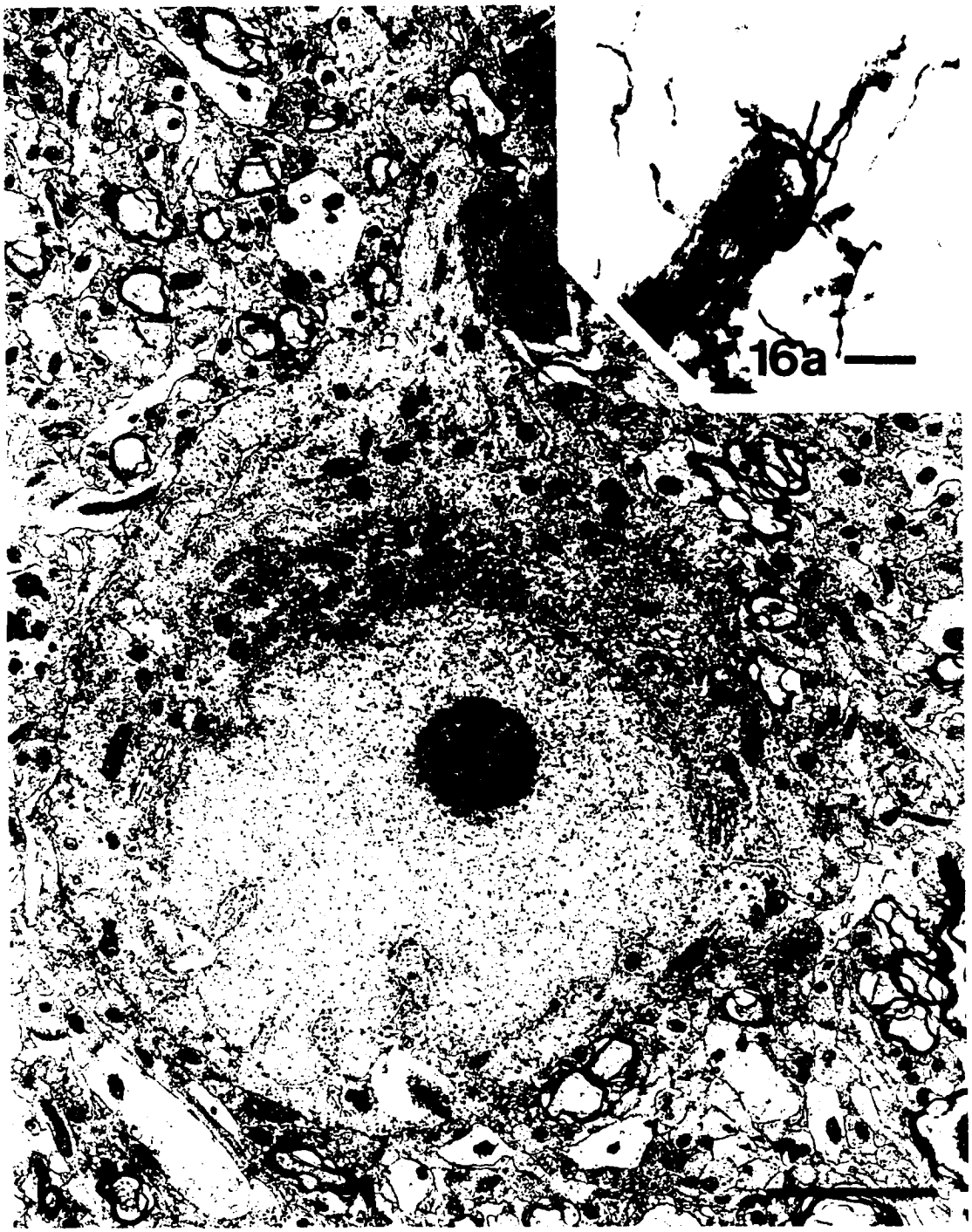

Figure 3.16: Golgi-impregnated Type V medium neuron in fetal striatal transplant. **a:** Light micrograph of Golgi-impregnated Type V medium neuron prior to gold-toning. Scale bar 25 μm. **b:** Electron micrograph of the neuron after gold-toning. Scale bar 3.0 μm.

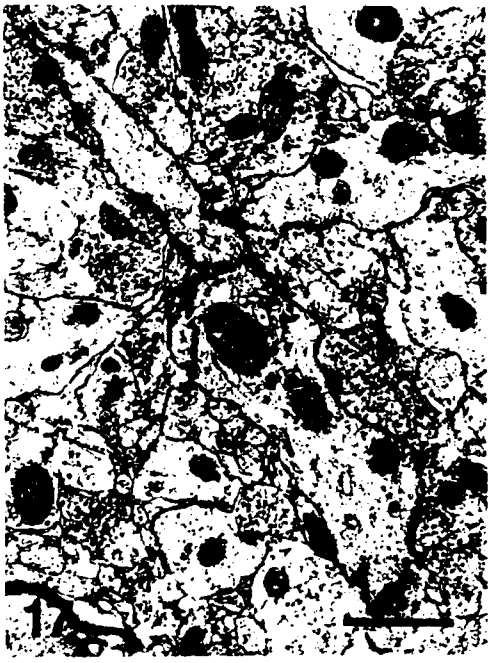

Figure 3.17: Varicose dendrite of the Type V medium neuron shown in Figure 14, receiving symmetrical synaptic input (arrowhead) from a bouton loosely packed with vesicles. Scale bar 1.0 μm.

REFERENCES

1. Björklund, A., Stenevi, U. and Svendgaard, N.A. (1976) Growth of transplanted monoaminergic neurones into the adult rat hippocampus along the perforant path. Nature 262: 787-790.
2. Björklund, A. and Stenevi, U. (1985) Neuronal Grafting in the Mammalian CNS. Amsterdam: Elsevier.
3. Bolam, J.P. (1984) Synapses of identified neurons in the neostriatuM. Ciba Found. Symp. 107: 30-47.
4. Bolam, J.P., Ingham, C.A. and Smith, A.D. (1984) The section-Golgi-impregnation procedure - 3. Combination of Golgi-impregnation with enzyme histochemistry and electron microscopy to characterize acetylcholinesterase-containing neurons in the rat neostriatum. Neuroscience 12:687-709.
5. Bolam, J.P., Powell, J.F., Wu, J.Y. and Smith, A.D. (1985) Glutamate decarboxylase-immunoreactive structures in the rat neostriatum: A correlated light and electron microscopic study including a combination of Golgi impregnation with immunocytochemistry. J. Comp. Neurol. 237: 1-20.

6. Chang, H.T., Wilson, C.J. and Kitai, S.T. (1982) A Golgi study of rat neostriatal neurons: Light microscopic analysis. J. Comp. Neurol. 208: 107-126.

7. Chang, H.T. and Kitai, S.T. (1982) Large neostriatal neurons in the rat: An electron microscopic study of gold-toned Golgi-stained cells. Brain Res. 8: 631-643.

8. Chung, J.W., Hassler, R. and Wagner, A. (1977) Degeneration of two of the nine types of synapses in the putamen after centre median coagulation in the cat. Exp. Brain Res. 28: 345-361.

9. Clarke, D.J., S.B. Dunnett, O. Isacson, D.J.S. Sirinathsinghji and A. Björklund (1988) Striatal grafts in rats with unilateral neostriatal lesions - I. Ultrastructural evidence of afferent synaptic inputs from the host nigrostriatal pathway. Neuroscience 24: 791-801.

10. Coyle, J.T. and Schwarcz, R. (1976) Lesion of striatal neurones with kianic acid provides a model of Huntington's chorea. Nature 263: 244-246.

11. Danner, H. and Pfister, C. (1979a) Untersuchungen zur Struktur des Neostriatum der Ratte. J. Hirnforsch. 20: 285-301.

12. Danner, H. and Pfister, C. (1979b) Zur Struktur des Neostriatum der Ratte. Gegenbaurs Morphol. Jahrb. 125(3): S. 349-364.

13. Deckel, A.W., Moran, T.H. and Robinson, R.G. (1986a) Behavioral recovery following kainic acid lesions and fetal implants of the striatum occurs independently of dopaminergic mechanisms. Brain Res. 363: 383-385.

14. Deckel, A.W., Moran, T.H., Coyle, J.T., Sanberg, P.R. and Robinson, R.G. (1986b) Anatomical predictors of behavioral recovery following fetal striatal transplants. Brain Res. 365: 249-258.

15. Deckel, A.W., Robinson, R.G., Coyle, J.T. and Sandberg, P.R. (1983) Reversal of long-term locomotor abnormalities in the kainic acid model of Huntington's disease by day 18 fetal striatal implants. Eur. J. Pharmacol. 93: 287-288.

16. DiFiglia, M., Pasik, P. and Pasik, T. (1976) A Golgi study of neuronal types in the neostriatum of monkeys. Brain Res. 114: 245-256.

17. DiFiglia, M., Schiff, L. and Deckel, A.W. (1988) Neuronal organization of fetal striatal grafts in kainate- and sham-lesioned rat caudate nucleus: Light and electron-microscopic observations. J. Neurosci. 8: 1112-1130.

18. DiMova, R., Vuillet, J. and Seite, R. (1980) Study of rat neostriatum using a combined Golgi-electron microscopic technique and serial sections. Neuroscience 5: 1581-1596.

19. Dunnett, S.B., Isacson, O., Sirinathsinghji, D.J.S., Clarke, D.J. and Björklund, A. (1988) Striatal grafts in rats with unistriatal lesions - III. Recovery from dopamine-dependent motor asymmetry and deficits in skilled paw reaching. Neuroscience 24: 813-820.

20. Fairen, A., Peters, A. and Saldanha, J. (1979) A new procedure for examining Golgi impregnated neurons by light and electron microscopy. J. Neurocytol. 6: 311-337.

21. Fox, C.A., Andrade, A.N., Hillman, D.E. and Schwyn, R.C. (1971/1972a) The spiney neurons of the primate neostriatum: A Golgi and electron microscopic study. J. Hirnforsch. 13: 181-201.

22. Fox, C.A., Andrade, A.N., Schwyn, R.C. and Rafols, J.A. (1971/1972b) The aspiney neurons and the glia in the primate striatum: A Golgi and electron microscopic study. J. Hirnforsch. 13: 341-362.

23. Freund, T.F., Bolam, J.P., Björklund, A., Stenevi, U., Dunnett, S.B., Powell J.F. and Smith, A.D. (1985) Efferent synaptic connections of grafted dopaminergic neurons reinnervating the host neostriatum: A tyrosine hydrooxylase study. J. Neurosci. 5: 603-616.

24. Gabbott, P.L. and Somogyi J. (1984) The "single" section Golgi-impregnation procedure: Methodological description. J. Neurosci. Methods 11: 221-230.

25. Hassler, R., Chung, J.W., Rinne, U. and Wagner, A. (1978) Selective degeneration of two out of nine types of synapses in the cat caudate nucleus after cortical lesions. Exp. Brain Res. 31: 67-80.

26. Hattori, T., Fibiger, H.C., McGeer, P.L. and Maler, L. (1973) Analysis of the fine structure of the dopaminergic nigrostriatal projection by electron microscopic autoradiography. Exp. Neurol. 41: 599-611.

27. Isacson, O., Brundin, P., Gage F.H. and Bjorklund A. (1985) Neuronal grafting in a rat model of Huntington's disease: Progressive neurochemical changes after ibotenate lesions and striatal tissue grafting. Neuroscience 16: 799-817.

28. Isacson, O., Dawbarn, D., Brundin, P., Gage, F.H., Emson, P.C. and Björklund, A. (1987) Neuronal grafting in a rat model of Huntington's disease: Striosomal-like organization of striatal grafts as revealed by acetylcholinesterase histochemistry, immunocytochemistry and receptor autoradiography. Neuroscience 22: 481-497.

29. Isacson, O., Brundin, P., Kelly, P.A.T., Gage, F.H. and Björklund, A. (1984) Functional neuronal replacement by grafted striatal neurones in ibotenic lesioned rat striatum. Nature 311: 458-460.

30. Isacson, O., Dunnett, S.B. and Björklund, A. (1986) Behavioral recovery in an animal model of Huntington's disease. Proc. Natl. Acad. Sci. USA 83: 2728-2732.

31. Izzo, P.N., Graybiel, A.M. and Bolam, J.P. (1987) Characterization of substance P- and [met]enkephalin-immunoreactive neurons in the caudate nucleus of the cat and ferret by a single section Golgi procedure. Neuroscience 20: 577-587.

32. Kemp, J.M. and Powell, J.P.S. (1971) The structure of the caudate nucleus of the cat. Light and electron microscopy. Phil. Trans. Roy. Soc. Lond. Ser. B. 262: 383-401.

33. Köhler, C. and Schwarcz, R. (1983) Comparison of ibotenic and kainate neurotoxicity in the rat brain: A histologic study. Neuroscience 8: 819-835.

34. Lu, E.J. and Brown, W.J. (1977) The developing caudate nucleus in the euthyroid and hypothyroid rat. J. Comp. Neurol. 171: 261-284.

35. McAllister, J.P., Walker, P.D., Zemanick, M.C., Weber, A.B., Kaplan, L.I. and Reynolds, M.A. (1985) Morphology of embryonic neostriatal cell suspensions transplanted into adult neostriata. Dev. Brain Res. 23: 282-286.

36. McGeer, E.G. and McGeer, P.L. (1976) Duplication of biochemical changes of Huntington's chorea by intrastriatal injection of glutamic and kainic acids. Nature 263: 517-519.

37. Mensah, P. and Deadwyler S. (1974) The caudate nucleus of the rat cell types and demonstration of a commissural system. J. Anat. 117: 281-293.

38. Pasik, P., Pasik, T. and DiFiglia, M. (1979) The internal organization of the neostriatum in mammals. In: I. Divac and R.G.E. Oberg (eds): The Neostriatum. New York: Pergamon Press, pp. 5-36.

39. Paxinos, G. and Watson, C. (1982) The Rat Brain in Stereotaxic Coordinates. Sydney: Academic Press.

40. Pritzel, M., Isacson, O., Brundin, P., Wiklund, L. and Björklund, A. (1986) Afferent and efferent connections of striatal grafts implanted into the ibotenic acid lesioned neostriatum in adult rats. Exp. Brain Res. 65: 112-126.

41. Redmond, D.E., Sladek, J.R., Roth, R.H., Collier, T.J., Elsworth, J.D., Deutch, A.Y. and Haber, S. (1986) Fetal neuronal grafts in monkeys given methylphenyltetrahydropyridine. Lancet 1: 1125-1127.

42. Roberts, R.C. and DiFiglia, M. (1988) Localization of immunoreactive GABA and enkephalin and NADPH-diapharase-positive neurons in fetal striatal grafts in the quinolinic-acid-lesioned rat neostriatuM. J. Comp. Neurol. 274: 406-421.

43. Seite, R., Vuillet-Luciani, J., Vio, M. and Cataldo, C. (1977) Sur la presence d'inclusions nucleaires dans certains neurones du noyau caude

du rat: repartition, frequence et organisation ultrastructurale. Biol. Cell. 30: 73-76.

44. Sirinathsinghji, D.J.S., Dunnett, S.B., Isacson, O., Clarke, D.J., Kendrick, K. and Björklund, A. (1988) Striatal grafts in rats with unilateral neostriatal lesions - II. In vivo monitoring of GABA release in globus pallidus and substantia nigra. Neuroscience 24: 803-811.

45. Somogyi, P. and Smith, A.D. (1979) Projection of neostriatal spiney neuron to the substantia nigra. Application of a combined Golgi-staining and horseradish peroxidase transport procedure at both the light and electron microscopic levels. Brain Res. 178: 3-15.

46. Somogyi, P., Bolam, J.P. and Smith, A.D. (1981) Monosynaptic cortical input and local axon collaterals of identified striatonigral neurons. A light and electron microscopic study using the Golgi-peroxidase transport-degeneration procedure. J. Comp. Neurol. 195: 567-584.

47. Somogyi, P. and H. Takagi (1982) A note on the use of picric acid-paraformaldehyde-glutaraldehyde fixative for correlated light and electron microscopic immunocytochemistry. Neuroscience 7: 1779-1783.

48. Gash, D.M. and Sladek, J.R. (1988) Transplantation into the Mammalian CNS D.M. Gash and J.R. Sladek, Progress in Brain Research, Vol. 78. Elsevier, Amsterdam.

49. Tanaka, D. (1980) Development of spiny and aspiny neurons in the caudate nucleus of the dog during the first postnatal month. J. Comp. Neurol. 192: 247-263.

50. Walker, P.D., Chovanes, G.I. and McAllister, J.P. (1987) Identification of acetylcholinesterase-reactive neurons and neuropil in neostriatal transplants. J. Comp. Neurol. 259: 1-12.

51. Walker, P.D. and McAllister, J.P. (1987) Minimal connectivity between neostriatal transplants and the host brain. Brain Res. 425: 34-44.

52. Wictorin, K. and Bjorklund, A. (1989) Connectivity of striatal grafts into the ibotenic acid-lesioned striatum - II. Cortical afferents. Neuroscience 30: 297-311.

53. Wictorin, K., Isacson, O., Fischer, W., Nothias, F., Peschansk, M. and Björklund, A. (1988) Connectivity of striatal grafts into the ibotenic acid-lesioned striatum - I. Subcortical afferents. Neuroscience 27: 547-562.

54. Wictorin, K., Simerly, R.B., Isacson, O., Swanson, L.W. and Björklund, A. (1989) Connectivity of striatal grafts into the ibotenic acid-lesioned striatum - III. Efferent projecting graft neurons and their relation to host afferents within the grafts. Neuroscience 30: 313-330.

Chapter 4

CHOLINE ACETYLTRANSFERASE- AND SUBSTANCE P-LIKE IMMUNOREACTIVE ELEMENTS IN FETAL STRIATAL GRAFTS IN THE RAT: A CORRELATED LIGHT AND ELECTRON MICROSCOPIC STUDY*

*(Published, Neuroscience 47 (1992) 621-639)

INTRODUCTION

The scientific basis for treatment of neuro-degenerative diseases through the use of fetal neuronal transplantation continues to develop. Transplanting fetal striatal tissue into the ibotenic acid-lesioned adult rat striatum, an animal model of Huntington's disease,[13,49] has proved to be invaluable in studying the neuroanatomical development of neuronal grafts.[12,22,48,59,77-79] The striatal lesions produce behavioral changes that can be partially reversed with fetal striatal implants.[17-21,24,32-35,64] A recent series of papers has shown that fetal striatal grafts are capable of establishing significant and appropriate afferent connections with the host cerebral cortex,[59,77,82,83] substantia nigra,[59,78,83] and thalamus,[59,78] and efferent connections with the host globus pallidus[59,79] and substantia nigra.[59,79] In addition, Helm et al.[28] have shown in an electron microscopic-Golgi study that the grafted neurons differentiate into all of the normal striatal cell types.[10,11] In situ hybridization histochemical studies of striatal grafts using oligodeoxyribonucleotide probes specific for several mRNAs, suggest that gene expression for neurotransmitters in striatal grafts is present, but different from that seen in the normal striatum.[51,65] In addition, several studies have demonstrated that striatal grafts contain many of the biochemically distinct cell types found in the normal striatum, including those expressing leave, substance P, cholecystokinin, neuropeptide Y, NADPH-diaphorase, calbindin-d28k, acetylcholinesterase, and choline acetyltransferase reactivity.[25,26,34,44,45,61-63,75] Additionally, Roberts and Di Figlia[61,62] examined GABA-, enkephalin-, NADPH-diaphorase-, and calbindin-d28k-positive striatal graft neurons at the electron microscopic level. Each

of these labeled cell types showed striking similarities to their counterparts in the normal striatum, although significant differences were also observed. Finally, Wichmann et al.[76] demonstrated that striatal grafts can partially restore acetylcholine release in the lesioned striatum.

The present project was undertaken in order to study choline acetytransferase-immunoreactive (ChAT-IR) and substance P-like immunoreactive (SP-IR) neurons at the electron microscopic level, and to compare their ultrastructural characteristics with immunoreactive elements typically seen in the normal striatum.

MATERIALS AND METHODS

A total of fifteen adult female Sprague-Dawley rats weighing 250-300 gms and seven pregnant female rats, 14-16 days of gestation, were used in this study.

Striatal Lesioning and Transplantation. The transplantation of fetal brain tissue into lesioned adult rat brain has been previously described[3] and was only slightly modified in this study. The animals were anesthetized with intraperitoneally injected chloropent (3.0 ml/kg) and received unilateral striatal injections of 0.25 ml of ibotenic acid (Sigma, 20 mg/ml), in 0.1 molar phosphate buffer (pH = 7.0) with a 2.0 ml Hamilton microsyringe at the following stereotaxic coordinates from bregma: A = 0.7 mm, L = 3.0 mm, and V = 4.5 mm.[55] Striatal implantation was performed two weeks after the lesioning. Female rats 14-16 days postgestation were anesthetized with intraperitoneally injected chloropent (3.0 ml/kg) and the fetuses were removed by caesarean section. The fetuses were kept in cold Hanks' solution without calcium or magnesium (modified Hanks' solution,

Sigma) containing 10 g/L of glucose and 10 units/ml of insulin. Striatal tissue was dissected from the dorsal ventricular ridge, resuspended in modified Hanks' solution by repeated suctioning through a fire-polished glass micropipette, and injected (2.5-3.5 µl) at the same stereotactic coordinates into the lesioned striatum. Three months following transplantation, the rats were anesthetized and perfused transcardially with 20 ml of 0.1 molar phosphate buffer (pH 7.4) followed by 500 ml of a fixative containing 4% paraformaldehyde, 0.1% glutaraldehyde, and 15% saturated picric acid, in 0.1 molar phosphate buffer (pH 7.4).[69] This was followed by 800 ml of a second fixative containing 4% paraformaldehyde, and 0.1% glutaraldehyde in 0.1 molar phosphate buffer. The brains were removed, placed in the second fixative for 12-16 hours at 4°C, sectioned coronally at 50 mm in 0.1 molar phosphate buffer on a Lancer vibratome, and rinsed for 2 hours in several changes of 0.1 molar phosphate buffer. In order to improve antibody penetration, the vibratome sections were sunk in 15% sucrose in 0.1 molar phosphate buffer (pH 7.4) and frozen in liquid nitrogen. Alternating sections were Nissl stained or processed for substance P- or choline acetyltransferase-immunohistochemistry.

Choline Acetyltransferase Immunohistochemistry and Substance P.

The sections were incubated in a primary antibody directed against choline acetyltransferase (Boehringer) diluted 1:1000 with 0.1 molar Tris buffered saline (pH 7.4)or substance P (Pel-Freez) diluted 1:500 with 0.1 molar Tris buffered saline (pH 7.4) containing 0.25% carrageenan (Sigma) and 0.05% sodium azide at 4°C constant agitation for 24-48 hours. The sections were

rinsed for 30 min in three changes of 0.1 molar Tris buffered saline followed by an incubation in a biotinylated secondary antibody (Vector) diluted with 0.1 molar Tris buffered saline containing 0.25% carrageenan for 2 hours at 4°C with constant agitation. After another rinsing, the sections were placed in ABC elite (Vector) for 30 min with constant agitation. The sections were then washed for 30 min in three changes of 0.1 molar phosphate buffer and placed in a diaminobenzidine/nickel solution for 35-45 min at room temperature with constant agitation. The DAB solution contained 50 mg diaminobenzidine, 200 mg B-D-glucose, 30 mg ammonium chloride, 0.4 glucose oxidase (Sigma) and 0.05 mg nickel sulfate per 100 ml of 0.1 molar phosphate buffer (pH 7.4).[36] Immunohistochemically-stained tissue from the striatal grafts was then examined and photographed at the light microscopic level. The relative frequency of immunoreactive neurons within the grafts was determined by comparing the number of immunoreactive neurons in the graft in a given section with the total cell count in an adjacent Nissl-stained section.

Processing for Electron Microscopy. The sections were then placed in 1.0% osmium tetroxide for 30 min, in two changes of 3.6% sodium chloride, and dehydrated in increasing concentrations of Quetol 523 M (Ted Pella, Inc.) and distilled water: 35%, 50%, and 70% for 10 min each; 80% and 90% for 15 min each; followed by 100% Quetol for 20 min. The sections were then floated in a 50% Quetol, 50% Maraglas solution (Ted Pella, Inc.) for 12 hours followed by pure Maraglas for 6 hours. The sections were flat-embedded on siliconized microscope slides and cured for

two days at 60°C. Tissue with identified immunoreactive cells was cut from the sections and fixed to epon blocks. Following serial ultrathin sectioning on a Reichert ultramicrotome, the sections were placed on formvar-coated grids, double-stained with uranyl acetate and lead citrate, and examined with a JEOL electron microscope.

RESULTS

Choline Acetyltransferase - Light Microscopy. Figure 1 shows a typical three-month old fetal striatal graft. At the light microscopic level ChAT-IR neurons were usually greater than 20 μm. in diameter (Fig. 4.2a,b,c), although there were several neurons with somatic diameters between 10 and 20 μm. (Fig. 4.2d). The somata of the large neurons were either oval, fusiform, or polygonal in shape and the perikarya, proximal dendrites and distal dendrites were usually all immunoreactive. The somata of the medium-sized neurons were round or oval. Overall, less than 0.1% of the neurons in the grafts were immunoreactive for ChAT and these neurons were evenly distributed throughout the graft. The large ChAT-IR neurons displayed between two and five primary dendrites which were moderately branched (Fig. 4.2). Although the neuropil surrounding the immunoreactive neurons did contain a moderate number of choline acetyltransferase-positive axons, there were few punctate structures, suggesting that there were few ChAT-IR boutons in the transplant.

Choline Acetyltransferase - Electron Microscopy. At the electron microscopic level, the ChAT-IR neurons could be classified into two groups based on somatic diameter. A total of eight large ChAT-IR neurons were examined at the electron microscopic level, each of which contained an indented nucleus surrounded by copious cytoplasm rich in mitochondria and endoplasmic reticulum (Figs. 4.3,4.4). The ChAT-immunoreaction product was quite dense in both the cytoplasm and nucleus in ChAT-IR neurons close to the surface of the section (Fig. 4.4), but became very light in cells deep in the section (Fig. 4.3). Three medium-sized ChAT-IR neurons were also examined at the electron microscopic level. Each contained a highly indented nucleus surrounded by a thin rim of cytoplasm (Fig. 4.5). The large cholinergic neurons in the grafts received occasional axosomatic contacts, while the medium-sized ChAT-IR neurons received dense axosomatic input (Fig. 4.6a).

In the neuropil surrounding the ChAT-IR neurons, numerous ChAT-IR dendrites could be easily identified. These dendrites were moderately to heavily stained with ChAT-immunoreaction product and contained numerous mitochondria. The proximal, middle, and distal dendrites all received axodendritic contacts from non-immunoreactive axon terminals (Fig. 4.6b,c,d). Because of the dense immunoreactivity of the dendrites, it could not be determined with certainty whether these axodendritic synaptic specializations were symmetric or asymmetric. In all of the material examined, no ChAT-IR dendrites were contacted by ChAT-IR boutons.

As predicted by the light microscopic observations, the number of ChAT-IR boutons in the transplants was small. These ChAT-IR boutons

were heavily stained with the nickel-enhanced diaminobenzidine reaction product and contained clear vesicles. Of the fifteen clearly reactive boutons found within the tissue, all made symmetric axodendritic contacts (Fig. 4.7a,b,c,d). No ChAT-immunoreactive boutons forming axosomatic or axospinous contacts were demonstrated in the grafts.

Substance P Light Microscopy. At the light microscopic level, substance P-like immunoreactive (SP-IR) neurons were between 10 and 25 μm. in diameter (Figs. 4.8a,b,c,d). Their somata were either round or polygonal in shape and were heavily stained with immunoreaction product. The dendrites of these cells were moderately to heavily stained proximally, but became non-reactive distally. Overall, less than 0.1% of the neurons in the grafts were immunoreactive for substance P, and these neurons were evenly distributed throughout the grafts. Some SP-IR neurons were surrounded by a terminal field of SP-IR axon terminals, while other stained neurons had very few immunoreactive terminals in the surrounding neuropil. In some instances, the terminal fields of a SP-IR neuron were close to the margin of the graft, and it seems probable that some of the immunoreactive axons did extend into the host brain. However, this could not be determined with certainty.

Substance P Electron Microscopy. A total of nine SP-IR neurons were examined at the electron microscopic level. These could be classified into two types based on ultrastructural characteristics. Type I immunoreactive neurons contained an unindented nucleus surrounded by a thin rim or

moderate amount of cytoplasm containing mitochondria and rough endoplasmic reticulum (Figure 4.9). In most instances, the cytoplasm was moderately to densely stained for substance P and few axon terminals contacted the perikarya. Type II SP-IR neurons contained an indented nucleus which was surrounded by copious cytoplasm rich in mitochondria, rough endoplasmic reticulum, and Golgi apparatus (Figure 4.10). Numerous non-immunoreactive axon terminals made axosomatic synapses onto these Type II immunoreactive neurons (Figure 4.11). SP-IR dendrites could be easily seen in the surrounding neuropil. These dendrites contained many mitochondria and received numerous axodendritic contacts (Figure 4.12). Because of the dense immunoreactivity within the dendrites, it could not be determined with certainty whether these axodendritic contacts were symmetrical or asymmetrical. In all of the axodendritic contacts examined, we found only one equivocal case of a SP-IR axon terminal contacting a SP-IR dendrite. Numerous SP-IR axon terminals making symmetric contacts with medium and small dendrites (Fig. 4.13a,b,c) and spines (Fig. 4.14) were observed in the neuropil. The axon terminals varied greatly in size and were consistently heavily stained. In addition, several SP-IR boutons were in close apposition to the somata of unstained graft neurons, but no clear synaptic specializations could be identified.

DISCUSSION

The mechanisms by which fetal striatal grafts in the ibotenic acid lesion rat striatum improve behavioral deficits are not clear at the present time, but may require the presence of normal striatal interneurons and projection neurons within the graft. In the present study, we used choline

acetyltransferase immunohistochemistry to study cholinergic neurons within the striatal grafts, neurons that function as interneurons in the normal striatum.[43,56,70,80] In addition, we used substance P-like immunohistochemistry to study substance P utilizing neurons, which function both as striatal interneurons[6,66,81] and projection neurons[68] in the normal striatum.

It is now recognized that the ChAT-positive neurons in the normal striatum are the "classical" large neurons demonstrated in previous Golgi studies in the rat.[7,10,23] Afferent connections to these cholinergic neurons have been demonstrated from the substantia nigra dopaminergic system[41] and from substance P utilizing striatal neurons.[5] Electron microscopic studies have also shown that the cholinergic neurons receive asymmetric synaptic input, suggesting that they receive input from the cerebral cortex and/or intralaminar nuclei of the thalamus.[5,66] In addition, the striatum exhibits a marked medial to lateral gradient in the density of cholinergic neuropil.[9]

Cholinergic interneurons have been shown to project to several different cell types within the striatum[37,56] and function as excitatory modulators.[2] Cholinergic axon terminals synapse with medium spiny striatal projection neurons,[37,56,72] which have been shown to use substance P, enkephalin, and/or GABA as their neurotransmitter. Therefore, the cholinergic system may have a strong influence on striatal output.

Substance P utilizing neurons within the neostriatum can be classified into two types based on ultrastructural characteristics.[8] One type represents the typical medium spiny neuron, which mainly projects to the globus

pallidus, entopeduncular nucleus, and substantia nigra, but also sends recurrent collaterals to other striatal neurons.[54,66,68,81] The second type represents one of the medium aspiny neurons,[8] which function mainly as striatal interneurons.[11,70] There is now considerable evidence that suggests that substance P has an overall excitatory role in substantia nigra.[27,16,38,50,58,74] Substance P injection unilaterally into the substantia nigra has been shown to cause an increase in the dopamine turnover in the ipsilateral striatum and also causes contralateral turning behavior,[30,38,71,73] while bilateral injections of substance P into the zona reticulata of substantia nigra produces increased grooming behavior.[39] Although the function role of substance P in the striatum has not been fully elucidated,[6] substance P has been shown to increase the electrical activity of striatal neurons.[42]

Choline Acetyltransferase-Light Microscopy

Previous ChAT-immunohistochemical studies of neurons in the rat striatum have demonstrated that cholinergic neurons have large somatic diameters (20-35 μm.) and oval, spindle-shaped, triangular, or polygonal perikarya.[31,40,56] Their long, sparsely branched dendrites characteristically have few dendritic spines. The cholinergic neurons are evenly distributed throughout the neostriatum and comprise approximately 1.7% of its total neuronal population.[56] In the present study, the large ChAT-IR neurons seen in the fetal striatal transplants were, in general, similar in size and shape to those seen in the normal striatum. However, less than 0.1% of the neurons displayed ChAT immunoreactivity in the transplants, which is markedly less than that seen in the normal striatum. In addition, the population of ChAT-IR graft neurons having somatic diameters less than 20 μm. has not been

demonstrated in the normal striatum. The large- and medium-sized ChAT-IR neurons were demonstrated in fetal striatal grafts previously by Liu et al.[45] These investigators suggested that these medium-sized neurons may represent small ChAT-immunoreactive interneurons usually seen in the cortex of the rat,[31] which were inadvertently dissected from the fetal rat brains along with the primordial striatum.

Choline Acetyltransferase - Electron Microscopy

Choline Acetyltransferase-Immunoreactive Neurons. The electron microscopic characteristics of ChAT-immunoreactive neurons in neostriatum has been thoroughly studied by Bolam et al.[4,7] in a combined choline acetyltransferase-immunohistochemical and Golgi study and was later expanded by Phelps et al.[56] in a more detailed choline acetyltransferase-immunohistochemical study. Both groups demonstrated that ChAT-IR neurons have round, fusiform, oval, or multipolar perikarya, which, at the ultrastructural level, are characterized by a deeply invaginated nucleus containing a prominent nucleolus. The abundant cytoplasm within these neurons contain numerous mitochondria, prominent Nissl bodies, and Golgi complexes, and characteristically received few symmetric axosomatic contacts. Each of these ultrastructural features are characteristic of the large cholinergic neurons in the striatal grafts. The large ChAT-immunoreactive neurons in the present study are also ultrastructurally identical to the large Type I striatal neurons demonstrated in previous electron microscopic-Golgi studies of the normal rat striatum [10,80] and of mature striatal grafts.[28]

Choline Acetyltransferase Immunoreactive Dendrites. Phelps et al.[56] demonstrated that the cholinergic neurons in the neostriatum receive most of their synaptic input on their dendrites. While the proximal dendrites of the ChAT-IR neurons receive moderate synaptic input, their secondary and tertiary dendrites receive numerous symmetric and asymmetric contacts from unlabeled boutons. Although the distal dendrites of the ChAT-immunoreactive dendrites in the fetal striatal grafts also received more synaptic input than the proximal dendrites, their synaptic input was probably less than that demonstrated in the normal striatum. The synaptic specializations of these cholinergic neurons were difficult to characterize due to the dense ChAT-immunoreaction product in the dendrites. Therefore, we cannot comment on whether the axodendritic contacts displayed asymmetric or symmetric synaptic specializations.

Choline Acetyltransferase Immunoreactive Boutons. Phelps et al.[56] also demonstrated that ChAT-positive axons within the normal striatum are either large diameter myelinated fibers or small diameter unmyelinated fibers. The fascicles of the internal capsule traversing the striatum also contained unmyelinated ChAT-immunoreactive fibers. They demonstrated that ChAT-immunoreactive boutons contained pleomorphic synaptic vesicles and made symmetric synaptic contacts with unlabeled dendrites, spines, and somata within the striatum. In addition, occasional synaptic contacts between ChAT-IR boutons and ChAT-labeled dendrites were demonstrated. In the present study, ChAT-IR boutons made symmetric contacts only with unlabeled dendrites. No axospinous or axosomatic contacts were identified. Whether this difference is due to the sparse innervation of the transplants by

ChAT-IR boutons, inadequate sampling, or represents a developmental abnormality of the grafts is currently only speculative.

Substance P - Light Microscopy

Initial studies on the distribution of substance P immunoreactivity in the brain of the rat by Ljungdahl et al.[46] and Cuello and Kanazawa[15] showed that small groups of substance P immunoreactive cells with diameters less than 25 μm were present in the rostral caudate nucleus, particularly in the ventral parts. In addition, there were single cells with a diameter between 15 and 25 μm, which were spread diffusely throughout the dorsal parts of the nucleus. The studies also showed that the striatum contained a network of fine substance P-like immunoreactive nerve terminals with a marked regional distribution, with the density of nerve terminals greatest in the anterior and ventral areas of the nucleus. In the present study, substance P-like immunoreactive neurons in fetal striatal transplants were similar in size and shape to those seen in normal striatum. However, the SP-IR neurons were never seen grouped together and the SP-IR neurons and axon terminals were also decreased in frequency compared to those in the normal striatum.[15]

Substance P - Electron Microscopy

Substance P-like Immunoreactive Neurons. The ultrastructural characteristics of substance P-like immunoreactive neurons and nerve terminals in the normal striatum have been fully characterized by Bolam et al.[8] These investigators reported that SP-IR neurons can be classified into two types. Type I neurons have characteristics typical of the medium-sized

spiny neurons reported in previous electron microscopic-Golgi and immunohistochemical studies. These neurons have round or oval nuclei which are not invaginated and the number of organelles in the sparse cytoplasm is typically low. In addition, boutons containing large, round or oval vesicles made symmetrical contacts with the perikarya of these neurons. The present study has also demonstrated the presence of Type I SP-IR neurons in striatal transplants. The nuclei and cytoplasmic characteristics of these neurons were similar to the SP-IR neurons found in the normal striatum. However, the numerous axosomatic contacts made on these neurons in the normal striatum were not present in the transplants. In the present study, we could not verify that the distal dendrites of these cells contained spines. However, in a previous electron microscopic-Golgi study of fetal striatal grafts, we demonstrated that all neurons with unindented nuclei were typical medium-sized, densely spiny neurons;[28] therefore, we can say with reasonable certainty that this Type I SP-IR neuron is of the medium-sized spiny type. The Golgi study also demonstrated that these neurons receive symmetric and asymmetric synaptic contacts on their dendritic shafts and spines, suggesting that they may receive input from the cerebral cortex or other host brain regions.[28,66]

The Type II SP-IR neurons described by Bolam et al.[8] were of medium size and were characterized by deeply invaginated nuclei. These neurons also contained sparse cytoplasm which contained very few organelles and their perikarya received only sparse synaptic input, mainly from small boutons, making symmetric axosomatic contacts. The Type II SP-IR neurons seen in fetal striatal transplants also contained an invaginated nucleus,

placing them in the aspiny category described in our previous electron microscopic-Golgi study.[28] However, the cytoplasm was abundant and contained numerous organelles, and the perikarya received numerous axosomatic contacts. There is currently no explanation for these differences in cellular ultrastructure and synaptic input.

Substance P-like Immunoreactive Terminals. Substance P-like immunoreactive nerve terminals have been shown to make two types of synaptic contacts in the normal rat brain. Bolam et al.[8] demonstrated that SP-IR nerve terminals in the striatum make symmetrical synaptic contacts with their postsynaptic targets. These investigators also demonstrated that these axon terminals were very similar to the boutons of recurrent axon collaterals of medium-sized spiny neurons. Somogyi et al.[67] demonstrated two types of substance P-like immunoreactive axon terminals in the normal rat substantia nigra. Type I boutons contained large vesicles and made symmetrical contacts only with dendrites, whereas Type II boutons contained smaller vesicles and formed asymmetrical synapses with both dendrites and perikarya. Pickel et al.[57] demonstrated that SP-IR axon terminals also make symmetric and asymmetric junctions with dendritic shafts and spines, respectively, in the rat nucleus accumbens. In the fetal striatal transplants, SP-IR boutons made only symmetric contacts with their postsynaptic elements, elegantly reproducing the anatomy of normal rat striatum. Whether SP–IR neurons in the fetal striatal grafts project to the host substantia nigra and form both Type I and Type II contacts is only speculative at this time. However, this connection is supported by several

studies which have demonstrated that fetal striatal grafts project to normal striatal targets.[59,79]

Frequency of Immunoreactive Neurons. In the present study, choline acetyltransferase- and substance P-like immunoreactive neurons in fetal striatal transplants were similar in size and shape to those seen in the normal striatum. However, both types of immunoreactive neurons were seen in decreased frequencies compared to the normal striatum. Roberts and Di Figlia[61,62] demonstrated that GABAergic, enkephalinergic and NADPH-diaphorase-positive neurons occurred in the similar frequencies in the grafts as in the normal striatum, and, therefore, it is unclear why our grafts contained relatively fewer immunoreactive neurons. One explanation could be that our fetal striatal grafts were contaminated with nonstriatal tissue, which, in effect, diluted the number of immunoreactive neurons in the transplant. In addition, in the present study the rats were not pretreated with colchicine prior to perfusion fixation and, therefore, the number of neurons immunoreactive for substance P was surely reduced compared to studies of the normal striatum which utilized colchicine. However, ChAT immunoreactivity would not be affected by colchicine treatment. Lastly, the decreased number of immunoreactive neurons could be a result of decreased afferent input to the striatal grafts. Multiple investigators have shown that substance P and substance P messenger RNA production is under dopaminergic control in the normal striatum.[1,14,52,53,60] Additionally, striatal cholinergic neurons are known to receive dopaminergic synaptic input in the rat.[41] Previous studies have demonstrated that catecholiminergic innervation

of fetal striatal grafts occurs in small patches and that the D1 and D2 receptors are underdeveloped.[12,29,34,45,47,78] In addition, Liu et al.[45] demonstrated that the large cholinergic neurons exist only in these dopaminergic patches. This data suggests that ChAT-IR and SP-IR neurons may be reduced in number in striatal grafts secondary to inadequate dopaminergic innervation from the host.

Figures and Tables

Figure 4.1: Photomicrograph demonstrating three month post-transplantation fetal striatal graft outlined by arrowheads. The transplant extends into the overlying cortex and there is a small area of necrosis in the lower part of the transplant. Scale bar = 0.2 cm.

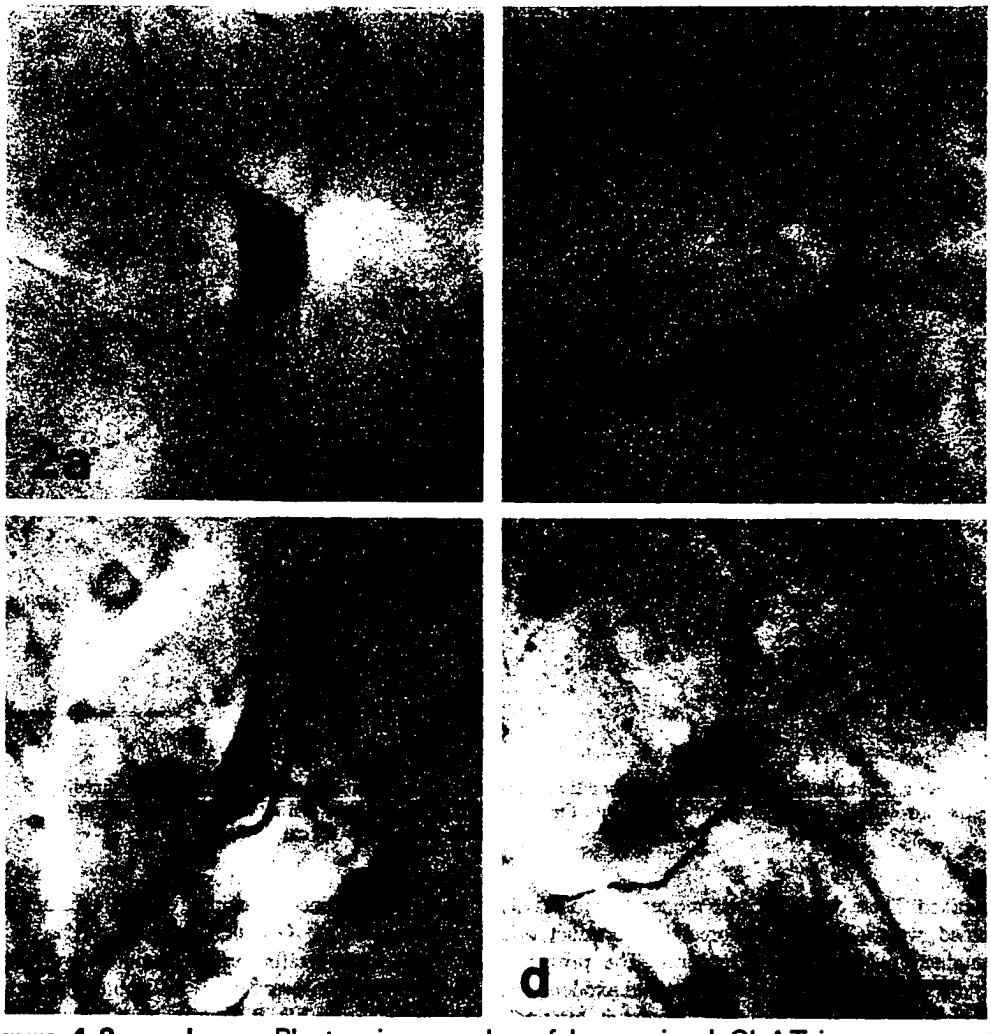

Figure 4.2: a, b, c. Photomicrographs of large-sized ChAT-immunoreactive neurons in a fetal striatal graft demonstrating oval, fusiform, and polygonal-shaped perikarya and sparsely branched dendrites. Scale bar = 25 μm. **D.** Photomicrograph of medium-sized ChAT-immunoreactive neuron in fetal striatal graft. The medium-sized neurons may represent ChAT-immunoreactive neurons in the cerebral cortex which were inadvertently transplanted with the primordial striatum. Scale bar = 25 μm.

Figure 4.3: **a.** Photomicrograph of a large ChAT-immunoreactive neuron in a fetal striatal graft. Scale bar = 50 μm. **b.** Electron micrograph of the ChAT-immunoreactive neuron demonstrating an indented nucleus, copious cytoplasm, numerous mitochondria, and rough endoplasmic reticulum. Scale bar = 4 μm.

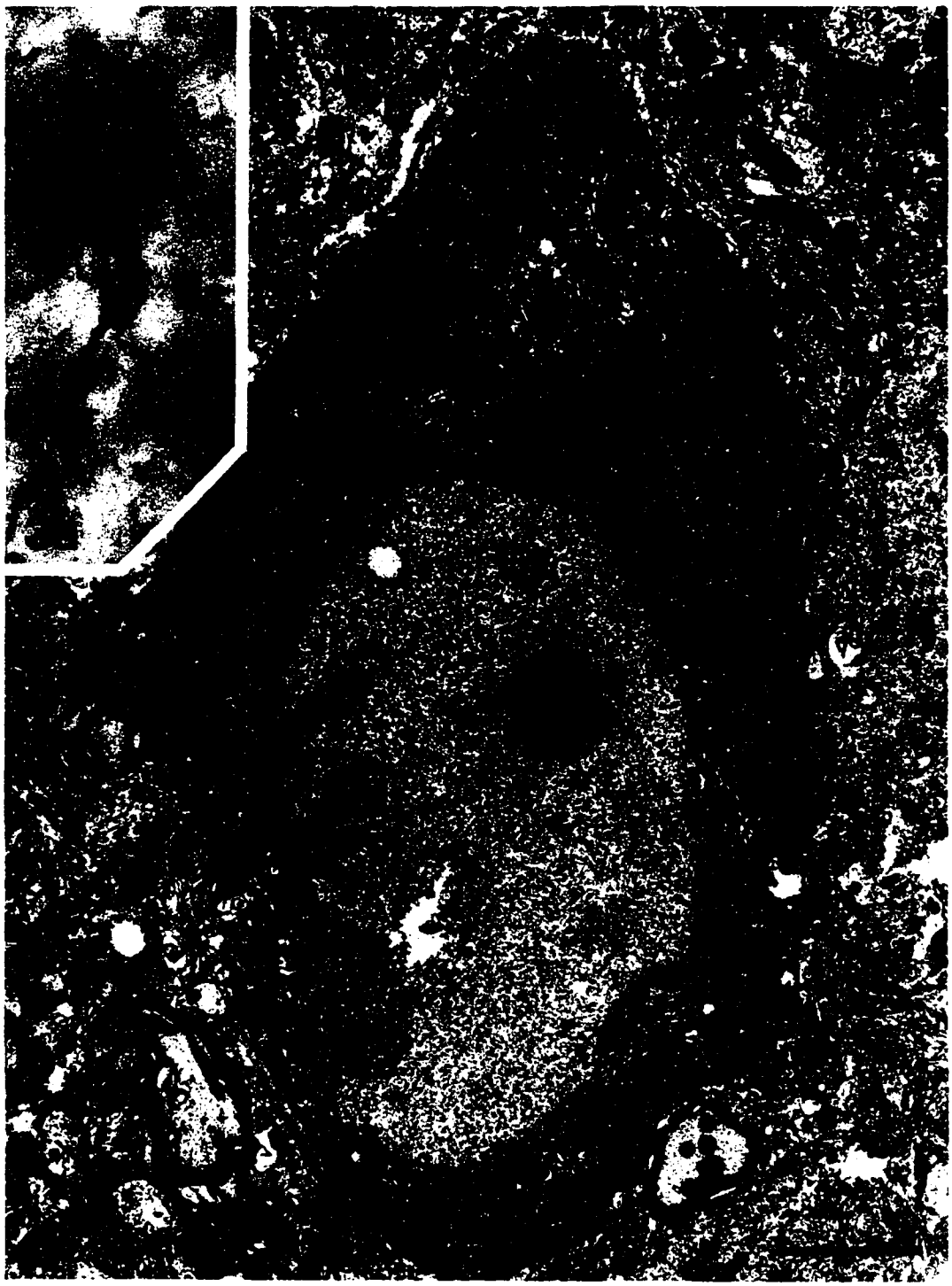

Figure 4.4: a. Photomicrograph of large ChAT-immunoreactive neuron in fetal striatal graft demonstrating a fusiform perikarya and a lightly stained primary dendrite. Scale bar = 20 μm. b. Photomicrograph of a semithin section of the neuron demonstrating a single, large nucleolus and densely immunoreactive cytoplasm. Scale bar = 15 μm. c. Electron micrograph of the ChAT-immunoreactive neuron demonstrating an eccentrically placed, indented nucleus surrounded by copious cytoplasm, both moderately labeled with ChAT-immunoreaction product. Scale bar = 7.5 μm.

Figure 4.5: a. Photomicrograph of ChAT-immunoreactive neuron in fetal striatal graft characterized by round, medium-sized perikarya and a long, heavily-stained dendrite. Scale bar= 20 μm. b. Electron micrograph of the ChAT-immunoreactive neuron demonstrating in a deeply indented nucleus and patches of ChAT-immunoreaction product in both the cytoplasm and nucleus (arrowheads). Scale bar = 3 μm.

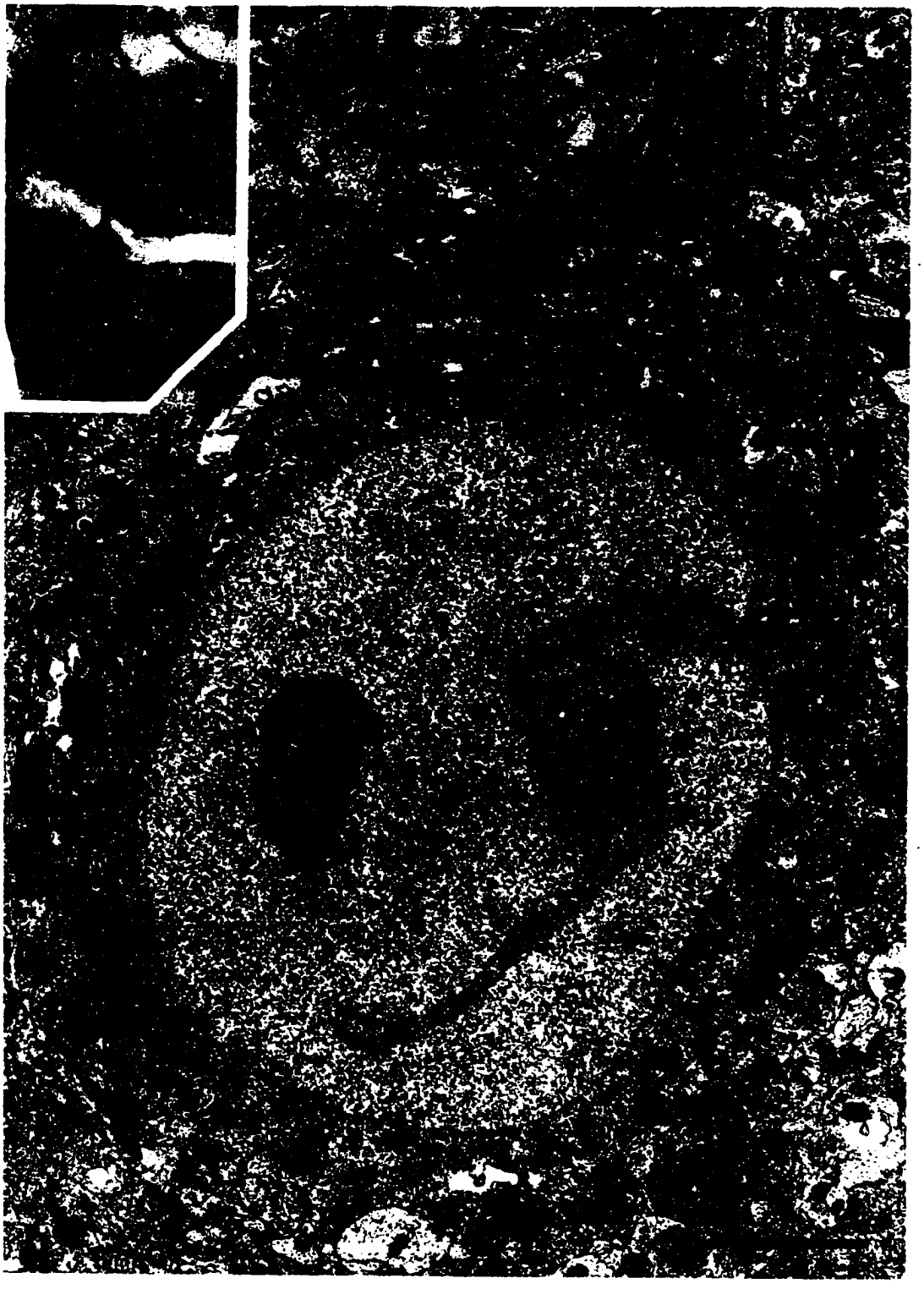

Figure 4.6: Ultrastructural detail of ChAT immunoreactive dendrites. a. Electron micrograph of a loosely packed axon terminal making a synapse (arrowhead) with the soma (S) of the ChAT-immunoreactive neuron demonstrated in Figure 4. Scale bar = 0.75 μm. **b.** Electron micrograph of a heavily stained, ChAT-immunoreactive dendrite receiving synaptic input (arrowheads) from a non-immunoreactive axon terminal. Scale bar = 1.0 μm. **c.** Electron micrograph of a ChAT-immunoreactive dendrite receiving synaptic input (arrowhead) from a non-immunoreactive axon terminal. Note the large mitochondria in the immunoreactive dendrite. Scale bar = 1.0 μm. d. Electron micrograph of a ChAT-immunoreactive distal dendrite receiving synaptic input (arrowhead) from a non-immunoreactive axon terminal. The adjacent non-immunoreactive axon terminal also made a synaptic contact with the dendrite in an adjacent section followed by serial thin-sectioning. Scale bar = 1.0 μm.

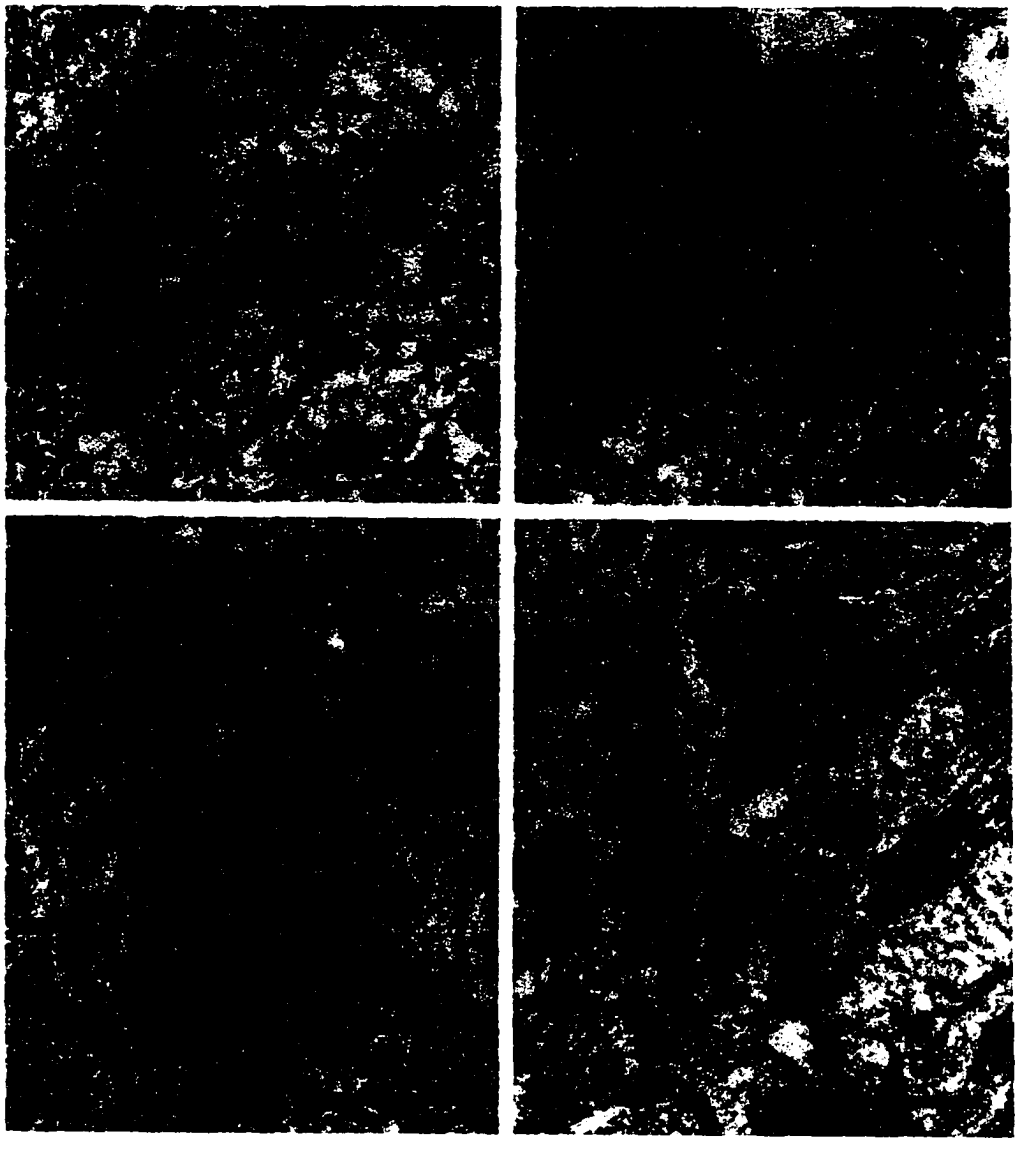

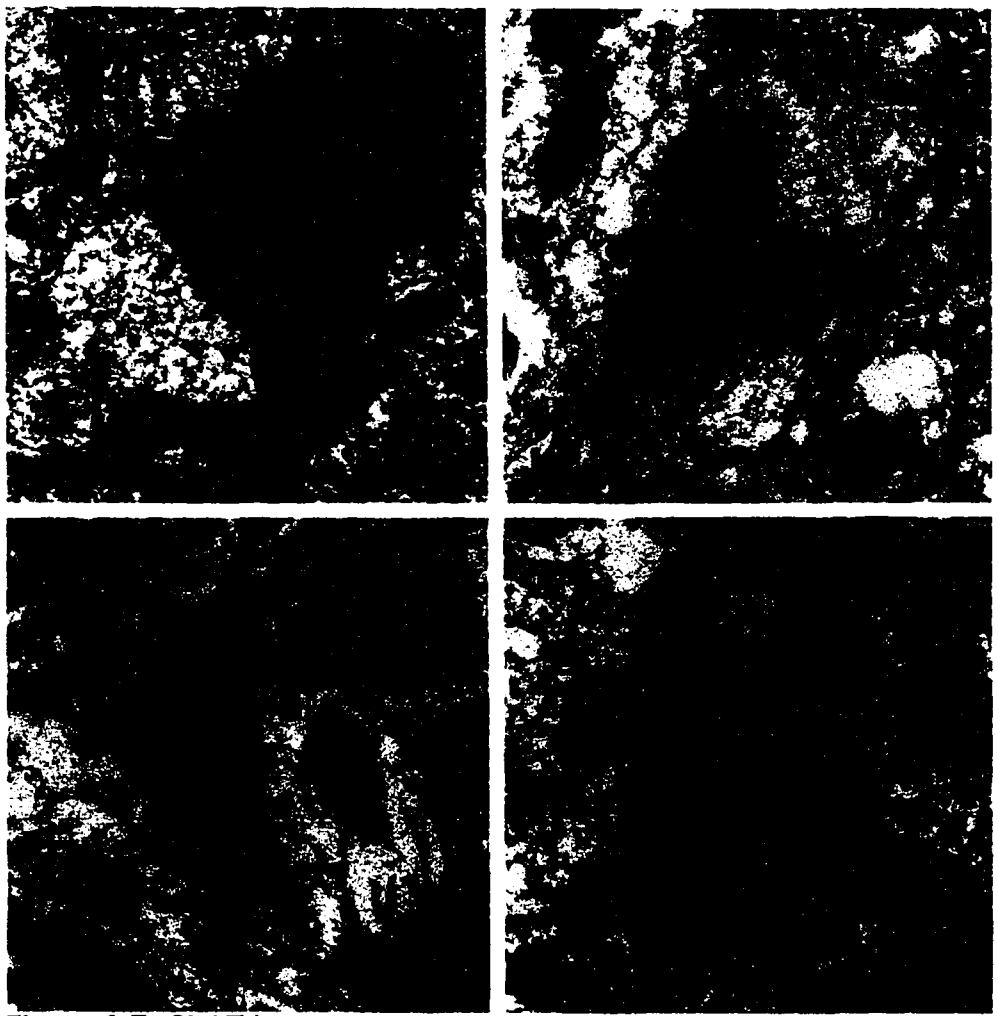

Figure 4.7: ChAT immunoreactive axon terminals. **a.** Electron micrograph of a large ChAT-immunoreactive axon terminal containing multiple round vesicles making a symmetric synaptic contact with an unlabeled dendrite (arrowheads). b. Electron micrograph of a ChAT-immunoreactive axon terminal making an asymmetric contact (arrowheads) with an unlabeled distal dendrite. c. Electron micrograph of a ChAT-immunoreactive axon terminal making a symmetric contact (arrowhead) with an unlabeled dendrite. d. Electron micrograph of a large ChAT-immunoreactive axon terminal containing multiple mitochondria making a symmetric contact (arrowheads) with an unlabeled dendrite. Scale bars = 0.5 μm.

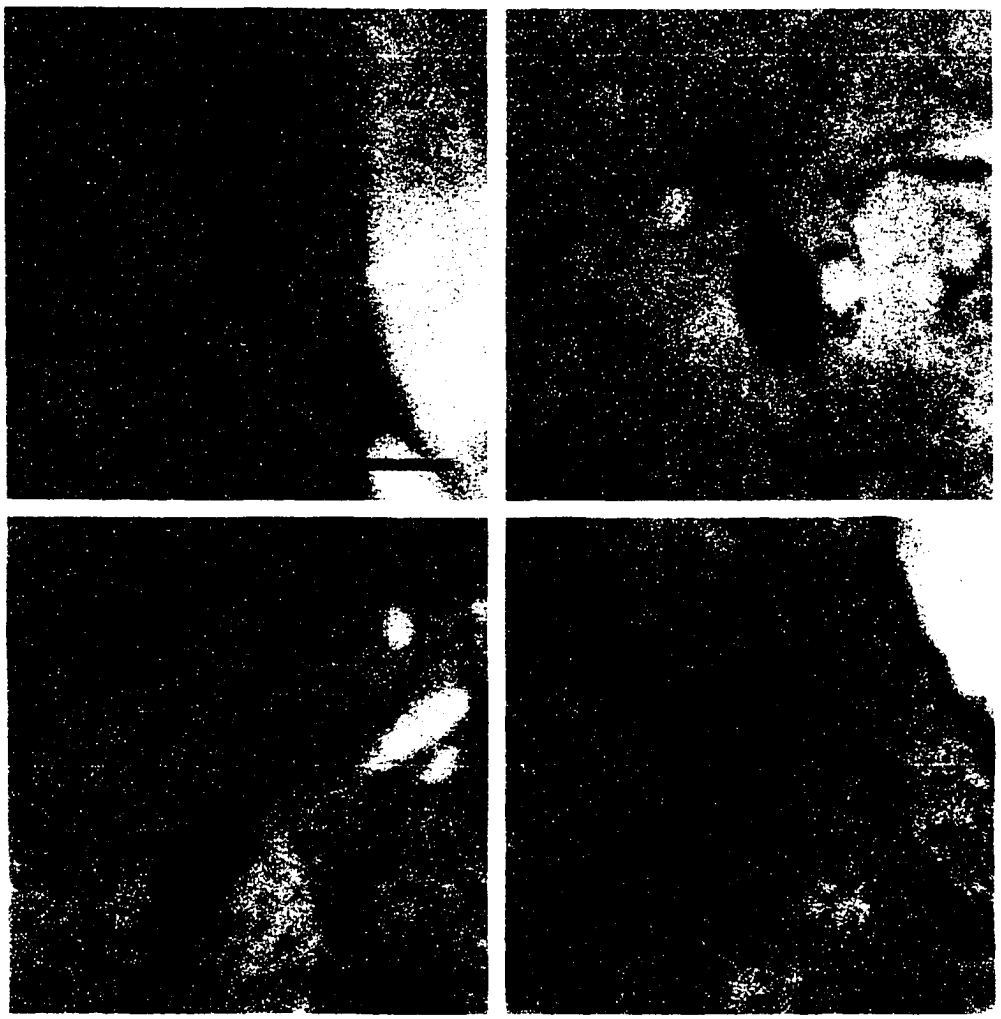

Figure 4.8: Photomicrographs of substance P-like immunoreactive neurons in a fetal striatal graft demonstrating polygonal- and oval-shaped perikarya. Scale bar = 20 μm. Note that the dendrites are moderately stained proximally, but become non-immunoreactive distally.

Figure 4.9: a. Photomicrograph of substance P-like immunoreactive neuron in neostriatal graft demonstrating a polygonally-shaped perikaryon and a moderately stained proximal dendrite. Scale bar = 10 μm. b. Semi-thin section of the neuron demonstrating dense immunoreaction product throughout the cytoplasm and light staining of the nucleus (Scale bar = 10 μm). c. Electron micrograph of the neuron demonstrating an unindented nucleus with a single nucleolus and a moderate amount of cytoplasm rich in mitochondria and rough endoplasmic reticulum. Note the absence of axosomatic contacts on the neuron. Scale bar = 3 μm.

Figure 4.10: **a.** Photomicrograph of substance P-like immunoreactive neuron in fetal striatal graft demonstrating an oval perikaryon surrounded by a neuropil rich in immunoreactive axon terminals. Scale bar = 20 μm. **b.** Electron micrograph of the neuron demonstrating dense immunoreaction product in the neuropil and nucleus. Note the highly indented nucleus, single nucleolus, and abundant Nissl substance. Scale bar 3.0 μm.

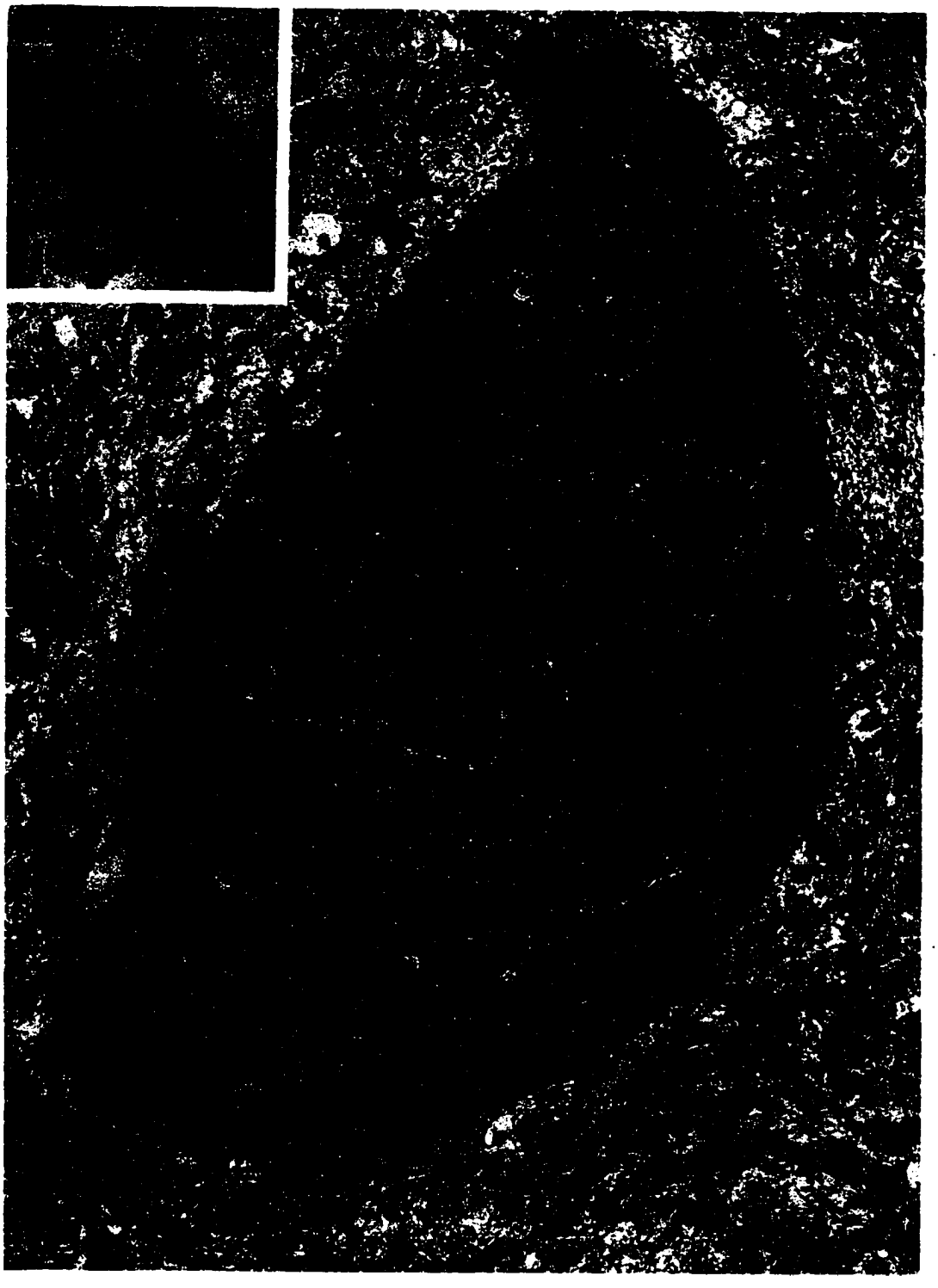

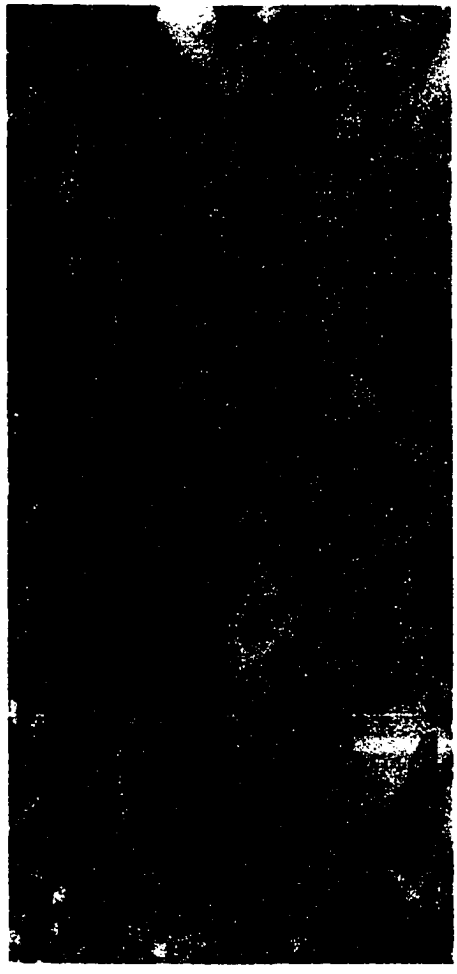

Figure 4.11: Electron micrograph demonstrating two non-immunoreactive axon terminals making synaptic contacts with the perikaryon of the substance P-like immunoreactive neuron demonstrated in Figure 4.10. The synaptic specializations seem to be symmetric, although the post-synaptic surfaces are obscured by the dense immunoreaction product. Scale bar = 0.5 μm.

Figure 4.12: Substance P-like immunoreactive dendrites. a. Electron micrograph of substance P-like immunoreactive dendrite containing numerous mitochondria which receive synaptic input from an unlabeled axon terminal (arrowhead). b., c. Electron micrographs of a substance P-like immunoreactive dendrites receiving synaptic input (arrowhead) from loosely packed unlabeled axon terminals. Scale bars = 0.75 μm.

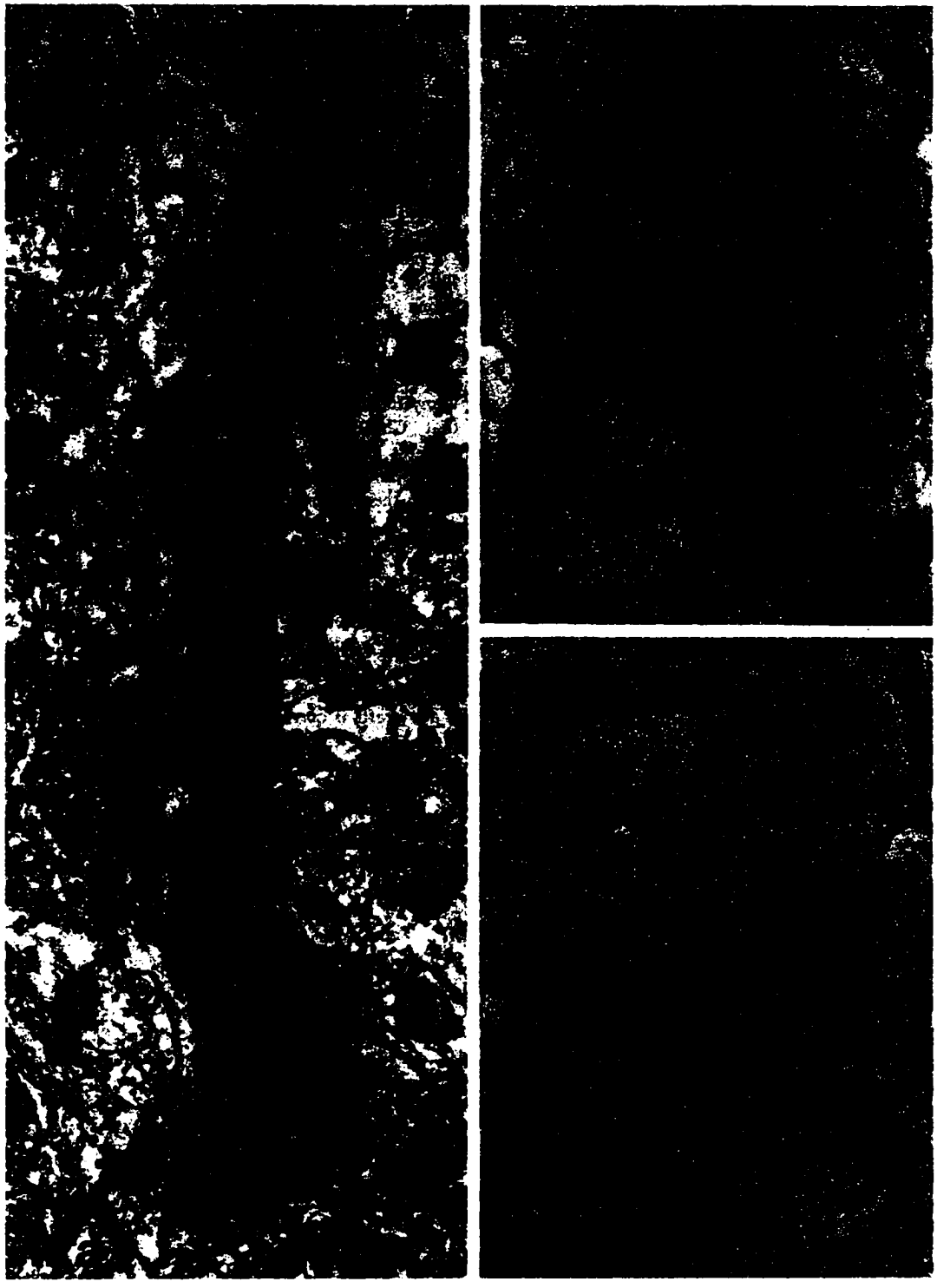

Figure 4.13: Substance P-like immunoreactive axon terminals. a. Electron micrograph of a large substance P-like immunoreactive axon terminal containing numerous mitochondria making a symmetric axodendritic contact with an unlabeled dendrite. Scale bar = 0.75 μm. b. Electron micrograph of a small non-immunoreactive dendrite receiving symmetric synaptic input from a substance P-like immunoreactive axon terminal (arrowhead). Scale bar = 0.75 μm. c. Substance P-like immunoreactive axon terminals making symmetric synaptic contacts with a small unlabeled dendrite (arrowheads). Scale bar = 0.5 μm.

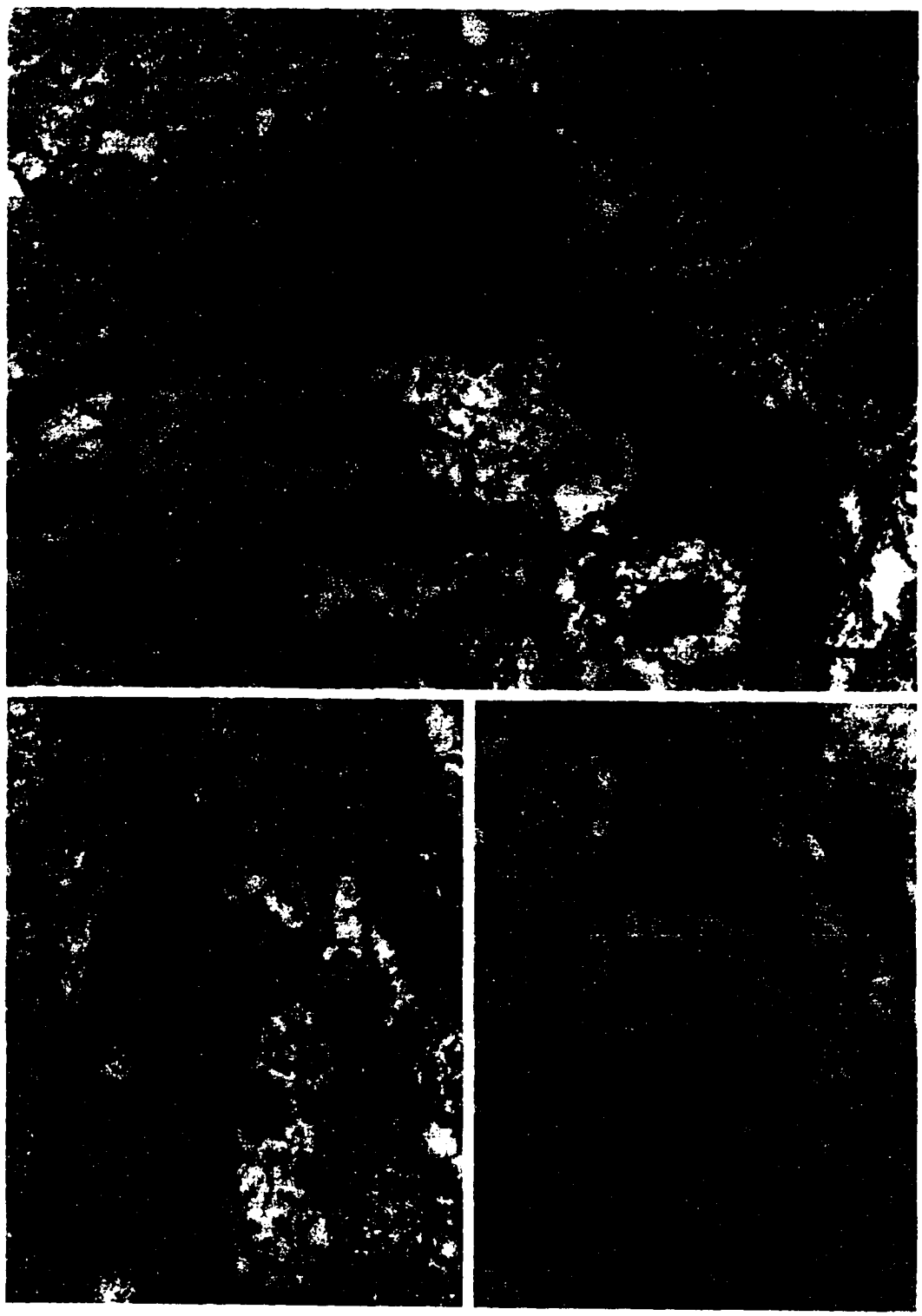

Figure 4.14: Electron micrograph of a substance P-like immunoreactive axon terminal making a synaptic contact with an unlabeled dendritic spine in a fetal striatal graft. Scale bar = 0.75 μm.

REFERENCES

1. Bannon, M.J., Elliott, P.J. and Bunney, E.B. (1987) Striatal tachykinin biosynthesis: regulation of mRNA and peptide levels by dopamine agonists and antagonist. Molec. Brain Res. 3:31-37.
2. Barnardi, G., Floris, V., Marciani, M.G., Morocutti, C. and Stanzione, P. (1976) The action of acetylcholine and L-glutamic acid on rat caudate neurons. Brain Res. 114:134-138.
3. Björklund, A. and Stenevi, U. (1985) Neuronal Grafting in the Mammalian CNS. Amsterdam: Elsevier.
4. Bolam J.P., Ingham, C.A., Wainer, B.H. and Smith, A.D. (1983) Golgi-impregnation of neurons containing acetylcholinesterase (AChE) or choline acetyltransferase (ChAT) in rat neostriatum: cholinergic pathways VI. Soc. Neurosci. Abstr. 9:964.
5. Bolam, J.P., Ingham, C.A., Izzo, P.N., Levey, A.I., Rye, D.B. Smith, A.D. and Wainer, B.H. (1986) Substance P-containing terminals in synaptic contact with cholinergic neurons in the neostriatum and basal forebrain: a double immunocytochemical study in the rat. Brain Res. 397:279-289.
6. Bolam, J.P. and Izzo, P.N. (1988) The postsynaptic targets of substance P-immunoreactive terminals in the rat neostriatum with particular reference to identified spiny striatonigral neurons. Exp. Brain Res. 70:361-377.
7. Bolam, J.P., Wainer, B.H., Smith, A.D. (1984) Characterization of cholinergic neurons in the rat neostriatum. A combination of choline acetyltransferase immunocytochemistry, Golgi-impregnation and electron microscopy. Neuroscience 12:711-718.

8. Bolam, J.P., Somogyi, P., Takagi, H., Fodor, I. and Smith, A.D. (1983) Localization of substance P-like immunoreactivity in neurons and nerve terminals in the neostriatum of the rat: a correlated light and electron microscopic study. J. Neurocytol. 12:325-344.

9. Burke R.E. and Karanas, A.L. (1990) Demonstration of a medial to lateral gradient in the density of cholinergic neuropil in the rat striatum. Neurosci. Lett. 108:58-64.

10. Chang, H.T. and Kitai, S.T. (1982) Large neostriatal neurons in the rat: an electron microscopic study of gold-toned Golgi-stained cells. Brain Res. Bull. 8:631-643.

11. Chang, H.T., Wilson, C.J. and Kitai, S.T. (1982) A Golgi study of rat neostriatal neurons: light microscopic analysis. J. Comp. Neurol. 208:107-126.

12. Clarke, D.J., Dunnett, S.B., Isacson, O. Sirinathsinghji, D.J.S. and Björklund, A. (1988) Striatal grafts in rats with unilateral neostriatal lesions. I. Ultrastructural evidence of afferent synaptic inputs from the host nigrostriatal pathway. Neuroscience 24:791-801.

13. Coyle, J.T. and Schwarcz, R. (1976) Lesion of striatal neurones with kainic acid provides a model of Huntington's chorea. Nature 263:244-246.

14. Cruz, C.J. and Beckstead, R.M. (1989) Nigrostriatal dopamine neurons are required to maintain basal levels of substance P in the rat substantia nigra. Neuroscience 30:331-338.

15. Cuello, A.C. and Kanazawa, I. (1978) The distribution of substance P-immunoreactive fibres in the rat central nervous system. J. Comp. Neurol. 178:129-156.

16. Davies, J. and Dray, A. (1976) Substance P in the substantia nigra. Brain Res. 107:623-627.

17. Deckel, A.W., Moran, T.H., Coyle, J.T. Sandberg, P.R. and Robinson, R.G. (1986) Anatomical predictors of behavioral recovery following fetal striatal transplants. Brain Res. 365:249-258.

18. Deckel, A.W., Moran, T.H. and Robinson, R.G. (1986) Behavioral recovery following kainic acid lesions and fetal implants of the striatum occurs independently of dopaminergic mechanisms. Brain Res. 363:383-385.

19. Deckel, A.W., Moran, T.H. and Robinson, R.G. (1988) Receptor characteristics and recovery of function following kainic acid lesions and fetal transplants of the striatum. I. Cholinergic systems. Brain Res. 474:27-38.

20. Deckel, A.W., Moran, T.H. and Robinson, R.G. (1988) Receptor characteristics and recovery of function following kainic acid lesions and fetal transplants of the striatum. II. Dopaminergic systems. Brain Res. 474:39-47.

21. Deckel, A.W., Robinson, R.G., Coyle, J.T. and Sandberg, P.R. (1983) Reversal of long-term locomotor abnormalities in the kainic acid model of Huntington's disease by day 18 fetal striatal implants. Eur. J. Pharmacol. 93:287-288.

22. Di Figlia, M., Schiff, L. and Deckel, A.W. (1988) Neuronal organization of fetal striatal grafts in kainate- and sham-lesioned rat caudate nucleus: Light and electron-microscopic observations. J. Neurosci. 8:1112-1130.

23. DiMova, R., Vuillet, J. and Seite, R. (1980) Study of rat neostriatum using a combined Golgi-electron microscopic technique and serial sections. Neuroscience 5:1581-1596.

24. Emerich, D.F., Zubricki, E.M., Shipley, M.T., Norman, A.B. and Sanberg, P.R. (1991) Female rats are more sensitive to the locomotor alterations following quinolinic acid-induced striatal lesions: Effects of striatal transplants. Exp. Neurol. 111:369-378.

25. Graybiel, A.M., Dunnett, S.B., Baughman, R.W. and Liu, F.-C. (1987) Cholinergic neurons and neuropil and tyrosine hydroxylase-positive fibers cluster together in circumscribed patches in intrastriatal grafts derived from embryonic striatal donor tissue. Neurosci. (Suppl.22):S265.

26. Graybiel, A.M., Liu, F.-C. and Dunnett, S.B. (1989) Intrastriatal grafts derived from fetal striatal primordia. I. Phenotypy and modular organization. J. Neurosci. 9:3250-3271.

27. Hall, M.E., Grantham, P.A. and Steward, J.M. (1985) Age and strain differences in some behavioral effects of intracranial substance P. Peptides 6:363-368.

28. Helm, G.A., Palmer, P.E. and Bennett, J.P. (1990) Fetal neostriatal transplants in the rat: a light and electron microscopic Golgi study. Neuroscience 37:735-756

29. Helm, G.A., Robertson, M.S., Jallo, G.I., Simmons, N. and Bennett, J.P. (1991) Development of D1 and D2 dopamine receptors and associated

second messenger systems in fetal striatal transplants. Exp. Neurol. 111:181-189.

30. Herrera-Marschitz, M., Christensson-Nylander, I., Sharp, T., Staines, W., Reid, M., Hökfelt, T., Terenius, L. and Ungerstedt, U. (1986) Striato-nigral dynorphin and substance P pathways in the rat. II. Functional analysis. Exp. Brain Res. 64:193-207.

31. Houser, C.R., Crawford, G.D., Barber, R. P., Salvaterra, P.M. and Vaughn, J.E. (1983) Organization and morphological characteristics of cholinergic neurons: an immunocytochemical study with a monoclonal antibody to choline acetyltransferase. Brain Res. 266:97-119.

32. Isacson, O., Brundin, P., Gage, F.H. and Björklund, A. (1985) Neuronal grafting in a rat model of Huntington's disease: progressive neurochemical changes after ibotenate lesions and striatal tissue grafting. Neuroscience 16:799-817.

33. Isacson O., Brundin, P., Kelly, P.A.T., Gage, F.H. and Björklund, A. (1984) Functional neuronal replacement by grafted striatal neurones in ibotenic acid lesioned rat striatum. Nature 311:458-460.

34. Isacson, O., Dawbarn, D., Brundin, P., Gage, F.H., Emson, P.C. and Björklund, A. (1987) Neuronal grafting in a rat model of Huntington's disease: striosomal-like organization of striatal grafts as revealed by acetylcholinesterase histochemistry, immunocytochemistry and receptor autoradiography. Neuroscience 22:481-497.

35. Isacson, O., Dunnett, S.B. and Björklund, A. (1986) Behavioral recovery in an animal model of Huntington's disease. Proc. Nat. Acad. Sci. USA 83:2728-2732.

36. Itoh, K.A., Konishi, A., Naura, S., Nakamura, N. and Sugimoto, T. (1979) Application of coupled oxidation to electron microscopic demonstration of horseradish peroxidase: cobalt-glucose oxidase method. Brain Res. 175:341-346.

37. Izzo, P.N. and Bolam, J.P. (1988) Cholinergic synaptic input to different parts of spiny striatonigral neurons in the rat. J. Comp. Neurol. 269:219-234.

38. James, T.A. and Starr, M.S. (1979) Effects of substance P injected into the substantia nigra. Brit. J. Pharmac. 65:423-429.

39. Kelley, A.E. and Iversen, S.D. (1978) Behavioral response to bilateral injections of substance P into the substantia nigra of the rat. Brain Res. 158:474-478.

40. Kimura H., McGeer P.L., Peng J.H. and McGeer E.G. (1981) The central cholinergic system studied by choline acetyltransferase immunohistochemistry in the cat. J. Comp. Neurol. 200:151-201.

41. Kubota Y., Inagaki, S., Shimada S., Kito S., Eckenstein F. and Tohyama M. (1987) Neostriatal cholinergic neurons receive direct synaptic inputs from dopaminergic axons. Brain Res. 413:179-184.

42. Le Gal La Salle, G. and Ben-Ari, Y. (1977) Microiontophoretic effects of substance P on neurons of the medial amygdala and putamen of the rat. Brain Res. 135:174-179.

43. Lehmann, J. and Langer, S.Z. (1983) The striatal cholinergic interneuron: Synaptic target of dopaminergic terminals? Neuroscience 10:1105-1120.

44. Liu, F.-C., Graybiel, A.M. and Dunnett, S.B. (1988) Modular organization of fetal striatal grafts. Soc. Neurosci. Abstr. 14:763.

45. Liu, F.-C., Graybiel, A.M., Dunnett, S.B. and Baughman, R.W. (1990) Intrastriatal grafts derived from fetal striatal primordia: II. Reconstitution of cholinergic and dopaminergic systems. J. Comp. Neurol. 295:1-14

46. Ljungdahl, A., Hökfelt T. and Nilsson, G. (1978) Distribution of substance P-like immunoreactivity in the central nervous system of the rat-I. Cell bodies and nerve terminals. Neuroscience 3:861-943.

47. Mayer E., Heavens, R.P. and Sirinathsinghji, D.J.S. (1990) Autoradiographic localisation of D1 and D2 dopamine receptors in primordial striatal tissue grafts in rats. Neurosci. Lett. 109:271-276.

48. McAllister, J.P., Walker, P.D., Zemanick, M.C., Weber, A.B., Kaplan, L.I. and Reynolds, M.A. (1985) Morphology of embryonic neostriatal cell suspensions transplanted into adult neostriata. Dev. Brain Res. 23:282-286.

49. McGeer, E.G. and McGeer, P.L. (1976) Duplication of biochemical changes of Huntington's chorea by intrastriatal injection of glutamic and kainic acids. Nature 263:517-519.

50. Melis, M.R. and Gale, K. (1984) Evidence that nigral substance P controls the activity of the nigrotectal GABAergic pathway. Brain Res. 295:389-393.

51. Morris, B.J., Wisden, W., Dunnett, S.B. and Sirinathsinghji, D.J.S. (1989) Cellular localisation of somatostatin mRNA and neuropeptide Y mRNA in foetal striatal tissue grafts. Neurosci. Lett. 103:121-126.

52. Nylander, I. and Terenius, L.H. (1987) Dopamine receptors mediate alterations in striato-nigral dynorphin and substance P pathways. Neuropharmacology 26:1295-1302.

53. Oblin, A., Zivkovic, B. and Bartholini, G. (1987) Selective antagonists of dopamine receptor subtypes differentially affect substance P levels in the striatum and substantia nigra. Brain Res. 421:387-390.

54. Park, M.R., Lighthall, J. W. and Kitai, S. T. (1980) Recurrent inhibition in the rat neostriatum. Brain Res. 194:359-369

55. Paxinos, G. and Watson,C. (1982) The Rat Brain in Stereotaxic Coordinates. Sydney: Academic Press.

56. Phelps, P.E., Houser, C.R. and Vaughn,J.E. (1985) Immunocytochemical localization of choline acetyltransferase within the rat neostriatum: A correlated light and electron microscopic study of cholinergic neurons and synapses. J. Comp. Neurol. 238:286-307.

57. Pickel, V.M., Joh, T.H. and Chan, J. (1988) Substance P in the rat nucleus accumbens: ultrastructural localization in axon terminals and their relation to dopaminergic afferents. Brain Res. 444:247-264.

58. Pinnock, R.D., Woodruff, G.N. and Turnbull, M.J. (1983) Actions of substance P, MIF, TRH and related peptides in the substantia nigra, caudate nucleus and nucleus accumbens. Neuropharmacology 22:687-696.

59. Pritzel, M., Isacson, O., Brundin, P., Wiklund, L. and Björklund, A.(1986) Afferent and efferent connections of striatal grafts implanted into the ibotenic acid lesioned neostriatum in adult rats. Exp. Brain Res. 65:112-126.

60. Ritter, J.K., Schmidt, C.J., Gibb, J.W. and Hanson, G.R. (1985) Dopamine-mediated increases in nigral substance P-like immunoreactivity. Biochem. Pharmacol. 34:3161-3166.

61. Roberts R.C. and Di Figlia, M. (1988) Localization of immunoreactive GABA and enkephalin and NADPH-diaphorase-positive neurons in fetal striatal grafts in the quinolinic-acid-lesioned rat neostriatum. J. Comp. Neurol. 274:406-421.

62. Roberts, R.C. and Di Figlia, M. (1990) Long-term survival of GABA-, enkephalin-, NADPH-diaphorase- and calbindin-d28k-containing neurons in fetal striatal grafts. Brain Res. 532:151-159.

63. Sanberg, P.R., Henault, M.A., Hagenmeyer-Houser, S.H., Giordano, M. and Russell, K.H. (1987) Multiple transplants of fetal striatal tissue in the kainic acid model of Huntington's disease: Behavioral recovery may not be related to acetylcholinesterase. In Azmitia, E. and Björklund, A. (eds): Cell and Tissue Transplantation in the Adult Brain. Ann. N.Y. Acad. Sci. 495:781-785.

64. Sirinathsinghji, D.J.S., Dunnett, S.B., Isacson, O., Clarke, D.J., Kendrick, K. and Björklund, A. (1988) Striatal grafts in rats with unilateral neostriatal lesions. II. In vivo monitoring of GABA release in globus pallidus and substantia nigra. Neuroscience 24:803-811.

65. Sirinathsinghji, D.J.S., Morris, B.J., Wisden, W., Northrop, A., Hunt, S.P. and Dunnett, S.B. (1990) Gene expression in striatal grafts - I. Cellular localization of neurotransmitter mRNAs. Neuroscience 34(3):675-686.

66. Somogyi, P., Bolam, J.P. and Smith, A.D. (1981) Monosynaptic cortical input and local axon collaterals of identified striatonigral neurons. A light and electron microscopic study using the Golgi-peroxidase transport-degeneration procedure. J. Comp. Neurol. 195:567-584.

67. Somogyi, P., Priestley, J.V., Cuello, A.C., Smith, A.D. and Bolam, J.P. (1982) Synaptic connections of substance P-immunoreactive nerve terminals in the substantia nigra: A correlated light and electron-microscopic study. Cell Tissue Res. 223:469-486.

68. Somogyi, P. and Smith, A.D. (1979) Projection of neostriatal spiny neuron to the substantia nigra. Application of a combined Golgi-staining and horseradish peroxidase transport procedure at both the light and electron microscopic levels. Brain Res. 178:3-15.

69. Somogyi, P. and Takagi, H. (1982) A note on the use of picric acid-paraformaldehyde-glutaraldehyde fixative for correlated light and electron microscopic immunocytochemistry. Neuroscience 7:1779-1783.

70. Takagi H., Somogyi P. and Smith A.D. (1984) Aspiny neurons and their local axons in the neostriatum of the rat: a correlated light and electron microscopic study of Golgi-impregnated material. J. Neurocytol. 13:239-265.

71. Tan, D.P. and Tsou, K. (1988) Different effects of tachykinins injected intranigrally on striatal dopamine metabolism. J. Neurochem. 51:1333-1337.

72. Wainer B.H., Bolam J.P., Freund T., Henderson Z., Totterdell, S. and Smith A.D. (1984) Cholinergic synapses in the rat brain: A correlated light and electron microscopic immunohistochemical study employing a

monoclonal antibody against choline acetyltransferase. Brain Res. 308:69-76.

73. Waldmeier, P.C., Kam, R. and Stocklin, K. (1978) Increased dopamine metabolism in rat striatum after infusions of substance P into the substantia nigra. Brain Res. 159:223-117.

74. Walker, R.J., Kemp, J.A., Yajima, H., Kitagawa, K., Woodruff, G.N. (1976) The action of substance P on mesencephalic reticular and substantia nigra neurones of the rat. Experientia 32:214-215.

75. Walker, P.D., Chovanes, G.I. and McAllister, J.P. (1987) Identification of acetylcholinesterase-reactive neurons and neuropil in neostriatal transplants. J. Comp. Neurol. 259:1-12.

76. Wichmann, T., Wistorin, K., Björklund, A. and Starke, K. (1988) Release of acetylcholine and its dopaminergic control in slices from striatal grafts in the ibotenic acid-lesioned rat striatum. Arch. Pharmacol. 338:623-631.

77. Wictorin, K. and Björklund, A. (1989) Connectivity of striatal grafts into the ibotenic acid-lesioned striatum. II. Cortical afferents. Neuroscience 30:297-311.

78. Wictorin, K., Isacson, O., Fischer, W., Nothias, F., Peschanski, M. and Björklund, A. (1988) Connectivity of striatal grafts into the ibotenic acid-lesioned striatum. I. Subcortical afferents. Neuroscience 27:547-562.

79. Wictorin, K., Simerly, R. B., Isacson, O., Swanson, L.W. and Björklund, A. (1989) Connectivity of striatal grafts into the ibotenic acid-lesioned striatum. III. Efferent projecting graft neurons and their relation to host afferents within the grafts. Neuroscience 30:313-330.

80. Wilson, C.J., Chang, H.T. and Kitai, S.T. (1983) Morphology and synaptic connections of a giant aspiny interneuron in the rat neostriatum. Soc. Neurosci. Abstr. 9:658.

81. Wilson, C.J. and Groves, P.M. (1980) Fine structure and synaptic connections of the common spiny neuron of the rat neostriatum: a study employing intracellular injection of horseradish peroxidase. J. Comp. Neurol. 194:599-615.

82. Xu, Z.C., Wilson, C.J. and Emson, P.C. (1989) Restoration of the corticostriatal projection in rat neostriatal grafts: electron microscopic analysis. Neuroscience 29:539-550

83. Zhou F.C. and Buchwald, N. (1989) Connectivities of the striatal grafts in adult rat brain: a rich afference and scant striatonigral efference. Brain Res. 504:15-30.

Chapter 5:

DESCRIPTIVE MORPHOLOGY OF DEVELOPING FETAL NEOSTRIATAL ALLOGRAFTS IN THE RHESUS MONKEY: A CORRELATED LIGHT AND ELECTRON MICROSCOPIC GOLGI STUDY

*(Published, Neuroscience 50 (1992) 163-179)

INTRODUCTION

Studies concerning the transplantation of fetal neurons for the treatment of neurodegenerative diseases have been performed primarily in rodents. Behavioral, biochemical, and neuroanatomical studies in rat models of Huntington's,[10,15-17,23,38,41,72] Alzheimer's,[2,3,11,26] and Parkinson's[2,8,31] disease have demonstrated that the use of fetal neuronal transplantation for the treatment of these diseases may be feasible in the near future. Huntington's disease is a genetic disorder characterized by the premature death of projection neurons in the caudate nucleus and putamen.[33,47,58] The rat model of Huntington's disease introduced by Coyle and Schwarz[13,45] and McGeer and McGeer,[49] which utilizes the injection of excitotoxic acids to lesion the neostriatum, has proved to be one of the most useful tools for the study of fetal neuronal transplants. The lesions produce behavioral deficits which can be partially reversed through the implantation of fetal neostriatal neurons into the lesioned area.[15,17,39-41] Biochemical studies suggest that this recovery is related to the restoration of GABAergic striatopallidal and striatonigral pathways.[60] This has been supported by neuroanatomical studies by Wictorin et al.[75] and Pritzel et al.,[56] which demonstrated that neostriatal grafts have significant efferent connections with the host globus pallidus, entopeduncular nucleus, and substantia nigra. Other studies[73,74,77] have demonstrated that the grafts receive afferent input from the host cerebral cortex, thalamus, and substantia nigra. Furthermore, Golgi-impregnation[35,48] and immunohistochemical[36,37,59,71] studies have demonstrated that the morphological and neurochemical differentiation of grafted neostriatal neurons is complete in six month old transplants.

Several groups of investigators have now extended neuronal transplantation studies into the primate. Morihisa et al.[53] attempted embryonic substantia nigra implants and host adrenal medulla implants into the caudate nucleus of rhesus monkeys after lesioning of the host substantia nigra. Their nigral transplants failed to survive, while their adrenal autografts appeared healthy 3 to 8 months after transplantation. Redmond et al.[57] subsequently demonstrated that fetal mesencephalic tissue transplanted into the MPTP-lesioned African green monkey can survive for extended periods of time and can lead to the partial reversal of behavioral abnormalities created by the destruction of dopaminergic neurons in the substantia nigra. These initial studies have been confirmed by other investigators.[12,25,28,61-64] It has been hypothesized that this behavioral improvement is directly related to the reinnervation of the host striatum by the transplanted dopaminergic neurons.

Multiple investigators have reported that lesioning of the primate striatum with either kainic acid or ibotenic acid can produce behavioral abnormalities, including chorea and athetosis, which suggests that such a lesion may also produce a useful model of Huntington's disease.[14,34,43] Isacson et al.[42] demonstrated that rat fetal neostriatal neurons transplanted into the lesioned baboon striatum survived for up to 6 weeks if the hosts are immunosuppressed with cyclosporin. The aims of the present study were to demonstrate that neostriatal allografts could survive in the lesioned primate striatum and to characterize the early development of these transplanted neurons using histologic staining, Golgi-impregnation, and electron microscopy. Because of the complex neuroanatomy of the primate neostriatum, including multiple cell types[1,9,20,24,29,30,46] as well as numerous

afferent and efferent connections,[4,65,66,76] the study of fetal striatal grafts in the lesioned primate striatum may be an ideal model to determine whether fetal neuronal grafts can eventually be used to treat human disease.

MATERIALS AND METHODS

One adult female Rhesus monkey and two pregnant Rhesus monkeys at an estimated 55-70 days of gestation were used in this study. One pregnant female was used initially as a fetal donor and was subsequently used as the recipient of a striatal graft after completely healing from the initial cesarean section.

Striatal lesioning and transplantation. Initially, the recipient monkeys were anesthetized with ketamine and pentobarbital and received T1 and T2 weighted magnetic resonance imaging (MRI) scans to localize the striatum. Several days after the initial MRI scan, the primates were again anesthetized with ketamine and pentobarbital and received four injections of 0.5 ml of ibotenic acid (Sigma, 20 mg/ml), in phosphate buffer (pH = 7.4) into the anterior putamen, utilizing stereotactic coordinates obtained from the MRI scans, with a 1.0 ml Hamilton microsyringe. Eight days following lesioning the animals again received MRI scans in order to verify correct placement of the lesion. Striatal implantation was performed nine days following the lesioning. A pregnant Rhesus monkey was anesthetized with ketamine and pentobarbital, and the fetus was exposed by Caesarean section. The brain was exposed and frontal cortex was resected with the use of a dissecting microscope. Striatal tissue was dissected from the dorsal ventricular ridge in order to obtain pure striatal precursors and resuspended in modified Hanks' solution without calcium and magnesium by repeated suctioning through a fire-polished glass micropipette. A 5.0 ml Hamilton syringe was then used to inject 5.0 ml of the cell suspension into the striatum while slowly withdrawing the syringe. Two injections were made using the same stereotactic coordinates as the lesion. Postoperatively one recipient monkey

received no immunosuppressant therapy. The other initially received cyclosporine (15 mg/kg/day) in two divided doses and prednisone (2.5 mg/day). The daily cyclosporine dose was tapered to 10 mg/kg/day over four weeks. Ten weeks following transplantation the recipient monkeys received a final MRI scan. The monkeys were then anesthetized and perfused transcardially with 50 ml of 0.12 mol/L phosphate buffer (pH 7.4) containing 0.25% procaine and 3% sucrose followed by 10 L of a fixative containing 1% paraformaldehyde, 4.0% glutaraldehyde and 3% sucrose in 0.1 mol/L phosphate buffer (pH 7.4). The head was removed four hours after perfusion and placed in the fixative overnight. The brain was removed, cut coronally at 0.5 cm with a brain knife, and photographed. The cerebral cortex was cut away from the slices and the blocks were then sectioned coronally at 80 m in 0.12 mol/L phosphate buffer containing 8% dextrose on a Lancer vibratome. The sections were rinsed for several hours in 0.12 mol/L phosphate buffer and were then histologically stained, Golgi-impregnated, or embedded for electron microscopy. Other coronal slices were paraffin-embedded, sectioned coronally at 10 m, and stained by the hematoxylin-eosin and Bielschowsky techniques.

Processing for electron microscopy. Vibratome sections were placed in 1% osmium for 1 h, followed by 3.6% sodium chloride for 30 min, and dehydrated in increasing concentrations of Quetol 523 M (Ted Pella, Inc.) in distilled water: 35%, 50%, and 70% for 10 min each; 80% and 90% for 15 min each; followed by 100% Quetol for 20 min. The sections were then floated in a 50% Quetol, 50% Maraglas solution (Ted Pella, Inc.) for 12 h followed by pure Maraglas for 6 h. The sections were flat-embedded on

siliconized microscope slides and cured for two days at 60°C. Tissue was then cut from the area of the transplant and fixed to epon blocks. Following serial thin-sectioning on a Reichert ultramicrotome, the sections were placed on formvar-coated grids, double-stained with uranyl acetate and lead citrate, and examined with a JEOL electron microscope.

Golgi impregnation. Vibratome sections were Golgi-impregnated by the "single section technique" previously described by Gabbott and Somogyi.[32] Briefly, the sections were post-fixed in 1% osmium tetroxide in 0.12 mol/L phosphate buffer for 30 min and free-floated in 3.5% potassium dichromate for 6 h. The sections were mounted between two microscope slides which were then taped together at the ends and immersed in 1.5% silver nitrate for 14 to 20 h. The sections were then mounted in glycerol and examined at the light microscopic level. Neurons well within the margins of the graft were then photographed and/or drawn using a drawing tube.

Gold toning. Sections of intereset were floated off into 0.1 mol/L phosphate buffer and gold-toned according to the method described by Fairen *et al.*[27] The tissue was placed in cold 0.04% gold chloride for 10-12 min, rinsed in cold distilled water for 20 min, and placed in 1% thiosulfate for 45 min. The sections were then reosmicated in 1% osmium tetroxide for 30 minutes and embedded as described above.

RESULTS

The striatal grafts in the monkey receiving no immunosuppression were small and showed evidence of necrosis. The two grafts in the immunosuppressed recipient were located in the anterior putamen and

measured approximately 0.4 cm x 0.8 cm (Fig. 5.1a). Grossly, the transplants appeared to be slightly darker than normal gray matter, had no evidence of hemorrhage or necrosis, and could be easily distinguished from the surrounding host brain. The vibratome sections of the grafts were more translucent than the host brain and, therefore, the graft tissue could be easily identified.

Light microscopy. The fetal striatal transplants were very cellular, containing neuronal, glial, and vascular elements (Fig. 5.1b). Hematoxylin-eosin and Nissl-stained sections demonstrated numerous neurons in various stages of development. The grafted neurons varied greatly in size, with the majority having somatic diameters between 8 and 20 μm, while a few neurons had somatic diameters up to 40 μm. In general, the medium neurons had nuclei displaying multiple nucleoli surrounded by sparse cytoplasm (Fig. 5.1c), whereas the larger neurons had a more developed nucleus and cytoplasm containing Nissl substance (Fig. 5.1d). The neuropil surrounding the transplanted neurons was incompletely developed compared to the surrounding normal striatum. Multiple inflammatory cells were seen in Virchow Robins space around some of the large blood vessels supplying the graft. However, there was no evidence of necrosis surrounding these perivascular infiltrates in the immunosuppressed recipient. The neurons were further characterized by Bielschowsky staining (Figs. 5.2a,b) and Golgi impregnation (Fig. 5.2c). The graft-host interface was clear and showed little gliosis.

Golgi-impregnation. The Golgi impregnated graft tissue was also clearly different from the host brain since the graft tissue was much less osmiophilic. The percentage of neurons and glial cells that were Golgi-impregnated within the transplant was much less than that of the surrounding normal brain. However, multiple neurons and glia cells could be identified within the transplant. Most of the Golgi-impregnated neurons had somatic diameters between 8 and 20 μm and were at various stages of maturation (Fig. 5.3). Some neurons were quite immature, displaying short, varicose dendrites with terminal growth cones and filopodia and very few, if any, dendritic spines (Fig. 5.3a). Other neurons had much longer and more elaborate dendrites, which, however, also had varicosities and growth cones (Fig. 5.3b). Cells in later stages of development were also demonstrated, some of which had dendrites measuring up to 150 mm which were aspinous proximally and moderately spined distally (Fig. 5.3c). These spines appeared to be longer and thinner than spines in the normal striatum. These neurons also had no evidence of somatic spines. Although Golgi-impregnated axons could be demonstrated within the transplant, the axons of Golgi-impregnated neurons could not be accurately characterized due to inadequate impregnation or to the axons projecting out of the given tissue section.

Electron Microscopy

Golgi impregnated cells. Electron microscopy was utilized to study the ultrastructure of several different cell types within the striatal transplant. Most of the medium-sized sparsely spined neurons contained an unindented nucleus, characteristic of the mature medium spiny neuron in the adult striatum.[20,22] However, the cytoplasm was under-developed and the nucleus

contained numerous nucleoli, typical of immature neurons (Fig. 5.4). The large neurons within the graft had long, sparsely spined dendrites and a well developed soma containing mitochondria, lysosomes, Nissl substance, and an indented nucleus displaying a single nucleolus (Fig. 5.5). These neurons were ultrastructurally similar to the mature large neurons seen in the normal primate striatum.[20,22] The dendrites of the neurons also received sparse axodendritic and axospinous contacts (Fig. 5.6). Well developed glial cells were also impregnated with the Golgi technique. One was examined at the electron microscopic level (Fig. 5.7).

Growth cones. Numerous growth cones were demonstrated in the striatal graft. Small mounds containing numerous large vesicles were seen protruding from many somatic membranes (Figs. 5.8a,b). The vesicles were pleomorphic in both size and shape, some appearing to form long tubular structures. The tips of many growing dendrites containing well developed microtubules also ended in growth cones void of organelles except large, clear vesicles (Fig. 5.8c).

Synapses. The neuropil surrounding the grafted neurons contained numerous growing dendrites which were contacted by axon terminals. Immature axodendritic synapses were frequently associated with coated vesicles (Fig. 5.9) and had little synaptic thickening (Fig. 5.10b). Other axon terminals made more mature appearing synapses with both small dendrites (Figs. 5.10a,c) and dendritic growth cones (Fig. 5.10d).

Vascular elements. The grafts contained numerous small blood vessels, most of which appeared to have intact junctional structures, suggesting that an intact blood brain barrier had been developed (Fig. 5.11).

However, other vessels were surrounded by a lymphocytic infiltrate, which, in the immunosuppressed recipient, was not associated with tissue necrosis. The blood vessels were usually associated with surrounding glial cells and numerous astrocytic foot processes.

Magnetic resonance imaging. The striatal grafts could be easily identified using T1 and T2 weighted MRI scans. Figure 5.12 demonstrates a T2 weighted scan which demonstrates the two large transplants in the anterior putamen, which correspond in both size and location to the transplants seen in Figure 5.1a. The low signal intensity in the center of the transplants probably represents iron, whereas the high signal intensity zone around the periphery of the transplant represents areas with a high water content. This "edema" correlates well with the large areas of extracellular space seen throughout the neuropil which was seen at the electron microscopic level.

DISCUSSION

In this paper, we have demonstrated that fetal striatal allografts transplanted in the lesioned Rhesus monkey striatum can survive for extended periods of time and that, ten weeks following transplantation, the grafts contained neurons at various stages of differentiation. Golgi impregnation and electron microscopic analysis confirmed that the striatal grafts consisted of maturing neuronal tissue, complete with differentiating neurons, developing neuropil, and numerous synapses. In addition, the study demonstrated that magnetic resonance imaging (MRI) can be used to localized and follow the growth patterns of fetal neuronal transplants in the brain of the primate.

The prenatal morphological development of the Rhesus monkey striatum has not been previously studied. However, Di Figlia et al.[19,21,22] performed Golgi and electron microscopic studies on the newborn Rhesus monkey neostriatum. They demonstrated that the Golgi-impregnated neurons within the newborn monkey can be classified into five neuronal types, as well as neurons which are too undifferentiated to classify. At this stage of development, most of these striatal neurons were characterized by varicose dendrites, terminal growth cones, and filopodia, characteristics typical of immature dendrites.[50-52,67-69] Their study demonstrated that the medium spiny neuron had an increasing spine density with increasing age, with the dendritic spine distribution the same as in the adult striatal neuron. Throughout all stages of maturation, these neurons had aspinous proximal dendrites and moderately to densely spined distal dendrites. In the present study, we have demonstrated that the transplanted fetal striatal neurons were at various stages of maturation. Some transplanted neurons exhibited the same immature dendritic features as the neurons described in the newborn primate. However, the spine density of the neurons in the present study was less than in the newborn primate, probably because the post-gestational age of the transplanted neurons (E125-140) was less than that of the newborn (E165).

At the electron microscopic level, Di Figlia et al.[22] confirmed that the newborn primate striatum contains somata and dendrites at various stages of maturation, displaying dendritic and axonal growth cones, filopodia, and varicosities. Multiple investigators have demonstrated that axospinous and axodendritic synapses are apparent in the neonatal primate, and that

axosomatic synapses tend to develop at a later age.[5,22] In the present study, we also demonstrated at the electron microscopic level that neurons at various stages of maturation are present in the fetal striatal transplants. The axonal and dendritic ultrastructure of the transplanted cells are similar to that of normal developing neurons.[7,18,44,55,67-69,70] The presence of axodendritic contacts in the neuropil demonstrates that connections are being formed by the transplanted neurons, even at this relatively early age. Whether the presynaptic boutons in the transplants are from host neurons, graft neurons, or both, will have to be determined in subsequent studies. The large areas of extracellular space seen in the striatal transplant were not seen by DiFiglia et al.[22] in the neonatal striatum, probably because the transplant was slightly more immature than the neonatal tissue.

It is now widely accepted that fetal neuronal transplants can ameliorate the behavioral and biochemical changes seen after the lesioning of various areas of the rat brain. Multiple investigators have now attempted to extend these studies into the primate, but most have reported difficulties with graft growth. Morihisa et al.[53] reported that no surviving catecholaminergic neurons were seen after three to eight months in their nigral transplants in the rhesus monkey. In contrast, Redmond et al.[57] and Sladek et al.[61] demonstrated that grafted dopaminergic neurons can survive and mature in the striatum of the African Green monkeys, although their transplants were of limited size. In the present study we have demonstrated that primate fetal striatal allografts can survive in enormous numbers for at least 10 weeks after transplantation. We believe that the success of these

transplants is dependent on technical considerations, appropriate fetal age, and postoperative immunosuppression.

During the transplantation procedure, the primate fetus was kept attached to the umbilical cord prior to the dissection of the brain in order that the blood supply to the fetal neurons was kept intact as long as possible. In addition, the time from which the first neuroblast was taken from the fetus to the time when the last transplant injection was made was less than 10 minutes, during which time the cell suspension was kept cold. These efforts to increase the oxygen supply and decrease the metabolic needs of the neuroblasts most likely added to the success of transplanting large numbers of viable neurons.

The fetal striatal neurons in the present study were obtained from Rhesus monkey fetuses which were between 55 and 70 days post-gestation, as opposed to 13-15 days post-gestation used in previous rat studies. Brand and Rakic[6] demonstrated in a ^{3}H-thymidine autoradiographic study that striatal neurons are generated during a 45-day period in the first half of gestation. Large striatal neurons with somatic diameters between 25 and 40 μm are generated between embryonic age 36 and 43 days, whereas small striatal neurons with somatic diameters between 13 and 22 μm are generated between embryonic age 36 and 70 days. Therefore, the fetal striatal tissue that was used in the present study contained most of the potential neuronal elements of the adult striatum, except for possibly a few small neurons which would have been generated for a short period after the harvest of the fetal cells. The window during which fetal striatal neurons can be successfully transplanted in the Rhesus monkey is currently not

known. Theoretically, any striatal neuroblasts present in the developing brain have the potential to be successfully transplanted. Since the generation of striatal neuroblasts begins at gestational age 36 days, it is possible that these initial cells could be transplanted at this stage. The optimal gestational age at which fetal striatal neuroblasts should be transplanted is probably 70 days, since at this time all of the striatal neurons have been generated and are still undifferentiated. It is currently not known whether neuroblasts with gestational ages later than 70 days can be used for transplantation, but it is probable that striatal neuroblasts can be successfully transplanted in cell suspensions up until they develop neuronal processes. Since Golgi and electron microscopic studies have not been performed on fetal primates, the gestational age at which this occurs is presently undetermined.

The importance of immunosuppression in the survival of primate neuronal allografts remains a controversial area. In this study striatal grafts in the non-immunosuppressed recipient were small and showed evidence of necrosis, whereas the striatal grafts in the immunosuppressed recipient were large and showed no evidence of necrosis. However, even in the immunosuppressed primate, the grafts produced a perivascular inflammatory response. The importance of these lymphocytic infiltrates to the extended survival of the grafts past 10 weeks is unclear. It is possible that the inflammatory response will be completely benign, since the grafted neural tissue was left completely intact. In future studies, the use of immunosuppression may prove to be essential for the healthy long-term survival of neural transplants in primates.

One of the major problems in studying the neuroanatomy of fetal grafts concerns the precise localization of the transplant within the host brain so that anterograde or retrograde tracers can be injected within the transplant in order to determine the grafts' afferent and efferent connections. Perschanski et al.[54] demonstrated that neuronal grafts can be visualized *in vivo* using MRI, although the resolution was relatively poor. In the present study, we have demonstrated that MRI can also be used to localize neuronal transplants within the primate brain. With the addition of an MRI-compatible stereotactic frame, accurate injections of these tracers could be obtained. In addition, an MRI-compatible frame could be used to inject neuroanatomical tracers within the host brain in order to anterogradely label the grafts' afferent fibers or retrogradely label the grafts' projection neurons. With larger magnets and improved software, the resolution of the MRIs should improve over the next decade, which will make it even easier to visualize the transplant and normal structures within the primate brain. It is also possible that MRI imaging can be used to follow graft rejection by monitoring graft size or imaging characteristics.

Many neuroscientists have hypothesized that the use of fetal neuronal tissue may be used in the future to treat human disease. However, the extension of these studies into the primate has been problematic. The cost of primate research has proved to be enormous, which has decreased the number of transplant studies done in the primate as well as the total number of animals used in each study. In addition, behavioral changes seen in the primate after lesioning of the striatum, substantia nigra, or basal forebrain are more complex than those seen in the rat, and it is, therefore, much more

difficult to study behavioral improvements after fetal transplantation. Finally, the inflammatory response seen in transplanted neuronal tissue in the primate, even after immunosuppression, is not seen in rat neuronal allografts. Further studies will need to be done in order to determine which immunosuppressant regimen will lead to the best graft survival in primates. Once these difficulties have been overcome, it will be possible to further delineate the neuroanatomy of the neuronal grafts within the primate, including their neurochemical differentiation, morphologic development, and afferent and efferent connectivity with the host brain.

Figures and Tables

Figure 5.1: Primate neostriatal grafts. a. Coronal section through the anterior putamen of a Rhesus monkey brain demonstrating two large fetal striatal transplants, 10 weeks post-transplantation (arrowheads). Note that there is no evidence of hemorrhage or necrosis within the transplants. Scale bar = 1 cm. **b:** Photomicrography of fetal striatal transplant demonstrating neuronal, glial and vascular elements (hematoxylin-eosin, H&E). Scale bar = 100 μm. c: High power magnification photomicrograph of a cluster of medium-sized neurons displaying multiple nucleoli and sparse cytoplasm within the transplant (H&E). Scale bar = 30 μm. d: High power photomicrograph displaying a large mature appearing neuron (arrow) within the striatal graft which is surrounded by numerous smaller and more immature neurons (H&E). Scale bar = 30 μm.

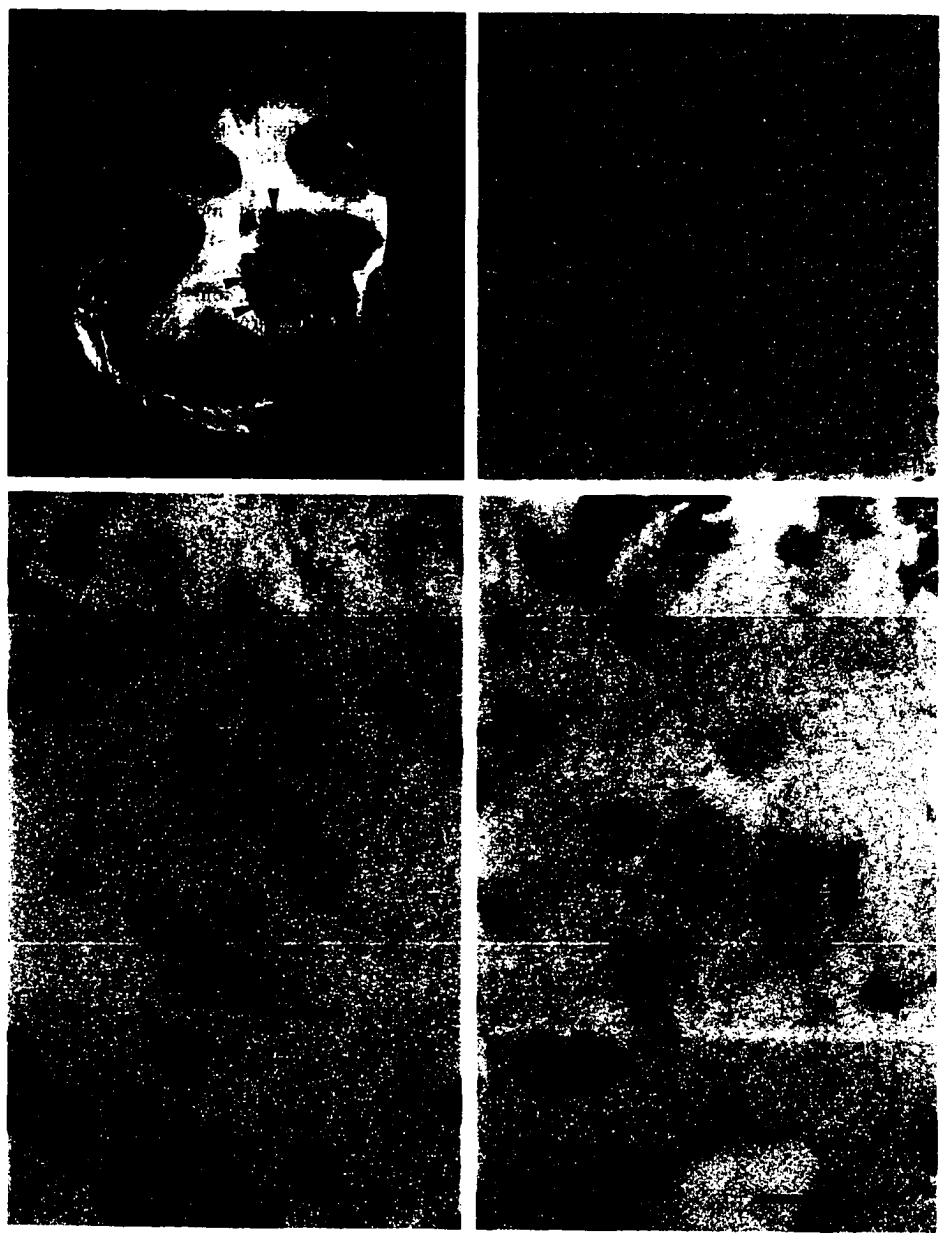

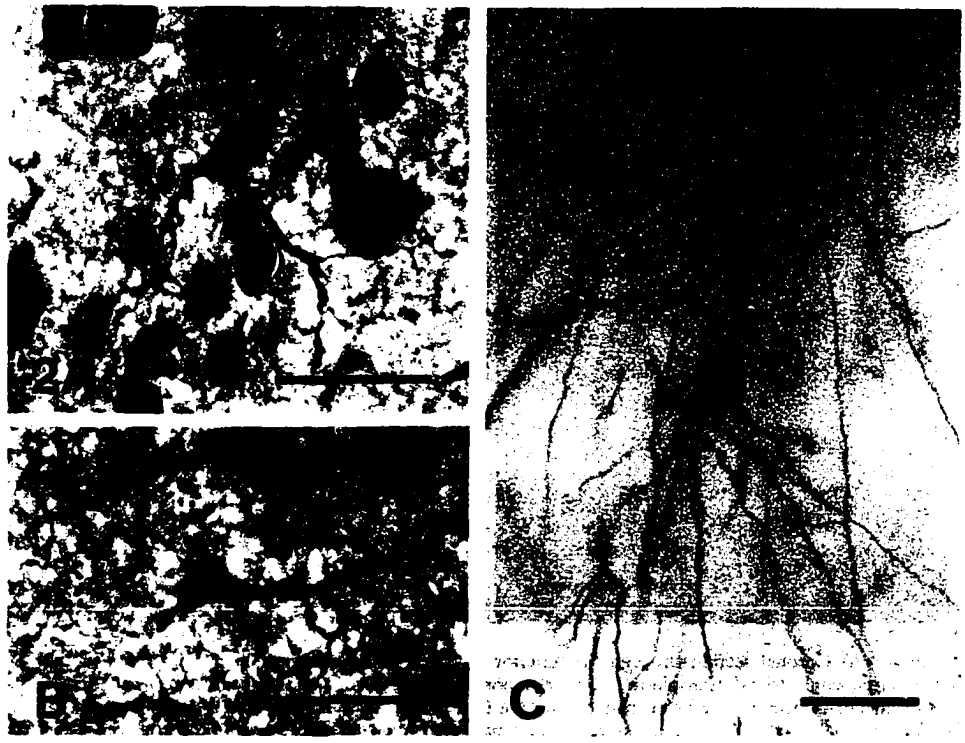

Figure 5.2: Neurons in neostriatal graft. **a, b:** High power photomicrographs of two grafted striatal neurons demonstrating long dendritic processes (Bielschowsky method). Scale bars = 30 μm. **c:** Photomicrograph of Golgi impregnated neuron within a striatal graft demonstrating long, moderately spined dendrites and a smooth, medium-sized soma. Scale bar = 50 μm.

Figure 5.3: Camera lucida drawings of Golgi-impregnated neurons within a primate fetal striatal graft. **a:** Undifferentiated neuron displaying varicose dendrites and terminal growth cones (open arrows). **b:** Maturing neuron displaying dendrites with varicosities, growth cones and filopodia (closed arrow). **c:** A more differentiated neuron displaying multiple dendritic spines and few dendritic varicosities. **d:** A neuron with dendrites at various stages of development. Some of the dendrites exhibit varicosities, growth cones and filopodia, while others have a more mature appearance, displaying multiple spines. Scale bars = 50 μm.

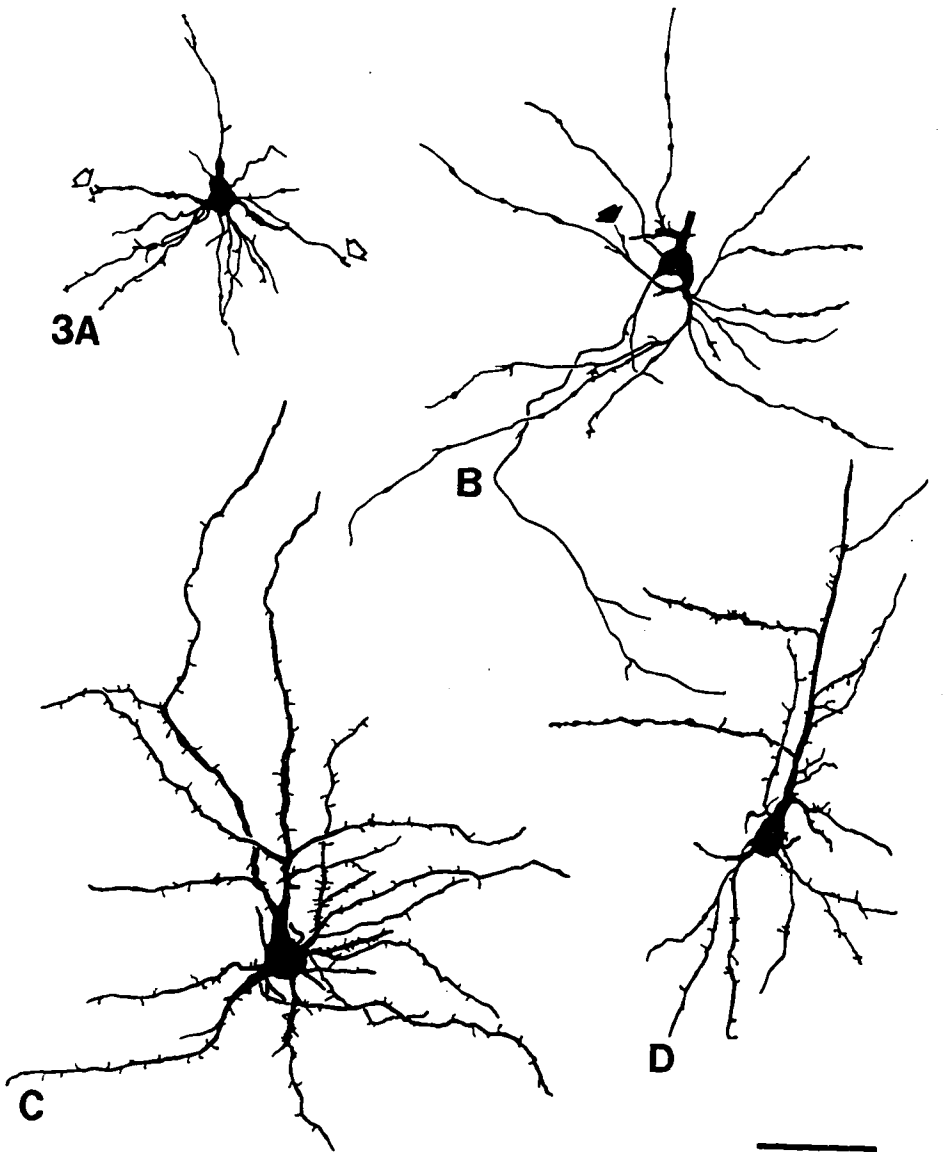

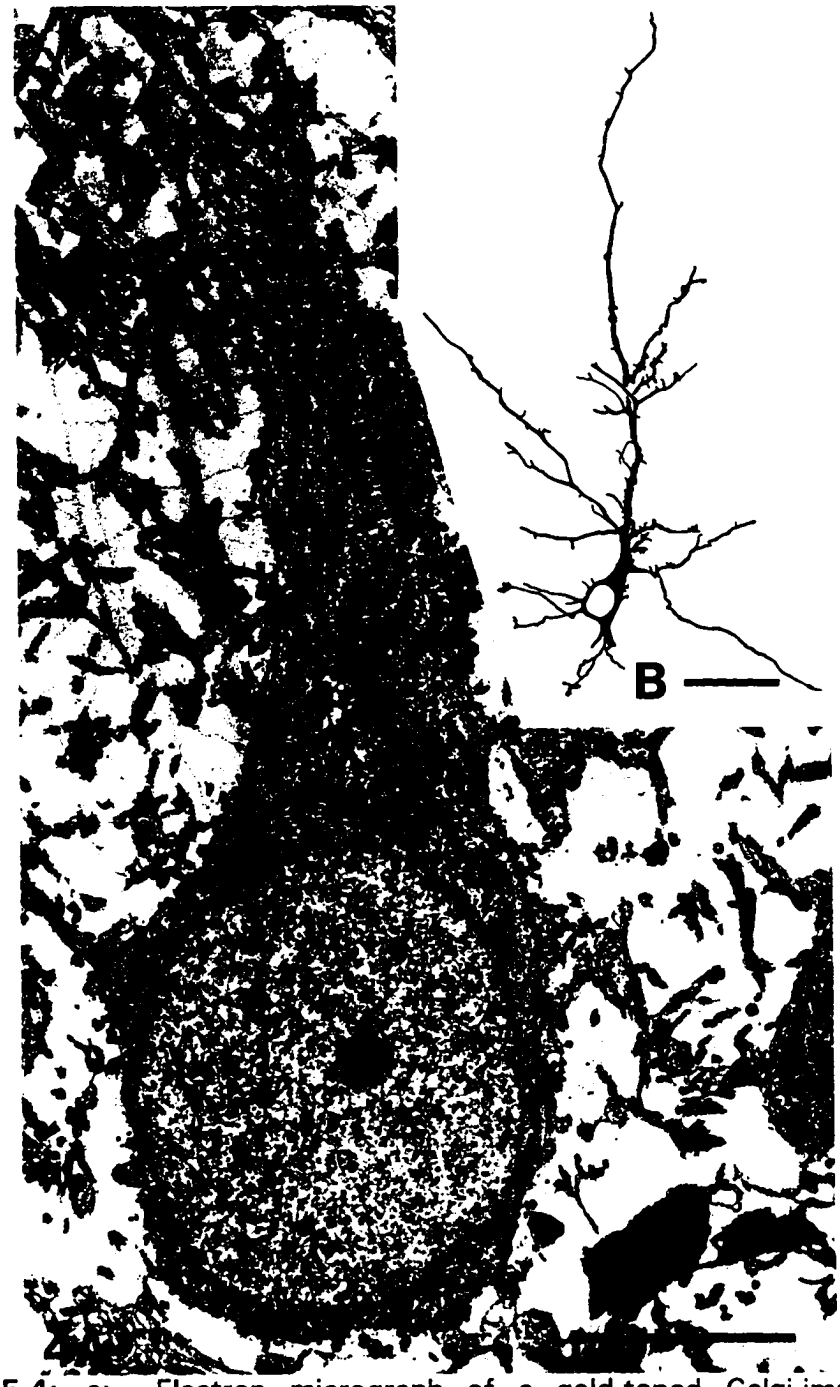

Figure 5.4: a: Electron micrograph of a gold-toned Golgi-impregnated neuron demonstrating a medium-sized soma containing sparse cytoplasm, an indented nucleus, and a large primary dendrite. Scale bar = 4 μm. b: Camera lucida drawing of the gold-toned Golgi-impregnated neuron seen in A demonstrating sparsely spined dendrites. Scale bar = 25 μm.

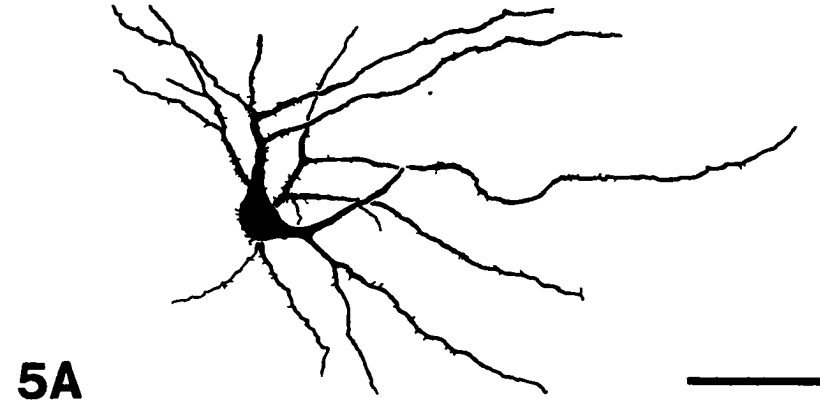

5A

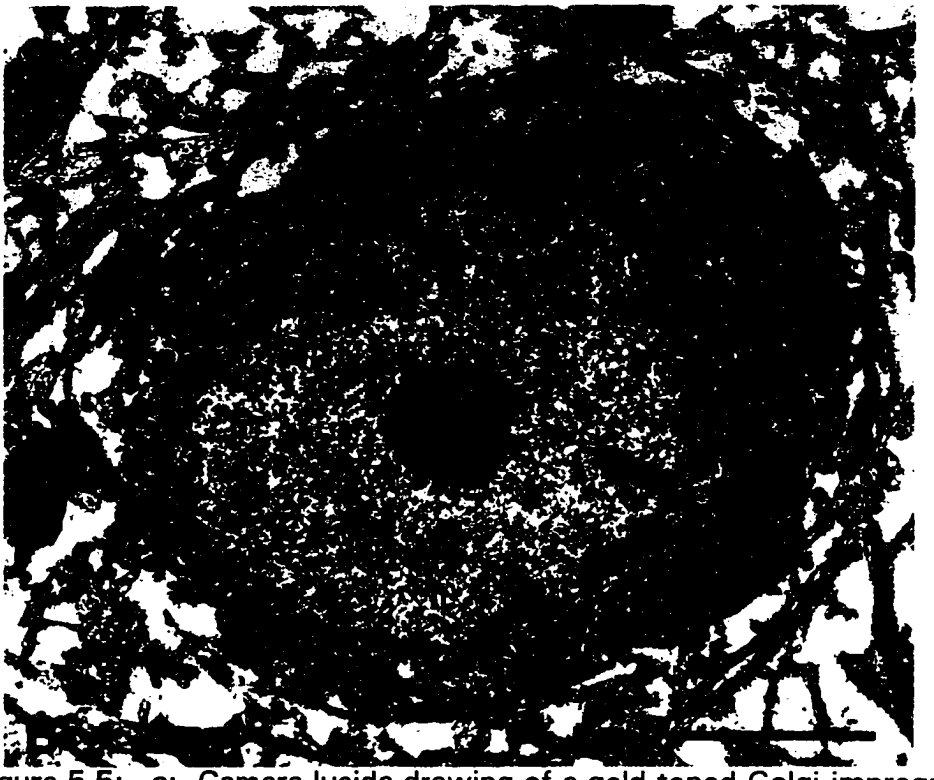

Figure 5.5: a: Camera lucida drawing of a gold-toned Golgi-impregnated neuron with a large somatic diameter, several somatic spines and long sparsely-spined dendrites. Scale bar = 100 μm. b: Electron micrograph of the neuron shown in A demonstrating a highly indented nucleus surrounded by copious cytoplasm rich in organelles. Scale bar = 5 μm.

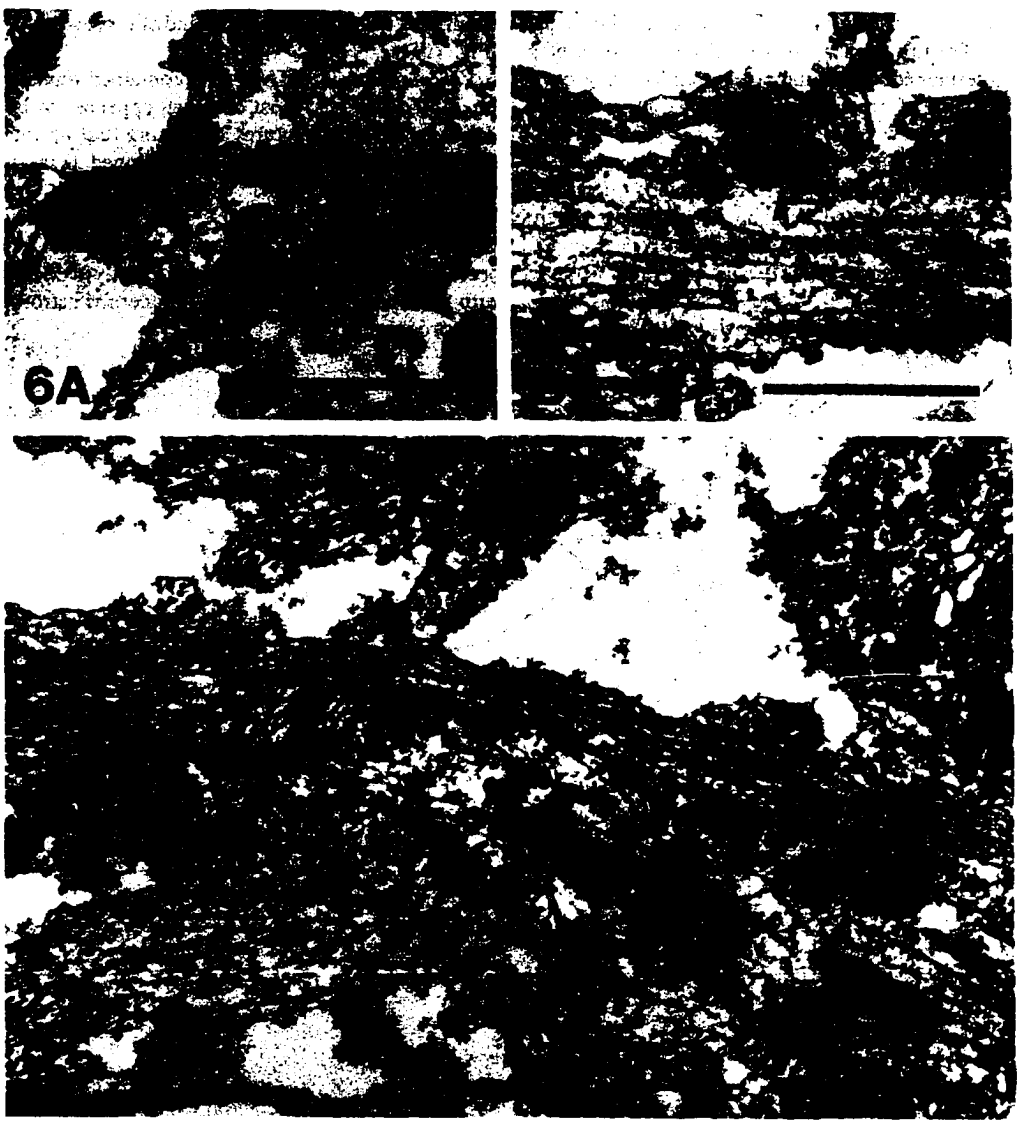

Figure 5.6: Electron micrographs of gold-toned Golgi-impregnated dendrites of the neuron shown in Fig. 5 which receive sparse axodendritic contacts (arrowheads). Scale bars = 1 μm.

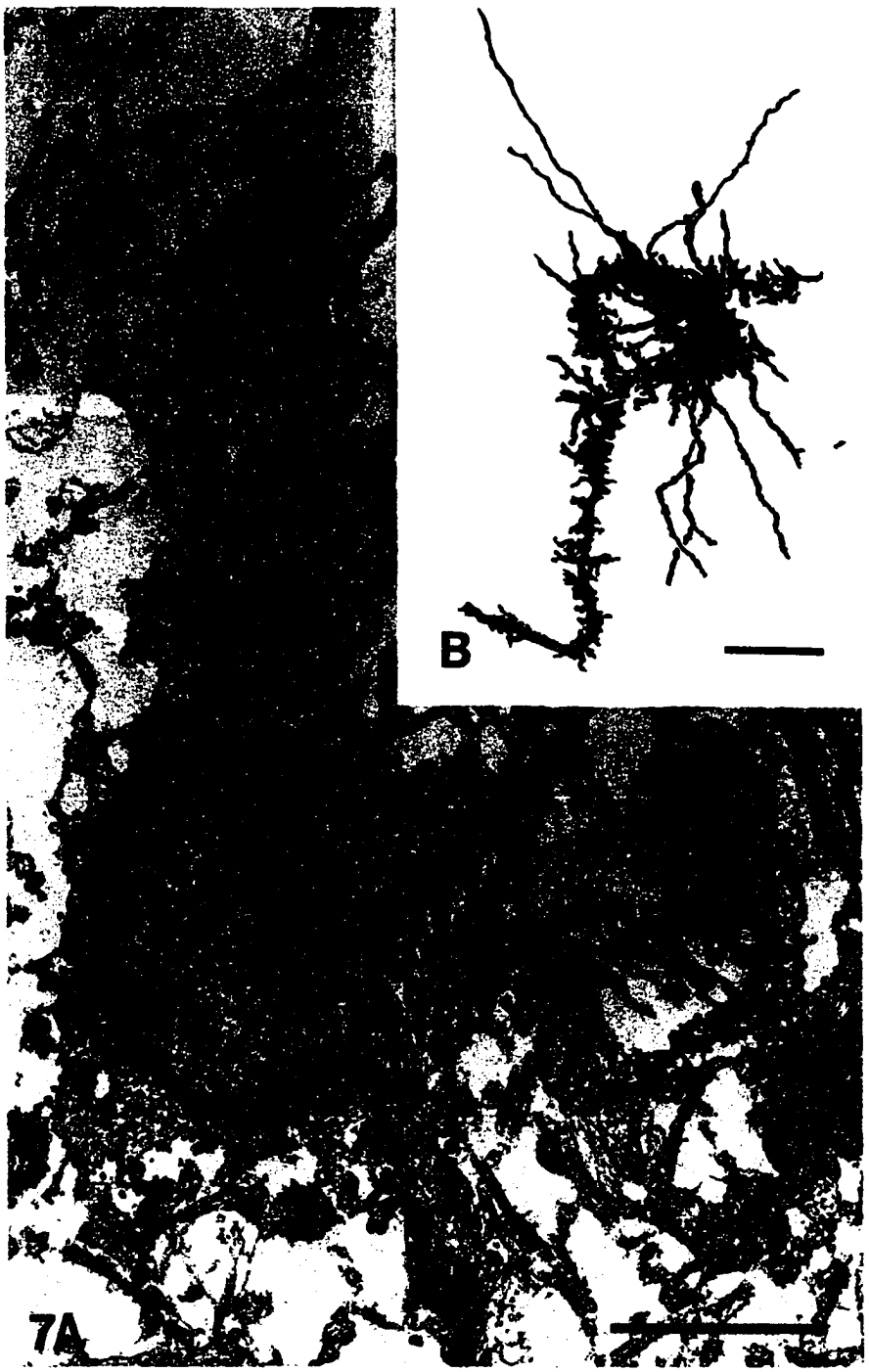

Figure 5.7: **a.** Electron micrograph of a gold-toned Golgi-impregnated fibrous astrocyte with a nucleus (n), a cytoplasm rich in filaments, and numerous processes. Scale bar = 2.5 μm. A camera lucida drawing of the cell is demonstrated in **b** (Scale bar = 10 μm).

Figure 5.8: a: Electron micrograph of a neuron in a transplant with a nucleus (n) and a bulge in the cytoplasmic membrane (arrowheads) containing numerous, pleomorphic large vesicles, probably representing a primordial dendritic growth cone. Scale bar = 2.0 μm. The structure is demonstrated at a larger magnification in b (Scale bar = 0.75 μm). c: A dendrite (d) within the transplant with a terminal growth (arrowheads) containing numerous large vesicles. Scale bar = 0.75 μm.

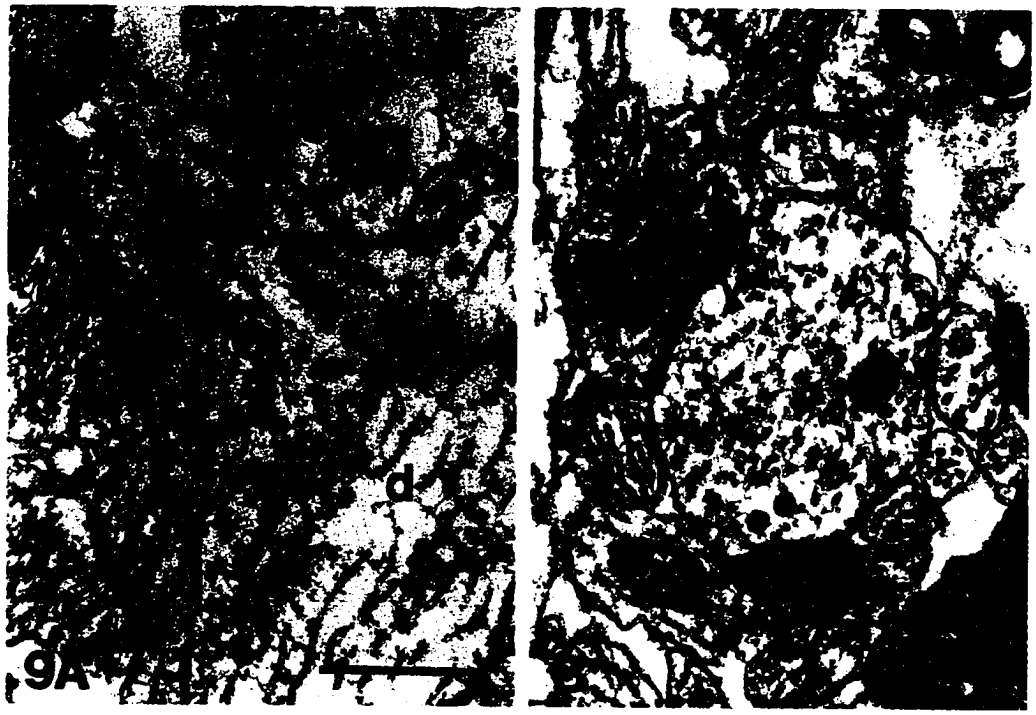

Figure 5.9: a: Electron micrograph of a dendrite (d) within a transplant which has a smaller dendrite forming a coated vesicle (arrowhead). The region is in close apposition to an axon terminal. b: Electron micrograph of an immature synapse which has apparently added a coated vesicle to its membrane (arrowhead) and has an associated coated vesicle in the dendrites cytoplasm. Scale bars = 0.5 μm.

Figure 5.10: Electron micrographs of axodendritic synapses (arrowheads) within the striatal allograft. **a**: A mature axodendritic contact with normal membrane thickenings. **b**: An immature synapse with underdeveloped membrane thickenings. **c**: A dendrite receiving numerous axonal contacts. **d**: An axon terminal contacting both a dendritic growth cone and a more mature dendrite. Scale bars = 0.75 μm.

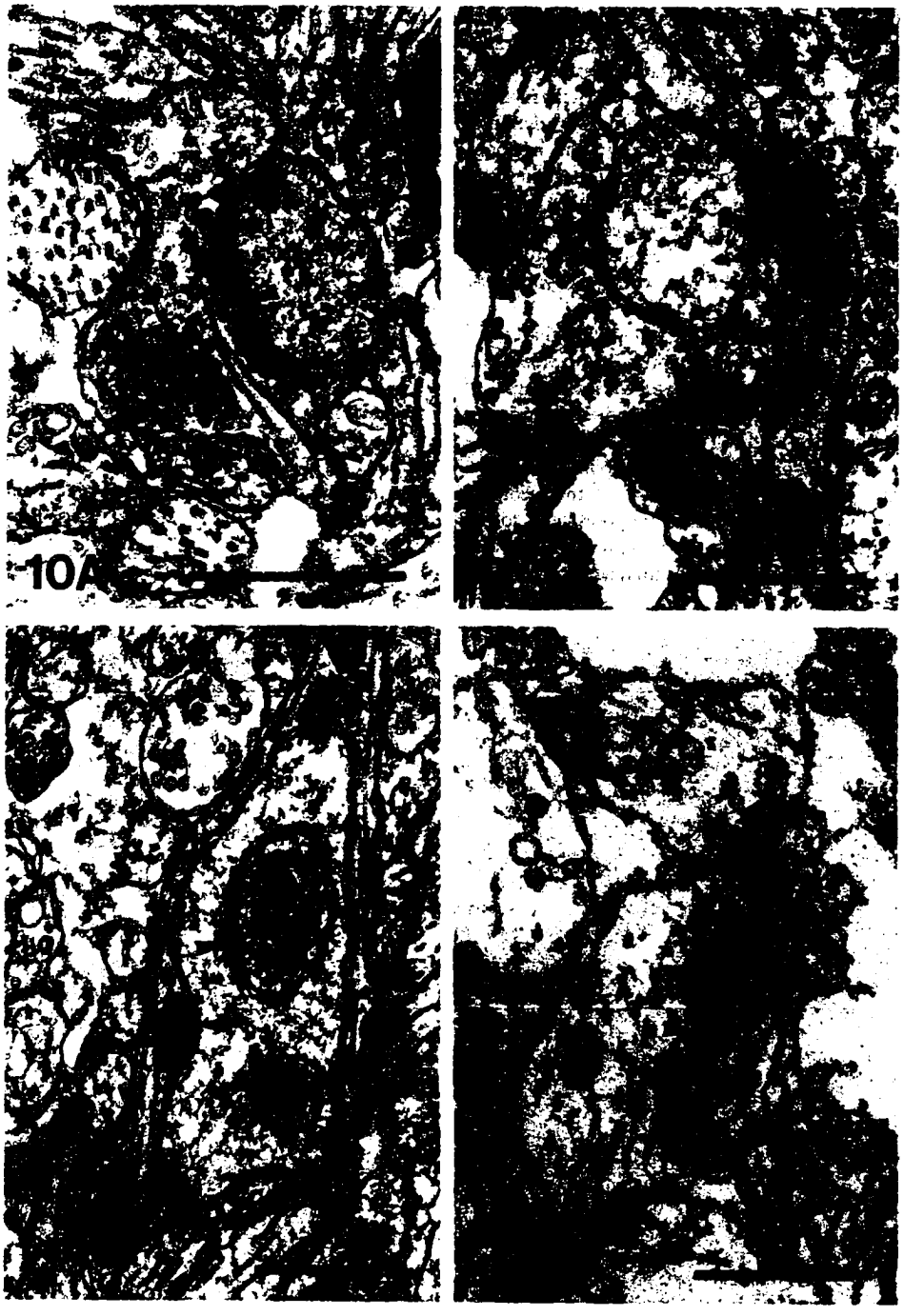

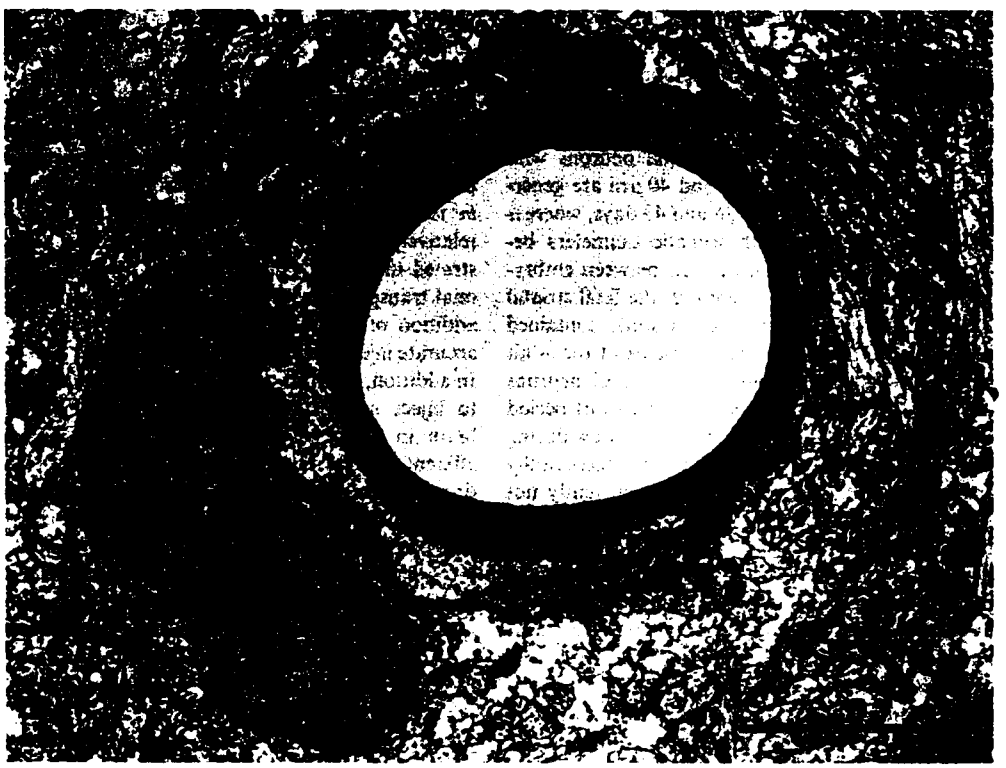

Figure 5.11: Electron micrograph of a small blood vessel within the transplant with an associated glial cell (g). Note the normal tight junctions formed by the endothelial lining of the capillary. Scale bar = 3.0 μm.

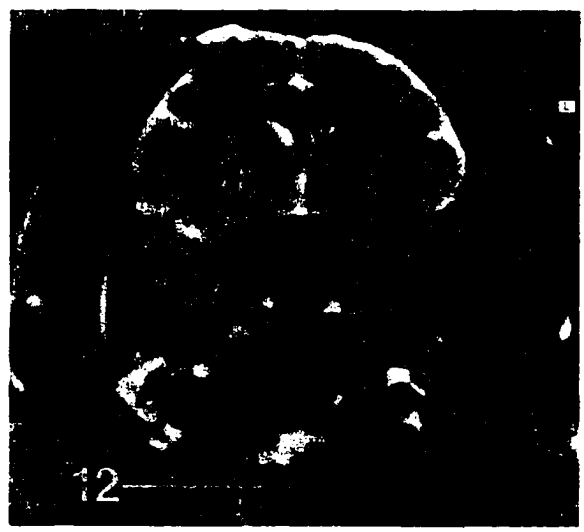

Figure 5.12: Magnetic resonance image (T2 weighted) of the primate brain 10 weeks after transplantation. The striatal transplants are characterized by a low signal center surrounded by a high signal zone (arrowheads), most likely representing high water content. t = temporal lobe, v = ventricle. Scale bar = 2.0 cm.

References

1. Adinolfi A. M. (1977) The postnatal development of the caudate nucleus: a Golgi and electron microscopic study of kittens. Brain Res. 133:251-266.
2. Björklund A. and Stenevi U. (1985) Neuronal Grafting in the Mammalian CNS. Elsevier, Amsterdam.
3. Björklund A., Stenevi U. and Svendgaard N. A. (1976) Growth of transplanted monoaminergic neurones into the adult rat hippocampus along the perforant path. Nature 262:787-790.
4. Bolam J. P. (1984) Synapses of identified neurons in the neostriatum. Ciba Found. Symp. 107:30-47.
5. Brand S. and Rakic P. (1979) Synaptogenesis in the caudate nucleus of the pre- and postnatal rhesus monkeys. Anat. Rec. 193:490 (Abstract)
6. Brand S. and Rakic P. (1979) Genesis of the primate neostriatum: ^{3}H-thymidine autoradiographic analysis of the time of neuron origin in the rhesus monkey. Neuroscience 4:767-778.
7. Bunge M. B. (1973) Fine structure of nerve fibers and growth cones of isolated sympathetic neurons in culture. J. Cell Biol. 56:713-735.
8. Carder R. K., Snyder-Keller A. M. and Lund R. D. (1988) Behavioral and anatomical correlates of immunologically induced rejection of nigral xenografts. J. Comp. Neurol. 277: 391-402.
9. Chang H. T., Wilson C. J. and Kitai S. T. (1982) A Golgi study of rat neostriatal neurons: Light microscopic analysis. J. Comp. Neurol. 208:107-126.

10. Clarke D. J., Dunnett S. B., Isacson O., Sirinathsinghji, D. J. S. and Björklund A. (1988) : Striatal grafts in rats with unilateral neostriatal lesions - I. Ultrastructural evidence of afferent synaptic inputs from the host nigrostriatal pathway. Neuroscience 24:791-801.

11. Clarke D. J., Gage F. H. and Björklund A. (1986) Formation of cholinergic synapses by intrahippocampal septal grafts as revealed by choline acetyltransferase immunocytochemistry. Brain Res. 369:151-162.

12. Collier T. J., Redmond D. E. Jr., Sladek C. D., Gallagher M. J., Roth R. H., Sladek J. R., Jr. (1987) Intracerebral grafting and culture of cryopreserved primate dopamine neurons. Brain Res. 436:363-366.

13. Coyle J. T. and Schwarcz R. (1976) Lesion of striatal neurones with kianic acid provides a model of Huntington's chorea. Nature 263:244-246.

14. Crossman A. R. (1987) Primate models of dyskinesia, the experimental approach to the study of basal ganglia-related involuntary movement disorders. Neuroscience 21:1-40.

15. Deckel A. W., Moran T. H. and Robinson R. G. (1986) Behavioral recovery following kainic acid lesions and fetal implants of the striatum occurs independently of dopaminergic mechanisms. Brain Res. 363:383-385.

16. Deckel A. W., Moran T. H., Coyle J. T., Sandberg P. R. and Robinson R. G. (1986) Anatomical predictors of behavioral recovery following fetal striatal transplants. Brain Res. 365:249-258.

17. Deckel A. W., Robinson R. G., Coyle J. T. and Sandberg P. R. (1983) Reversal of long-term locomotor abnormalities in the kainic acid model of Huntington's disease by day 18 fetal striatal implants. Eur. J. Pharmacol. 93:287-288.

18. Del Cerro M. P. and Snider R. S. (1968) Studies on the developing cerebellum. Ultrastructure of the growth cones. J. Comp. Neurol. 133:341-362.

19. DiFiglia M., Pasik P. and Pasik T. (1976) Quantitative morphology of monkey neostriatum: one-week old vs. adult. Neurosci. Abstr. 2:61.

20. DiFiglia M., Pasik P. and Pasik T. (1976) A Golgi study of neuronal types in the neostriatum of monkeys. Brain Res. 114:245-256.

21. DiFiglia M., Pasik P. and Pasik T. (1979) Developmental aspects of neostriatal organization in monkeys. Appl. Neurophysiol. 42:81-83.

22. DiFiglia M., Pasik P. and Pasik T. (1980) Early postnatal development of the monkey neostriatum: a Golgi and ultrastructural study. J. comp. Neurol. 19:303-331.

23. DiFiglia M., Schiff L. and Deckel A. W. (1988) Neuronal organization of fetal striatal grafts in kainate- and sham-lesioned rat caudate nucleus: Light and electron-microscopic observations. J. Neurosci. 8:1112-1130.

24. DiMova R., Vuillet J. and Seite R. (1980) Study of rat neostriatum using a combined Golgi-electron microscopic technique and serial sections. Neuroscience 5:1581-1596.

25. Dubach M., Schmidt R. H., Martin R., German D. C. and Gowden D. M. (1988) Transplant improves hemiparkinsonian syndrome in

nonhuman primate: Intracerebral injection, rotometry, tyrosine hydroxylase immunohistochemistry. Progress in Brain Research, Vol. 78 (eds Gash D. M. and Sladek J. R. Jr.), pp. 491-496. Elsevier, New York.

26. Dunnett S. B., Low W.C., Iversen S.D., Stenevi U. and Björklund A. (1982) Septal transplants restore maze learning in rats with fornix-fimbria lesions. Brain Res 251, 335-348.

27. Fairen A., Peters A. and Saldanha J. (1979) A new procedure for examining Golgi impregnated neurons by light and electron microscopy. J. Neurocytol. 6,311-337.

28. Fine A., Hunt S. P., Oertel W. H., Nomoto M., Chang P. N., Bond A., Waters C., Temlett J. A., Annett L., Dunnett S., Jenner P. and Marsden C. D. (1988) Transplantation of embryonic marmoset dopaminergic neurons to the corpus striatum of marmosets rendered parkinsonian by 1-methyl-4-phenyl-1,2,3,6-tetrahydropyridine. Progress in Brain Research, Vol. 78 (eds Gash D. M. and Sladek J. R., Jr), pp. 479-489. Elsevier, New York.

29. Fox C. A., Andrade A. N., Hillman D. E. and Schwyn R. C. (1971/1972) The spiney neurons of the primate neostriatum: a Golgi and electron microscopic study. J. Hirnforsch. 13:181-201.

30. Fox C. A., Andrade A. N., Hillman D. E. and Schwyn R. C. (1971/1972) The aspiney neurons and the glia in the primate striatum: a Golgi and electron microscopic study. J. Hirnforsch. 13:341-362.

31. Freund T. F., Bolam J. P., Björklund A., Stenevi U., Dunnett S. B., Powell J. F. and Smith A. D. (1985) Efferent synaptic connections of

grafted dopaminergic neurons reinnervating the host neostriatum: a tyrosine hydroxylase study. J. Neurosci. 5:603-616.

32. Gabbott P. L. and Somogyi J. (1984) The "single" section Golgi-impregnation procedure: Methodological description. J. Neurosci. Methods 11:221-230.

33. Graveland G. A., Williams R. S. and DiFiglia M. (1985) Evidence for degenerative and regenerative changes in neostriatal spiny neurons in Huntington's disease. Science 227:770-773.

34. Hantraye P., Richie D., Maziere M. and Isacson O. (1990) A primate model of Huntington's disease: Behavioral and anatomical studies of unilateral excitotoxic lesions of the caudate-putamen in the baboon. Exp. Neurol. 108:91-104.

35. Helm G. A., Palmer P. E. and Bennett J. P., Jr. (1991) Fetal neostriatal transplants in the rat: A light and electron microscopic Golgi study. Neuroscience 37:735-756.

36. Helm G. A., Palmer P. E. and Bennett J. P. Jr. (1992) Choline acetyltransferase and substance P-like immunoreactive elements in fetal striatal grafts. a correlated light and electron microscopic study. Neuroscience 47:621-639.

37. Helm G. A., Robertson M. W., Jallo G. I., Simmons N. and Bennett J. P. Jr. (1991) Development of D1 and D2 dopamine receptors and associated second messenger systems in fetal striatal transplants. Exp. Neurol. :181-189.

38. Isacson O., Brundin P., Gage F. H. and Björklund A. (1985) Neuronal grafting in a rat model of Huntington's disease: progressive

neurochemical changes after ibotenate lesions and striatal tissue grafting. Neuroscience 16:799-817.

39. Isacson O., Brundin P., Kelly P. A. T., Gage, F. H. and Björklund A. (1984) Functional neuronal replacement by grafted striatal neurones in ibotenic lesioned rat striatum. Nature 311: 458-460.

40. Isacson O., Dawbarn D., Brundin P., Gage F. H., Emson P. C. and Björklund A. (1987) Neuronal grafting in a rat model of Huntington's disease: striosomal-like organization of striatal grafts as revealed by acetylcholinesterase histochemistry, immunocytochemistry and receptor autoradiography. Neuroscience 22: 481-497.

41. Isacson O., Dunnett S. B. and Björklund A. (1986) Behavioral recovery in an animal model of Huntington's disease. Proc. Nat. Acad. Sci. U. S. A. 83:2728-2732.

42. Isacson O., Riche D., Hantraye P., Sofroniew M. V. and Maziere M. (1989) A primate model of Huntington's disease: cross-species implantation of striatal precursor cells to the excitotoxically lesioned baboon caudate-putamen. Exp. Brain Res. 75:213-220.

43. Kanazawa I., Tanaka Y. and Cho F. (1986) "Choreic" movement induced by unilateral kainate lesion of the striatum and l-DOPA administration in monkey. Neurosci. Lett.71:241-246.

44. Kawana E., Sandri C. and Akert K. (1971) Ultrastructure of growth cones in the cerebellar cortex of the neonatal rat and cat. Z. Zellforsch. 115:284-298.

45. Köhler C. and Schwarcz R., (1983) Comparison of ibotenic and kainate neurotoxicity in the rat brain: a histologic study. Neuroscience 8:819-835.

46. Lu E. J. and Brown W. J. (1977) The developing caudate nucleus in the euthyroid and hypothyroid rat. J. Comp. Neurol. 171:261-284.

47. Martin J. B. (1984) Huntington's disease: new approaches to an old problem. Neurol 34:1059-1072.

48. McAllister J. P., Walker P. D., Zemanick M. C., Weber A. B., Kaplan L. I. and Reynolds M. A. (1985) Morphology of embryonic neostriatal cell suspensions transplanted into adult neostriata. Dev. Brain Res. 23:282-286.

49. McGeer E. G. and McGeer P. L. (1976) Duplication of biochemical changes of Huntington's chorea by intrastriatal injection of glutamic and kainic acids. Nature 263:517-519.

50. Morest D. K. (1969) The differentiation of cerebral dendrites: a study of the post-migratory neuroblast in the medial nucleus of the trapezoid body. Z. Anat. Entwickl.-Gesch. 128:271-289.

51. Morest D. K. (1969) The growth of dendrites in the mammalian brain. Z. Anat. Entwickl.-Gesch. 128:290-317.

52. Morest D. K. (1970) A study of neurogenesis in the forebrain of opossum pouch young. Z. Anat. Entwickl.-Gesch. 130:265-305.

53. Morihisa J. M., Nakamura R. K. and Freed W. J. (1984) Adrenal medulla grafts survive and exhibit catecholamine-specific fluorescence in the primate brain. Exp. Neurol. 84:643-653.

54. Peschanski M., Rudin M., Isacson O., Delepierre M. and Roques B. P. (1988) Magnetic resonance imaging of intracerebral neural grafts. Progress in Brain Reserch, Vol. 78. (eds Gash D. M. and Sladek J. R. Jr.), pp. 619-624. Elsevier, New York.

55. Povlishock J. T. (1976) The fine structure of the axons and growth cones of the human fetal cerebral cortex. Brain Res. 114:379-389

56. Pritzel M., Isacson O., Brundin P., Wiklund L. and Björklund A. (1986) Afferent and efferent connections of striatal grafts implanted into the ibotenic acid lesioned neostriatum in adult rats. Exp. Brain Res. 65: 112-126.

57. Redmond D. E., Sladek J. R., Roth R. H. Collier T. J., Elsworth J. D., Deutch A. Y. and Haber S. (1986) Fetal neuronal grafts in monkeys given methylphenyltetrahydropyridine. Lancet 1:1125-1127.

58. Reiner A., Albin R. L., Anderson K. D., D'Amato C. J., Penney J. B. and Young A. B. (1988) Differential loss of striatal projection neurons in Huntington's disease. Proc. Natl. Acad. Sci. U.S.A. 85:5733-5737.

59. Roberts R. C. and DiFiglia M. (1988) Localization of immunoreactive GABA and enkephalin and NADPH-diaphorase-positive neurons in fetal striatal grafts in the quinolinic-acid-lesioned rat neostriatum. J. Comp. Neurol. 274:406-421.

60. Sirinathsinghji D. J. S., Dunnett S. B., Isacson O., Clarke D. J., Kendrick K. and Björklund A. (1988) Striatal grafts in rats with unilateral neostriatal lesions - II. *In vivo* monitoring of GABA release in globus pallidus and substantia nigra. Neuroscience 24:803-811.

61. Sladek J. R. Jr., Collier T. J., Haber S. N., Roth R. H. and Redmond D. E. Jr. (1986) Survival and growth of fetal catecholamine neurons transplanted into primate brain. Brain Res. Bull. 17:809-818,

62. Sladek J. R. Jr., Collier T. J., Haber S. N., Deutch A. Y., Elsworth J. D., Roth R. H. and Redmond D. E. Jr. (1987) Reversal of parkinsonism by fetal nerve cell transplants in primate brain. Ann. N. Y. Acad. Sci. 495, 641-657.

63. Sladek J. R. and Gash D. M. (1988) Nerve cell grafting in Parkinson's disease. J. Neurosurg. 68:337-351.

64. Sladek J. R. Jr., Redmond D. E. Jr., Collier T. J., Haber, S. N., Elsworth J. D., Deutch A. Y. and Roth R. H. (1987) Transplantation of fetal dopamine neurons in primate brain reverses MPTP induced parkinsonism. Progress in Brain Research, Vol. 71 (eds Seil F. J, Herbert E. and Carlson B. M.), pp. 309-323. Elsevier, New York.

65. Somogyi P. and Smith A. D. (1979) Projection of neostriatal spiney neuron to the substantia nigra. Application of a combined Golgi-staining and horseradish peroxidase transport procedure at both the light and electron microscopic levels. Brain Res. 178:3-15.

66. Somogyi P., Bolam J. P. and Smith A. D. (1981) Monosynaptic cortical input and local axon collaterals of identified striatonigral neurons. a light and electron microscopic study using the Golgi-peroxidase transport-degeneration procedure. J. Comp. Neurol. 195: 567-584.

67. Tanaka D. Jr. (1977) Dendritic development of small caudate neurons in the puppy: a Golgi study. Anat. Rec. 187:781. (Abstract)

68. Tanaka D. (1980) Development of spiny and aspiny neurons in the caudate nucleus of the dog during the first postnatal month. J. Comp. Neurol. 192:247-263.

69. Tanaka D. Jr. and Alexander B. (1978) Golgi and electron microscopic evidence for growth cones in the caudate nucleus of the neonatal dog. Exp. Neurol. 60:614-623.

70. Tennyson W. M. (1970) The fine structure of the axon and growth cone of the dorsal root neuroblast of the rabbit embryo. J. Cell Biol. 44:62-79.

71. Walker P. D., Chovanes G. I. and McAllister J. P. (1987) Identification of acetylcholinesterase-reactive neurons and neuropil in neostriatal transplants. J. Comp. Neurol. 259:1-12.

72. Walker P. D. and McAllister J. P. (1987) Minimal connectivity between neostriatal transplants and the host brain. Brain Res. 425:34-44.

73. Wictorin K. and Björklund A. (1989) Connectivity of striatal grafts into the ibotenic acid-lesioned striatum - II. Cortical afferents. Neuroscience 30:297-311.

74. Wictorin K., Isacson O., Fischer W., Nothias F., Peschansk M. and Björklund A. (1988) Connectivity of striatal grafts into the ibotenic acid-lesioned striatum - I. Subcortical afferents. Neuroscience 27: 547-562.

75. Wictorin K., Simerly R. B., Isacson O., Swanson L. W. and Björklund A. (1989) Connectivity of striatal grafts into the ibotenic acid-lesioned

striatum - III. Efferent projecting graft neurons and their relation to host afferents within the grafts. Neuroscience 30:313-330.

76. Wilson C. J. and Groves P. M. (1980) Fine structure and synaptic connections of the common spiny neuron of the rat neostriatum: a study employing intracellular injection of horseradish peroxidase. J. Comp. Neurol. 194:599-615.

77. Xu Z. C., Wilson C. J. and Emson P. C. (1989) Restoration of the corticostriatal projection in rat neostriatal grafts: electron microscopic analysis. Neuroscience 29:539-550.

Chapter 6

DEGENERATION OF LONG-TERM FETAL NEOSTRIATAL ALLOGRAFTS IN THE RHESUS MONKEY: AN ELECTRON MICROSCOPIC STUDY*

*(Published, Experimental Neurology 123 (1993) 174-180)

INTRODUCTION

The potential use of fetal neuronal transplants for the treatment of Parkinson's and Huntington's disease has been firmly established in behavioral, biochemical, and neuroanatomical studies performed primarily in rodents.[1,2] The rat model of Huntington's disease introduced by Coyle and Schwarcz [5] and McGeer and McGeer [19] utilizes the injection of excitotoxic amino acids to lesion the striatum, leading to selective neuronal losses and behavioral deficits which closely resemble Huntington's disease. Fetal striatal neurons implanted into the lesioned striata have been shown to ameliorate partially these biochemical and behavioral deficits.[7,8,12,13,15,16,22,24] Despite these encouraging results in rodents, the extension of these studies into the primate has been limited. Several investigators have now reported that excitotoxic lesioning of the primate striatum can produce behavioral abnormalities similar to the human disease.[6,10,18] In addition, Isacson et al [17] reported that rat fetal neostriatal neurons implanted into the lesioned baboon striatum can survive for up to six weeks if the hosts are immunosuppressed, while Hantraye et al [11] showed that the grafts can improve behavioral deficits in the lesioned primates. In a previous study, we have demonstrated that fetal neostriatal allografts in the Rhesus monkey can survive for up to three months.[14] At this time, the grafts contain neurons at various stages of maturation, numerous growth cones, developing dendrites, and mature and immature synapses, as assessed by Golgi impregnation and electron microscopy. The aims of the present study were to investigate whether neostriatal allografts could survive for longer periods of time in the lesioned primate striatum and to characterize the

grafts at the electron microscopic level. Anatomical studies assessing long-term survival of neuronal transplants in non-human primates and behavioral analysis of the effects of long-term graft survival are essential before this approach should be utilized in the clinical setting.

EXPERIMENTAL PROCEDURES

One adult female Rhesus monkey and two pregnant Rhesus monkeys (Hazelton Research Products) at an estimated 55 to 70 days of gestation were used in the study. One pregnant female was used as a fetal donor and subsequently as the recipient of striatal grafts after completely healing from the initial Caesarean section. All animal studies were performed under the auspices of a protocol approved by the University of Virginia Animal Research Committee.

Initially, the recipient monkeys were anesthetized with Ketamine and Pentobarbital and received T_1 and T_2 weighted magnetic resonance imaging (MRI) scans to localize the striatum. Several days after the initial MRI scan, the primates were again anesthetized with Ketamine and Pentobarbital and received four injections of 0.5 μL of ibotenic acid (Sigma, 20 mg/ml), in phosphate buffer (pH 7.4) into the anterior putamen, utilizing stereotactic coordinates obtained from the MRI scans. Several days after lesioning, the animals again received MRI scans in order to verify correct placement of the lesion. Striatal implantation was performed nine days after lesioning using techniques described previously. [14] Eight months following transplantation, the recipient monkeys were anesthetized and perfused transcardially with 50 mL of 0.12 mol/L phosphate buffer (pH 7.4) containing 0.25% Procaine and 3% sucrose followed by 10 liters of a fixative containing 4%

paraformaldehyde, 1% glutaraldehyde, and 3% sucrose in 0.1 mol/L phosphate buffer (pH 7.4). The heads were removed four hours after perfusion and placed in the fixative overnight. The brain was removed and cut coronally at 0.5 cm with the brain knife. The cerebral cortex was cut away from the slices and the blocks were then sectioned at 80 M. in 0.12 mol/L phosphate buffer containing 8% dextrose on a Lancer vibratome. The sections were rinsed for several hours in 0.12 mol/L phosphate buffer and were then Golgi impregnated or examined at the electron microscopic level as described in a previous study. [14]

RESULTS

Light Microscopy. The 8 month neostriatal transplants obtained in this study were significantly smaller than the three-month transplants obtained in our previous primate study. [14] The grafts were between 1.0 and 1.5 mm in diameter and contained a high number of glial cells as well as small regions of necrosis (Fig. 6.1). However, clearly visible neurons of various sizes were seen amongst the glia. Because of the dense gliosis, it was difficult to determine the exact sizes of most of the grafted neurons and the development of the surrounding neuropil at the light microscopic level. However, many of the neuronal nuclei in the grafts were pyknotic compared to the neuronal nuclei in the surrounding normal striatum. Unfortunately, no neurons within the striatal graft stained properly with the Golgi impregnation method, despite normal impregnation of the surrounding primate striatum.

Electron Microscopy. At the electron microscopic level, the neostriatal allografts were characterized by marked gliosis, as well as light and dense neuronal degeneration. There were, however, a moderate number of normal

appearing neurons in the graft. These implanted neurons could be classified into three types based on ultrastructural features and somatic diameter. Large neurons with a somatic diameter greater than 20 μm consistently contained a large, indented nucleus with a single nucleolus surrounded by copious cytoplasm rich in mitochondria, rough endoplasmic reticulum, and polyribosomes (Fig. 6.2). However, these neurons contained numerous lipofuscin granules characteristic of aging neurons. Medium-sized neurons with somatic diameters between 10-20 μm contained unindented nuclei and sparse cytoplasm, typical for the "medium spiny" striatal neuron, while others contained an indented nucleus, characteristic of several types of medium-sized aspiny neurons.

The majority of the neurons, however, showed evidence of degeneration, with small pyknotic nuclei surrounded by a thin rim of cytoplasm containing scant Nissl substance. The neurons were surrounded by numerous filamentous astrocytes which seemed to occupy most of the neuropil with their glial processes. Interspersed amongst the glial processes were occasional axodendritic and axospinous synapses. These synapses had well developed synaptic specializations and appeared to be quite mature (Fig. 6.3). The numerous coated vesicles and pits seen commonly in three month striatal primate grafts were not seen in the present study. In addition, no dendritic growth cones were seen within the transplants. Throughout the graft there was no evidence of lymphocytic infiltration, which one would expect if there was any immunologic rejection of the graft by the host.

DISCUSSION

In this paper we have demonstrated that fetal striatal allografts transplanted into the lesioned Rhesus monkey striatum can survive for up to eight months, although the transplants are characterized by neuronal degeneration, premature neuronal aging, and marked gliosis. However, the neurons also contain axodendritic and axospinous synapses suggesting that some of the neurons may be functional. Whether the axon terminals originate from other transplanted neurons or from the host brain is currently only speculative.

Gopinath et al. [9] have previously reported that fetal mesencephalic transplants in the rat develop normally for approximately 180 days after being implanted into the adult rat striatum. After this time, the dopaminergic neurons age prematurely, showing a reduction in rough endoplasmic reticulum and an increase in large vacuoles and lipofuscin granules. In addition, there is a marked reduction in neuronal densities of the transplants. Although there have been numerous studies performed on fetal rat and primate nigral transplants, no other studies have reported these changes seen with aging. [21,26] It is possible that these other studies of nigral transplants have not had long enough survival times to produce these changes, or that these morphological changes were simply not recognized. However, Roberts and DiFiglia [23] have demonstrated long-term survival (16 months) of fetal neostriatal grafts in the rat. The transplanted neurons express GABA, enkephalin, and NADPH-diaphorase immunoreactivity similar to the host striatum and showed no evidence of degeneration. Other studies have also suggested that striatal allografts are stable in the rat. The reason

for the neuronal instability in primate striatal allografts, as compared to the relative neuronal stability in rat striatal allografts, is currently only speculative.

Since a limited number of animals received neuronal grafts in this study, it is possible that the degenerative changes were simply due to individual variability or technical differences. However, a more intriguing explanation for the neuronal degeneration is that the transplanted neurons do not receive the appropriate afferent input from or do not make sufficient efferent connections with the host brain. This could, in theory, lead to inadequate neurotrophic substances reaching the neurons, subsequently causing them to degenerate or age prematurely. Previous neuroanatomical studies of rat neostriatal allografts by Wictorin et al [32] and Pritzel et al [20] have demonstrated significant efferent connectivity with the host globus pallidus, entopeduncular, and substantia nigra, while several investigators have demonstrated that the grafts receive afferents from the host cerebral cortex, [30,34] thalamus, [33] and substantia nigra. [4,31] However, Walker and McAllister [31] demonstrated only minimal connectivity between the striatal grafts and the surrounding host brain. Many of the synapses seen in the transplants in the present study were asymmetric, suggesting that the cortical-striatal pathway may have been established by the grafts. [3,27] More recent studies concerning the implantation of human fetal striatum into the rat brain have demonstrated massive fiber outgrowth into appropriate target regions. [29] Whether the human neurons have a greater potential to grow axons over long distances because they develop more slowly or whether they are not affected by the neurite growth inhibitors present on

oligodendrocytes in the rat central nervous system is currently not known. [25,29] The connectivity of the fetal striatal allografts in the primate may be hampered by the significant distances from the grafts to their efferent targets or by neurite growth inhibitors possibly present in the primate central nervous system.

Figures and Tables

Figure 6.1: **a.** Light micrograph of a Nissl-stained 8 month fetal striatal transplant (t) in the lesioned Rhesus monkey striatum (l) demonstrating a moderate number of neurons surrounded by large numbers of glial cells. The allograft's cellularity can be compared to that of the normal monkey neostriatum(s). Scale bar = 0.5 mm. **b.** A large neuron within the transplant (arrowhead in A.) contains a moderate amount of nissl-substance and is surrounded by numerous glial cells. Scale bar = 10 μm. **c.** A polygonally-shaped medium-sized neuron within the graft contains a large amount of Nissl substance. Scale bar = 10 μm.

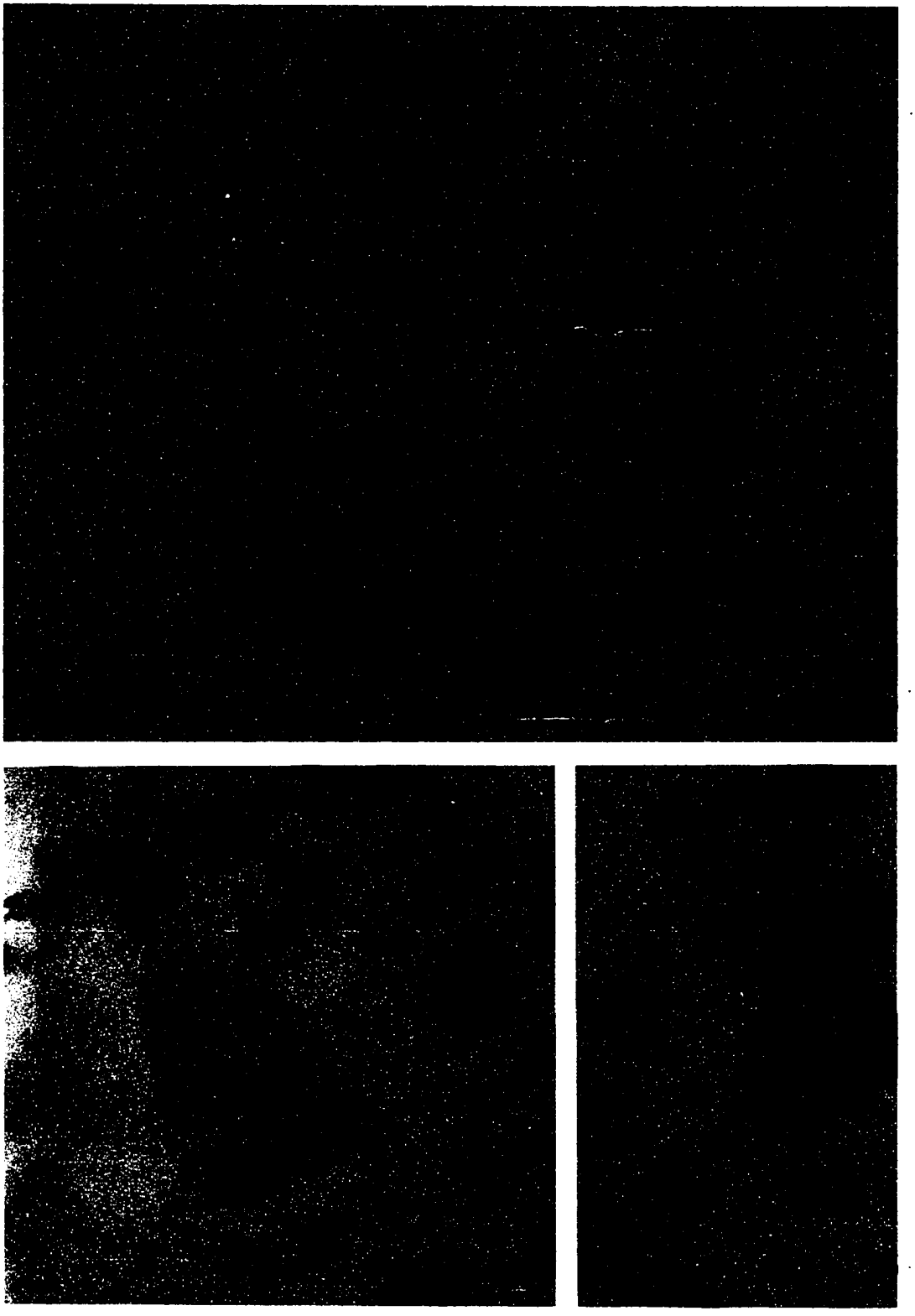

Figure 6.2: Electron micrograph of a large neuron in the striatal graft demonstrating a large, indented nucleus (N) surrounded by copious cytoplasm rich in rough endoplasmic reticulum (ER) and mitochondria. Note the numerous lipofucsin granules (arrowheads) indicating premature aging of the neuron. Scale bar = 4.0 μm.

Figure 6.3: Electron micrographs of an eight month fetal striatal graft demonstrating: **a.** Two axodendritic synapses (arrow and arrowhead). **b.** An axodendritic synapse (arrowhead) and an axospinous synapse (arrow). **c.** An axodendritic synapse (arrowhead) onto a medium sized dendrite. **d.** A large axon terminal synapsing on a dendrite (arrowheads). Note the dense glial fibers in the surrounding neuropil. Scale bars = 1.0 μm.

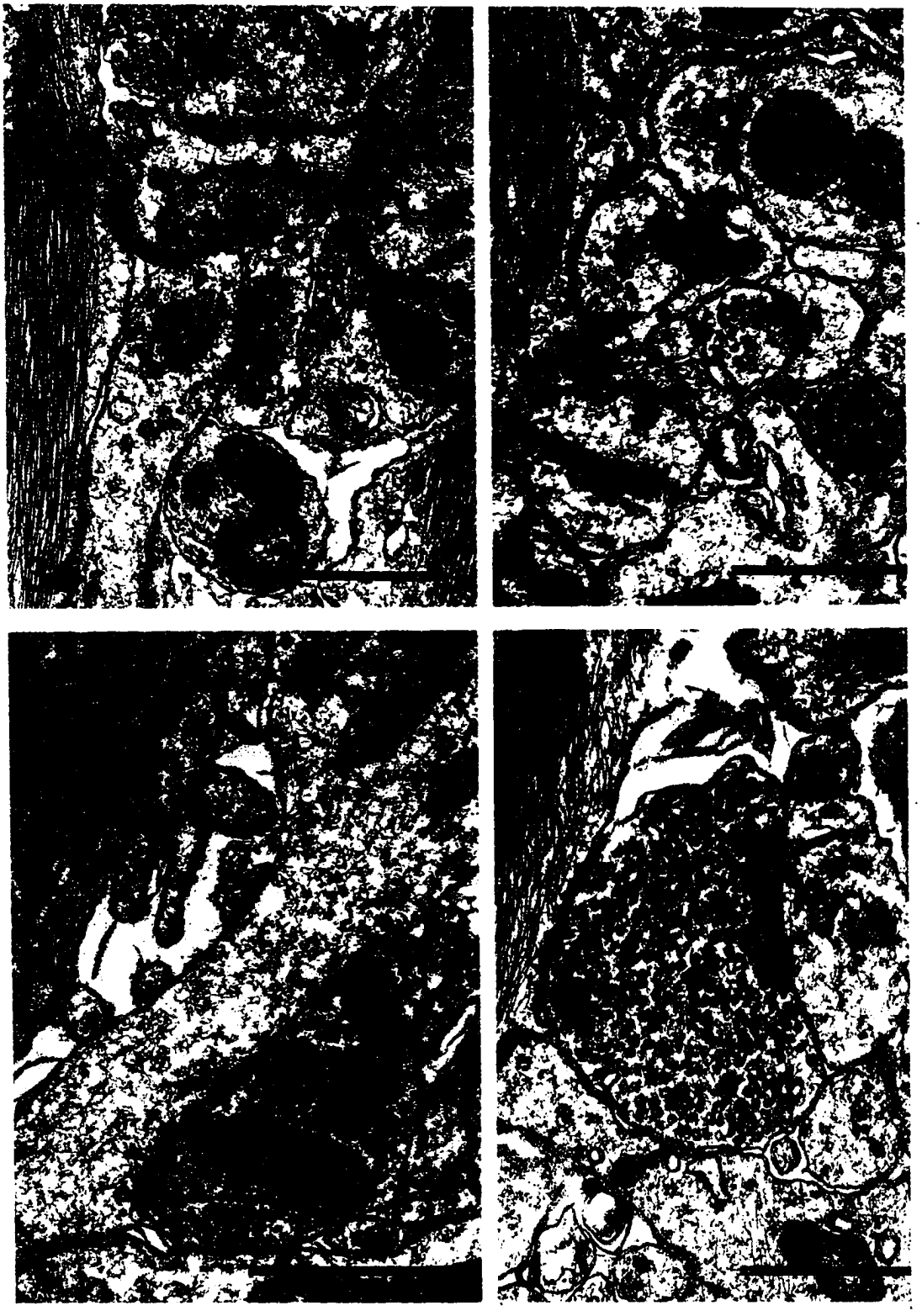

REFERENCES

1. BJÖRKLUND A. AND STENEVI U. 1985. Neuronal Grafting in the Mammalian CNS. Elsevier, Amsterdam.
2. BJÖRKLUND A., STENEVI U. AND SVENDGAARD N. A. 1976. Growth of transplanted monoaminergic neurones into the adult rat hippocampus along the perforant path. Nature 262:787-790.
3. BOLAM J. P. 1984. Synapses of identified neurons in the neostriatum. Ciba Found. Symp. 107:30-47.
4. CLARKE D. J., DUNNETT S. B., ISACSON O., SIRINATHSINGHJI, D. J. S. AND BJÖRKLUND A. 1988. Striatal grafts in rats with unilateral neostriatal lesions - I. Ultrastructural evidence of afferent synaptic inputs from the host nigrostriatal pathway. Neuroscience 24:791-801.
5. COYLE J. T. AND SCHWARCZ R. 1976. Lesion of striatal neurones with kianic acid provides a model of Huntington's chorea. Nature 263: 244-246.
6. CROSSMAN A. R. 1987. Primate models of dyskinesia, the experimental approach to the study of basal ganglia-related involuntary movement disorders. Neuroscience 21:1-40.
7. DECKEL A. W., MORAN T. H. AND ROBINSON R. G. 1986. Behavioral recovery following kainic acid lesions and fetal implants of the striatum occurs independently of dopaminergic mechanisms. Brain Res. 363: 383-385.
8. DECKEL A. W., ROBINSON R. G., COYLE J. T. AND SANDBERG P. R. 1983. Reversal of long-term locomotor abnormalities in the kainic acid model of Huntington's disease by day 18 fetal striatal implants. Eur. J. Pharmacol. 93:287-288.

9. GOPINATH G., SHETTY A.K., AND TANDON P.N. 1991. Ageing changes in the transplants of fetal substantia nigra grafted to striatum of adult rat. Neuroscience 40(2):429-443.

10. HANTRAYE P., RICHE D., MAZIERE M. AND ISACSON O. 1990. A primate model of Huntington's disease: Behavioral and anatomical studies of unilateral excitotoxic lesions of the caudate-putamen in the baboon. Exp. Neurol. 108:91-104.

11. HANTRAYE P., RICHE D., MAZIERE M., AND ISACSON O. 1992. Intrastriatal transplantation of cross-species fetal striatal cells reduces abnormal movements in a primate model of Huntington disease. Proc Nat. Acad. Sci. USA 89(9): 4187-4191.

12. HELM G. A., PALMER P. E. AND BENNETT J. P. JR. 1992. Choline acetyltransferase and substance P-like immunoreactive elements in fetal striatal grafts. a correlated light and electron microscopic study. Neuroscience 47:621-639.

13. HELM G. A., ROBERTSON M. W., JALLO G. I., SIMMONS N. AND BENNETT J. P. JR. 1991. Development of D1 and D2 dopamine receptors and associated second messenger systems in fetal striatal transplants. Exp. Neurol. 111:181-189.

14. HELM GA, PALMER PE, SIMMONS NE, DIPIERRO C, BENNETT JP JR. 1992. Descriptive morphology of developing fetal neostriatal allografts in the Rhesus monkey: A correlated light and electron microscopic study. Neuroscience 50:163-179.

15. ISACSON O., BRUNDIN P., GAGE F. H. AND BJÖRKLUND A. 1985. Neuronal grafting in a rat model of Huntington's disease: progressive

neurochemical changes after ibotenate lesions and striatal tissue grafting. Neuroscience 16:799-817.

16. ISACSON O., BRUNDIN P., KELLY P. A. T., GAGE, F. H. AND BJÖRKLUND A. 1984. Functional neuronal replacement by grafted striatal neurones in ibotenic lesioned rat striatum. Nature 311:458-460.

17. ISACSON O., RICHE D., HANTRAYE P., SOFRONIEW M. V. AND MAZIERE M. 1989. A primate model of Huntington's disease: cross-species implantation of striatal precursor cells to the excitotoxically lesioned baboon caudate-putamen. Exp. Brain Res. 75:213-220.

18. KANAZAWA I., TANAKA Y. AND CHO F. 1986. "Choreic" movement induced by unilateral kainate lesion of the striatum and l-DOPA administration in monkey. Neurosci. Lett. 71:241-246.

19. MCGEER E. G. AND MCGEER P. L. 1976. Duplication of biochemical changes of Huntington's chorea by intrastriatal injection of glutamic and kainic acids. Nature 263:517-519.

20. PRITZEL M., ISACSON O., BRUNDIN P., WIKLUND L. AND BJÖRKLUND A. 1986. Afferent and efferent connections of striatal grafts implanted into the ibotenic acid lesioned neostriatum in adult rats. Exp. Brain Res. 65:112-126.

21. REDMOND D. E., SLADEK J. R., ROTH R. H. COLLIER T. J., ELSWORTH J. D., DEUTCH A. Y. AND HABER S. 1986. Fetal neuronal grafts in monkeys given methylphenyltetrahydropyridine. Lancet 1:1125-1127.

22. ROBERTS R. C. AND DIFIGLIA M. 1988. Localization of immunoreactive GABA and enkephalin and NADPH-diaphorase-positive neurons in fetal

striatal grafts in the quinolinic-acid-lesioned rat neostriatum. J. Comp. Neurol. 274:406-421.

23. ROBERTS R.C. AND DIFIGLIA M. 1990. Long-term survival of GABA-enkephalin-, NADPH-diaphorase and calbindin-d28k-containing neurons in fetal striatal grafts. Brain Res. 532:151-159.

24. SIRINATHSINGHJI D. J. S., DUNNETT S. B., ISACSON O., CLARKE D. J., KENDRICK K. AND BJÖRKLUND A. 1988. Striatal grafts in rats with unilateral neostriatal lesions - II. *In vivo* monitoring of GABA release in globus pallidus and substantia nigra. Neuroscience 24:803-811.

25. SCHNELL, L. AND SCHWAB, M. D. 1990. Axonal regeneration in the rat spinal cord produced by an antibody against myelin-associated neurite growth inhibitors. Nature 343:269-272.

26. SLADEK J. R. JR., COLLIER T. J., HABER S. N., ROTH R. H. AND REDMOND D. E. JR. 1986. Survival and growth of fetal catecholamine neurons transplanted into primate brain. Brain Res. Bull. 17:809-818,

27. SOMOGYI P., BOLAM J. P. AND SMITH A. D. 1981. Monosynaptic cortical input and local axon collaterals of identified striatonigral neurons. A light and electron microscopic study using the Golgi-peroxidase transport-degeneration procedure. J. Comp. Neurol. 195:567-584.

28. WALKER P. D. AND MCALLISTER J. P. 1987. Minimal connectivity between neostriatal transplants and the host brain. Brain Res. 425: 34-44.

29. WICTORIN K., CLARKE D.J., BOLAM J.P., BRUNDIN P., GUSTAVII B., LINDVALL O., AND BJÖRKLUND, A. 1990. Extensive efferent projections of intra-striatally transplanted striatal neurons as revealed by a

species-specific neurofilament marker and anterograde axonal tracing. In S.B. Dunnett and S.-J. Richards (Eds. Progress in Brain Research, Vol. 82, pp. 391-399. Elsevier Science Publishers, New York.

30. WICTORIN K. AND BJÖRKLUND A. 1989. Connectivity of striatal grafts into the ibotenic acid-lesioned striatum - II. Cortical afferents. Neuroscience 30:297-311.

31. WICTORIN K., ISACSON O., FISCHER W., NOTHIAS F., PESCHANSK M. AND BJÖRKLUND A. 1988. Connectivity of striatal grafts into the ibotenic acid-lesioned striatum - I. Subcortical afferents. Neuroscience 27: 547-562.

32. WICTORIN K., SIMERLY R. B., ISACSON O., SWANSON L. W. AND BJÖRKLUND A. 1989. Connectivity of striatal grafts into the ibotenic acid-lesioned striatum - III. Efferent projecting graft neurons and their relation to host afferents within the grafts. Neuroscience 30:313-330.

33. XU Z.C., WILSON C.J., AND EMSON P.C. 1991. Restoration of thalamostriatal projections in rat neostriatal grafts. An electron microscopic analysis. J. Comp. Neurol. 303:22-34.

34. XU Z. C., WILSON C. J. AND EMSON P. C. 1989. Restoration of the corticostriatal projection in rat neostriatal grafts: electron microscopic analysis. Neuroscience 29:539-550.

Chapter 7

THE UTILIZATION OF TYPE I COLLAGEN GEL, DEMINERALIZED BONE MATRIX AND BONE MORPHOGENETIC PROTEIN-2 (rhBMP-2) TO ENHANCE AUTOLOGOUS BONE LUMBAR SPINAL FUSION*

*(In Press, Journal of Neurosurgery, 1996)

INTRODUCTION

Spinal fusion continues to play a significant role in both neurological and orthopedic surgery in the treatment of numerous pathological conditions of the spine, including trauma, tumors, congenital anomalies, and degenerative disease. Although internal fixation with instrumentation, such as Harrington rods, Luque rings, and Steffi plates, is useful for short-term spinal stability, bony fusion is always required for long-term stability. The ideal spinal fusion technique creates a strong, healthy bone mass between the vertebrae with a high rate of fusion, needs little technical expertise, and has a low complication rate. It has now been well established in both clinical and laboratory studies that autologous bone is the "gold standard" grafting material for achievement of arthrodesis in the spine. Obtaining an autologous bone graft from the iliac crest is now a standard procedure, but is also associated with risks of infection, bleeding, and increased post operative pain.[27,40] In order to avoid donor site morbidity, allografts, xenografts and synthetic grafts have been studied experimentally, but there is a risk of transmission of infectious agents and none are superior to autologous bone alone.[35]

During the last ten years, the cellular mechanisms that regulate bone formation have been extensively studied.[36,37] Osteoinductive growth factors such as the bone morphogenetic proteins (BMPs) have been demonstrated to

induce bone formation through endochondral mechanisms, leading to their potential use in both fusions of the spine and fractured long bones.[37] Manipulation of the support proteins in the extracellular space around a fusion site may also improve bony fusion. For example, isotonic, neutral pH gels of purified Type I collagen have been shown to provide a matrix onto which osteoblasts freely migrate, leading toward enhanced healing of critical size defects in the rat skull.[28] The aim of the present study was to determine whether isotonic, neutral pH Type I collagen gel, demineralized bone matrix (DBM), an excellent source of bone growth factors, and recombinant human bone morphogenetic protein-2 (rhBMP-2) can be utilized to improve the rate and strength of autologous bony fusions in the decompressed canine lumbar spine.

MATERIALS AND METHODS

A total of 40 adult female beagles were used in this study. The method for lumbar decompression and fusion utilized at the University of Virginia Health Sciences Center for the treatment of spinal stenosis was used in this study, which consists of a unilateral bony decompression of laminae, facets, and pedicles with undercutting of the spinous processes followed by a contralateral autologous bony fusion. Group I (10 dogs) received a unilateral decompression with the usual contralateral bony fusion. Group II (7 dogs) received a unilateral decompression with a contralateral

fusion using autologous bone and DBM. Group III (10 dogs) received a unilateral decompression with contralateral fusion using autologous bone in a Type I collagen gel. Group IV (7 dogs) received a unilateral decompression with a contralateral fusion using autologous bone and DBM in a Type I collagen gel. Group V (6 dogs) received a unilateral decompression with a contralateral fusion using autologous bone and recombinant human bone morphogenetic protein-2 (rhBMP-2).

The animals were anesthetized with Tiletamine 50%/Zolazepam 50% (10 mg/kg), intubated and placed under halothane anesthesia. The lower back was shaved, prepped, and draped in sterile fashion, and a midline incision was made over the spinous process from L3 to S1. The lumbodorsal fascia was incised bilaterally at the margin of the spinous processes and the paraspinous musculature was dissected off of the spinous processes and laminae using scissors and periosteal elevators. At this point, hemilaminectomies, facetectomies, and pediculectomies were performed on the left side at the L4, L5, and L6 levels. All removed bone was saved in normal saline solution, while the removed ligaments were discarded. Adequate hemostasis was obtained with bipolar cautery.

Attention was then directed toward the right-sided bony fusion. The facet joints from the inferior facet of L3 to the superior facet of L7 were decorticated and the bone saved as usual. In Group I, the autologous bone

was then placed over the laminae and facets between L3 and L7. In Group II, 2.0 gm of dog DBM was added to the autologous bone. In Group III, 3.0 cc of a solution of Type I collagen was added to the bone chips. Group IV grafts contained the autologous bone, 2.0 gm of dog DBM, and 3.0 cc of the Type I collagen gel solution. In Group V, 2.0 mg of recombinant human bone morphogenetic protein-2 (rhBMP-2, Genetics Institute) was added to the autologous bone, with or without a bovine collagen carrier. The fascial layer was then closed in an interrupted fashion using 3.0 Nurolon sutures. Subcutaneous tissue was closed in an interrupted fashion using 3.0 Vicryl sutures and the skin was closed with interupted stitches using 3.0 Dermalon. The dogs received post operative analgesia as needed and post operative antibiotics for three days.

Preparation of Type I Dog Collagen. Tail tendons from assorted species of dogs were stripped from their fascial sheaths and cut into thin strips. The remainder of the preparation was carried out at 4°C. The strips were soaked in 0.5 M acetic acid while stirring for at least 2 days, and the mixture was then filtered through sterile gauze using positive pressure. Following centrifugation of the filtrate for 25 minutes at 5000 G, the supernatant was fractionated using sodium chloride (0.1 gram/ml) added very slowly over 6-10 hours while stirring. After all of the sodium chloride had been added, the solution was allowed to stir for 18-25 hours. It was

then centrifuged again for 25 minutes at 5000 g, and the pellet was resuspended in 0.5 M acetic acid. Lyophilization indicated a solution of 8 mg/ml, and an SDS gel indicated a high level of purity of the collagen isolated by this method when compared to standard Type I collagen.

The collagen preparation was then dialyzed against 330 ml Dulbecco's Modified Eagle's Medium (DMEM) plus 670 ml 0.5 M acetic acid, 670 ml DMEM plus 330 ml 0.5 M acetic acid, and 2000 ml DMEM for 15 minutes, 15 minutes, and 45 minutes, respectively. A few drops of chloroform added to the final step for germicidal purposes were allowed to evaporate during the dialysis.

Collagen gels were prepared by combining 1.40 ml collagen solution in DMEM, 0.20 ml 5x DMEM, and 0.16 ml 20x sodium bicarbonate and titrating carefully just to the point of color change (from yellow to pink) with 0.5 M sodium hydroxide.

Preparation of Demineralized Bone Matrix. Demineralized bone matrix was prepared from segments of femora and tibiae of freshly sacrificed adult canines. All soft tissue was removed and the bones were washed in sterile deionized water on ice, extracted with a 1:1 chloroform-methanol mixture (30 ml/g), air-dried overnight, and pulverized in a Wiley Mill with crushed dry ice. The resulting powder was rinsed with serial changes of sterile deionized water to bring the pH to 3.5 or more and was then lyophilized and stored at

70°C. Random samples were taken for cultures which demonstrated no bacterial or fungal contamination. Previous studies have demonstrated the osteoinductive activity of this preparation.[2,15]

Computerized Tomography. Each dog in the study received a complete CT scan of the spine from L2-L7 before surgery and 1 week, 3 months, and 6 months post operatively. Dogs were imaged under general anesthesia with Tiletamine 50%/Zolazepam 505 (10 mg/kg) in the supine position. Scanning was performed using a Picker PQ-2000 (software version 4.2). Axial images with 2.0 mm collimation and 1.5 mm table increment were performed using the standard algorethm, with 130 KV, 150 mA and 2 second scan time. The field of view of 24 cm, with a display field of view of 12 cm.

Volumetric analysis was performed on a Voxel Q workstation (Picker International, Cleveland, OH). A binary image was created by setting the window to zero (0) Houndsfield units (HU). A level of HU was chosen, since preliminary data demonstrated that this level most accurately correlated with the volume of cortical bone. Volumetric data was generated based on slice thickness and number of pixels per slice with attenuation values greater than or equal to 100 HU. Regions of interest (ROI) were manually created to include only posterior elements. The ROI was further subdivided by drawing a coronal line bisecting the spinal canal. The volume of the posterior

elements were then compared between the pre-operative scans and the post-operative scans obtained prior to euthanasia.

Histological Methods. One experimental animal from groups I-IV was euthanized 12 weeks post operatively with an overdose of sodium pentabarbital. No histology was performed on the group V spines since our rhBMP-2 resources limited this group to only six animals, all of which were used for biomechanical studies. The lumbar spine was removed, grossly cleaned of musculature, and fixed in 10% buffered formalin for 5 days. After rinsing in cold tap water for one hour, the specimen was placed in a decalcifying solution (Baxter Laboratories), which was changed at 2.5, 5, 10, 24, 36, and 48 hours. After decalcifying for a total of 72 hours, the specimen was rinsed in cold tap water for 30 minutes and returned to 10% buffered formalin.

The bone was then treated by a 12 hour course in a Histomatic Tissue Processor (Fisher Scientific) and embedded in paraffin. Using a Tissue Tek Accu-Cut microtome (Miles Scientific), 5 μm sections were cut and placed on slides. After drying overnight, the slides were deparaffinized, stained with hematoxylin and eosin, and mounted with Permount (Fisher).

Biomechanical Testing. Twelve (Group V) or twenty-four (Groups I-IV) weeks post operatively the remainder of the experimental animals were given an overdose of sodium pentobarbital. The lumbar spine was removed,

grossly cleaned of musculature, and placed in one liter of 30% hydrogen peroxide at a temperature of 60°C. After ten minutes in the acidic solution, the specimens were dipped in cold water to neutralize the hydrogen peroxide and loose pieces of residual tissue were removed using forceps. This method resulted in bony specimens completely free of soft tissue, except for the annulus fibrosis of the intravertebral discs. The specimens were then ultrasonically cleaned in cold water for 35-45 minutes to ensure complete removal of the hydrogen peroxide and any residual soft tissue. The samples were then photographed and stored in a sodium chloride solution.

In order to clamp onto the vertebral bodies during biomechanical testing, the vertebral bodies were placed into a mold and Cerro metal was poured around the vertebral bodies and allowed to cool. Cerro metal, an alloy of bismuth, tin, cadium, and lead, melts at 70°C and was therefore ideal for this purpose. After removal of the metal from the mold, the entire vertebral segment or individual vertebral interspaces could be tested biomechanically. The vertebral bodies were fixed to an apparatus to measure the angle of deflection in flexion and extension of the spine as a function of applied force, typically at 50 gm intervals. Plots of extension and flexion angles versus applied torque were generated and a straight line was fitted to the data in each case. Correlation coefficients of almost all of the fits were nearly unity. This implied for the small angle of deflection in

the cases studied, mechanical stiffness of the fusions could be modeled by the standard Newtonian expression $\tau = K\Delta\varnothing$ where K is the slope of the fitted line and $\Delta\varnothing$ is the angle of deflection.

RESULTS

Gross Examination. After cleaning the spines of soft tissue, the specimens clearly demonstrated a complete unilateral decompression (Fig 7.1a) and contralateral bony fusion (Figs 7.2a,c; 7.3a,c). Uniformily, the fusion masses in groups I, III, and V were composed of solid cortical bone, uninterrupted by areas of soft tissue (Figs 7.2c; 7.3a,c; 7.4), while the DBM groups (II and III) displayed fusion masses which were porous, containing areas of solid bone interspersed with areas of soft connective tissue (Fig 7.2a). Secondly, it was readily apparent that the fusion masses were much larger in the dogs which received rhBMP-2 (Group V) spines than in the control group (Fig 7.3c; 7.4). Gross inspection of the fusion sites clearly demonstrated which intervertebral levels were solidly fused by the bone graft and which levels displayed pseudoarthroses. The Group V spines had an average solid fusion of 3.00±0.63 ($p = .002$) continuous intervertebral levels, whereas the control group solidly fused only 1.57±0.79 continuous intervertebral levels. The collagen alone group (III) solidly fused 1.725±0.99 ($p > .05$) levels, while the two DBM groups (II, IV) displayed no solid

intervertebral fusion sites. In summary, only the rhBMP-2 significantly increased the number of fused levels compared to the control group, whereas the DBM significantly inhibited solid fusion (see Table 7.1). The collagen gel had no significant effect on the number of levels solidly fused.

Histologic Examination. Three months post operatively the histologic appearance of the fusion sites of Groups I and III were quite similar. The fusion mass consisted of well formed lamellar and woven bone surrounding well developed marrow spaces. The autologous bone graft fused solidly with the adjacent spinous processes and laminae, even though these structures were not decorticated during surgery (Figs 7.5a,b). It appeared, however, that the interface between the fusion mass and host bone in the dogs receiving collagen gel was more solid and continuous that the dogs receiving autologous bone alone (Fig 7.5c). There was no evidence of lymphocytic infiltration in the Group III bone graft, suggesting that the Type I canine collagen gel was not immunologically rejected from the host dog. However, since the specimens were examined three months post operatively, there may have been a more acute inflammatory reaction which could not be appreciated at this point.

Interestingly, the groups receiving DBM consistently demonstrated large areas of fibrous tissue, primitive mesenchymal appearing cells, and regions of endochondral ossification within the fusion mass (Fig 7.5d). The

bone grafts were not as firmly fused to the spinous processes and laminae as they were in the other two groups. As in Group III, there was no evidence of immunologic rejection of the implanted collagen gel or demineralized bone matrix in these animals.

Radiographic Examination. Axial CT scans and their three dimensional (3-D) reconstructions were used in the study to verify complete removal of the appropriate laminae, facets and pedicles (Fig 7.1b), confirm correct placement of the autograft on the contralateral side and to assess the volume and morphology of the fusion mass over time (Figs. 7.2b,d; 7.3b,d). The bone grafts in groups I, III and V were typically smooth, had few irregularities, and had no regions devoid of bone (Figs 7.2d; 7.3a,c). The grafts containing DBM characteristically displayed large regions devoid of bone, giving the fusion masses an irregular surface (Fig 7.2b). Unfortunately, the CT images and 3-D reconstructions could not accurately demonstrate vertebral levels that were solidly fused and those which demonstrated pseudoarthroses. However, volumetric analysis at the fusion mass was very useful in determining the amount of bone present at the fusion site. In control animals, the average change in volume of the posterior elements in group I was 0.26 ± 0.71 cm^3. Therefore, the volume of bone present in the fusion mass was minimally more than the amount of bone that was placed at surgery. However, the addition of rhBMP-2 in

group V increased the amount of bone in the posterior elements by 10.42±6.57 cm^3 ($p=0.036$). The volume changes in groups II, III and IV did not differ significantly from control animals (Table 7.2).

Biomechanical Analysis. A summary of the biomechanical properties of the fused lumbar spine in both flexion and extension is given in Table 7.3. Biomechanical testing clearly demonstrated that the addition of DBM to autologous bone grafts significantly weakened the spinal fusions, mainly because the inclusion of soft tissue within the fusion mass prevented solid intervertebral fusion. There was no significant difference between the biomechanical strength of the fused lumbar spines between groups I, III and V. As will be discussed later, the fact that the group V spines were no stiffer than the control spines, despite the markedly increased volume of bone, was probably due to the significantly higher number of spinal levels that were solidly fused in the group V animals.

DISCUSSION

Unilateral lumbar decompression with a contralateral posterior spinal fusion utilizing autologous bone from the decompressed side is one of the techniques used at our institution for the treatment of lumbar spinal stenosis. Application of this technique in the canine has proved to be a useful experimental model to test spinal fusion graft materials. Despite the large volume of bone obtained from this spinal decompression, solid bony

fusions did not typically occur at all of the operated levels in animals treated with autograft alone. Therefore, this model is useful for studying new techniques which could potentially improve the rate and strength of spinal fusions. In this study attempts were made to enhance the standard autologous bone graft fusions with osteoinductive (rhBMP-2 and DBM) and osteoconductive (Type I collagen gel) agents. Bone morphogenetic protein clearly had the strongest positive effect on autologous bone spinal fusions in this study, whereas the collagen gels had little affect. DBM markedly decreased the rate of spinal fusion.

BMPs were originally isolated from extracts of demineralized bone.[30,31,32] These proteins are a class of related growth and differentiation factors within the transforming growth factor (TGF-B) super family based on primary amino acid sequence homology.[4] Through molecular cloning eleven related members have been currently identified and named BMP-2 through BMP-12. Each protein can individually induce the formation of cartilage and bone in both *in vivo* and *in vitro* assay systems.[24,34,37] *In situ* hybridization studies have demonstrated that BMP messenger RNAs are expressed in the embryonic limb, implicating them as being crucial in the formation of skeletal tissues during development.[33,36] Recently, a mammalian serine/threonine kinase receptor (CFK-43A) has been shown to specifically bind BMP-2 and BMP-4 with high affinity.[16,38] The receptor binds the other BMPs as well,

but with much lower affinity. Interestingly, it does not bind TGF-B. As expected CFK-43A messenger RNA has been shown to be expressed in developing limb buds in a complimentary fashion to the transcripts for its ligands.

There have been several recent animal studies demonstrating the utility of BMPs in the healing of skeletal defects. Yasko, et al, demonstrated that rhBMP-2 promoted bone formation in a dose related manner in rats with 5 mm segmental defects in the femur.[39] This study was extended by Gerhart, et al, who demonstrated that two centimeter femur defects in sheep could be consistently healed with rhBMP-2 alone at a rate similar to autograft alone.[13] Finally, Toriumi, et al, demonstrated that rhBMP-2 can effectively heal three centimeter mandibular defects.[29] In addition, another osteoinductive protein, rhOP-1 has been demonstrated to be effective in healing large segmental osteoperiosteal defects in rabbits, dogs and monkeys.[5] This protein has also been demonstrated to be of potential value in posterior spinal stabilization without the use of autograft.[6] The present study demonstrates that the addition of rhBMP-2 to autologous bone spinal fusions can significantly increase the volume of bone at the fusion site as well as increase the number of levels successfully fused in multilevel lumbar fusions.

Interestingly, the present study did not demonstrate any positive effects of rhBMP-2 on the biomechanical properties of the fused spines. This is not consistent with the fact that there were significantly larger amounts of bone at the fusion site in the animals receiving BMP with the autograft. We believe that this discrepancy can be explained by the fact that in the autograft control group, fewer levels were typically fused and therefore biomechanical testing was performed over fewer segments. Therefore, average number of fused levels which were achieved in the autograft alone group (1.57±0.79) could not be adequately compared to the number of fused levels in the autograft plus BMP group. In more recent studies in our laboratory, we have demonstrated that in one level posterior spinal fusions using autograft alone versus autograft enhanced with rhBMP-2, the rhBMP-2 group had significantly more bone at the fusion site and produced a significantly stronger spinal fusion than the autograft alone group. Clearly, recombinant bone morphogenic proteins will be extremely useful as an additive to autologous bone spinal fusions and may well be useful as a bone graft substitute alone. It is also possible that a cocktail of bone growth factors may be of even greater benefit in enhancing spinal fusions, although there is currently no data available supporting this approach.

Although several studies have evaluated the use of demineralized bone matrix in spinal fusions, all of the studies used histology and/or volume of bone at the fusion site to assess its clinical utility.[12,14,18] None of the studies actually looked at the rate of solid bony fusion in the spine. Guizzardi, et al, demonstrated histologically that demineralized bone matrix can induce bone formation in posterior spinal fusions.[14] In addition, Frenkel, et al, demonstrated that demineralized bone matrix gels could induce osteoid production in posterior spinal fusions in dogs.[12] However, both studies did not determine the biomechanical strength of the fused region or whether the spinal levels were solidly fused. Lastly, Lovell, et al, demonstrated radiographically that in posterior spinal fusions in dogs, demineralized bone matrix plus autograft can increase the amount of bone compared to autograft alone.[18] However, these investigators did not determine whether these fusions were solid or whether they exhibited pseudoarthroses. In the present study, we demonstrated that demineralized bone matrix may increase the amount of bone deposition at the fusion site through endochondral mechanisms, but that the DBM particles lead to a decreased rate of solid fusion with consistent evidence of pseudoarthroses. Although it was clear from our histologic analysis that the DBM stimulated cartilage and bone formation, the DBM groups also contained increased fibrous tissue between the bone chips leading to decreased stability of the fused region.

Since previous studies using identical demineralized bone matrix material performed at the University of Virginia demonstrated excellent bone formation, it is unclear why the DBM had such a deleterious effect on spinal fusion in the present study.[2] It is possible that with more refined techniques, demineralized bone matrix with higher concentrations of bone growth factors can be produced in the future.

Native, neutral, pH isotonic gels of type I collagen have been shown to promote osteoblast differentiation and migration *in vitro* and promote the healing of critical size skull defects *in vivo*.[28] The osteoconductive Type I collagen gels used in this study may have provided a better cellular environment than pepsinated bovine collagen or aldehyde cross-linked bovine skin collagen, which are currently commercially available and have shown little potential to promote bone repair in several other studies.[1,7,8,9,25,26] Collagen may act primarily as an osteoconductive matrix and secondarily as a binding agent for osteoinductive growth factors.[3,10,20,23] In this study, Type I collagen gel seemed to improve the interface between the fusion mass and adjacent lamina and spinous processes, suggesting that the gels may fill the spaces between autologous bone chips and host bone, providing a continuous osteoconductive matrix for the growth of osteogenic cells. However, the gels did not significantly increase the amount of bone formation or increase the biomechanical properties of the fusion mass. One

difficulty with the gels used in the present study is that they were extremely loose and liquefied with mild repetitive agitation. Therefore, it is possible that the large segmental movements, which typically occur in the lumbar regions in dogs, may have disrupted the collagen matrix before the gels could influence bone deposition at the fusion site. Secondly, since the collagen was placed at the fusion site as a chilled liquid solution which subsequently gelled *in situ*, it is possible that blood or serous drainage at the surgical site may have diluted the collagen, thereby preventing its successful gelling. In either case, although some of the spinal fusions in this group demonstrated very large fusion masses, some of which were comparable to the BMP group, many of the spines were no better than the autologous bone group. The data suggests that some type of osteoconductive collagen, especially ones with better physical properties, could be extremely useful in improving bone deposition between the bone chips in autolgous bone grafts.

Figures and Tables

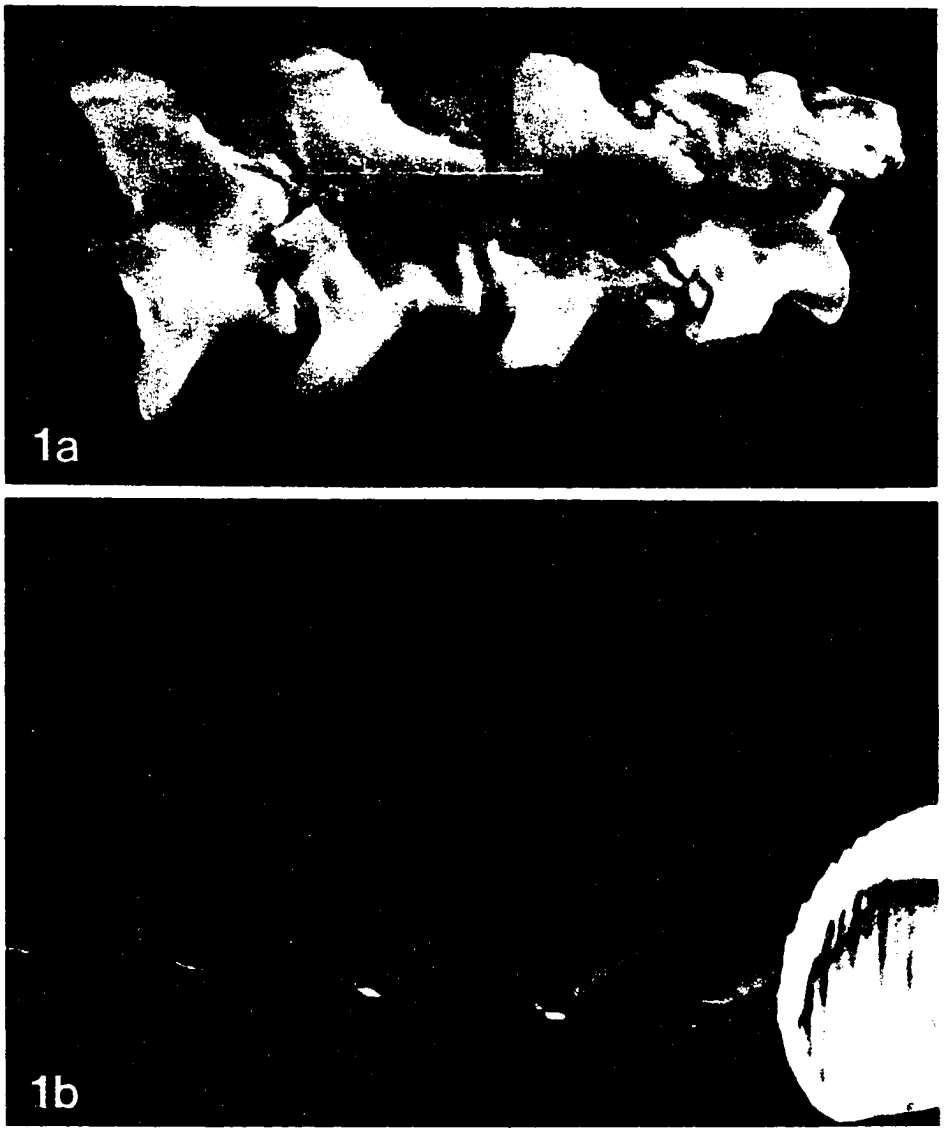

Figure 7.1: **a.** Posteriolateral view of lumbar spine demonstrated the unilaterally decompressed spinal canal, with hemilaminectomies, facetectomies and pediculectomies. **b.** 3-D CT reconstruction of the lumbar spine shown in a. demonstrating the utility of 3-D reconstruction in evaluating spinal decompression.

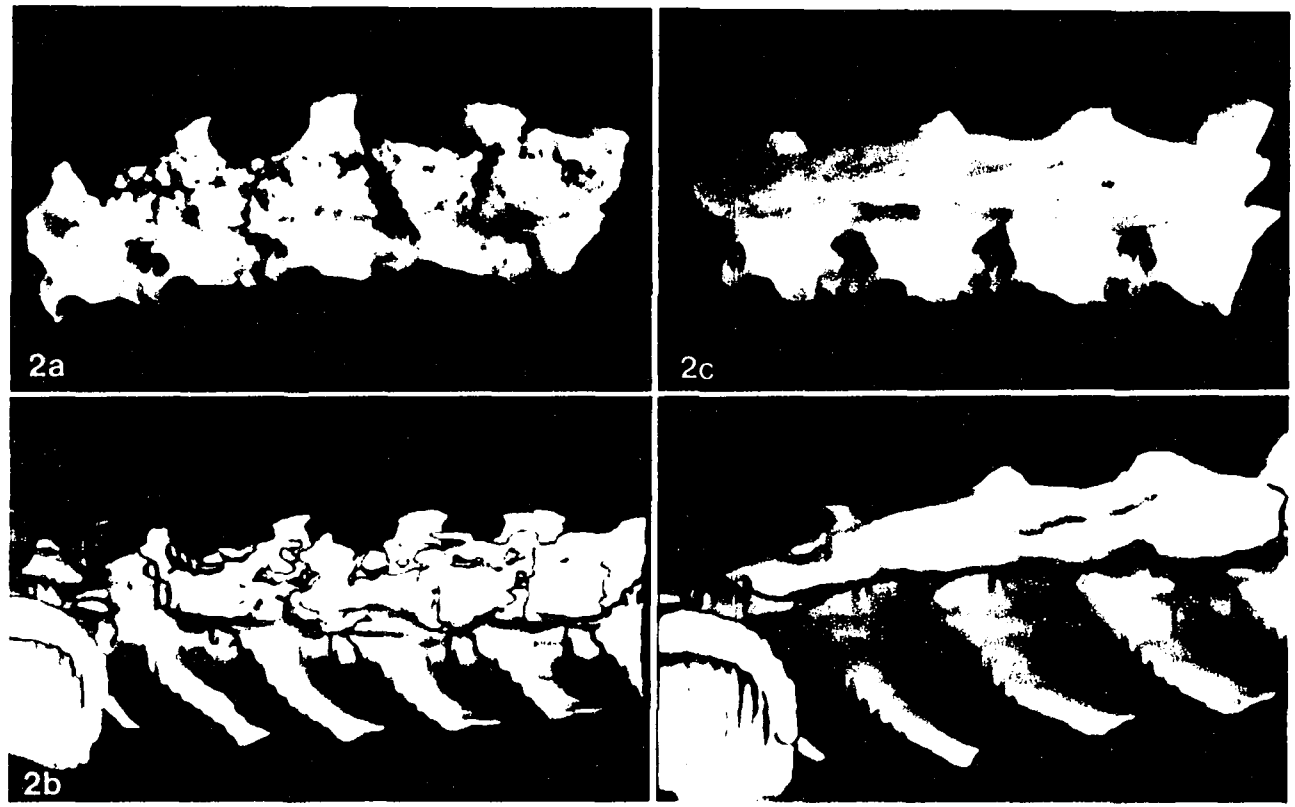

Figure 7.2: Group I and II spinal fusions. **a.** Lateral view of a Group II (DBM & autologous bone) spinal fusion **b.** 3-D CT reconstruction of the spinal fusion shown in a. **c.** Lateral views of the best Group I (autologous bone alone) spinal fusion. **d.** 3-D CT reconstruction of the spinal fusion shown in c.

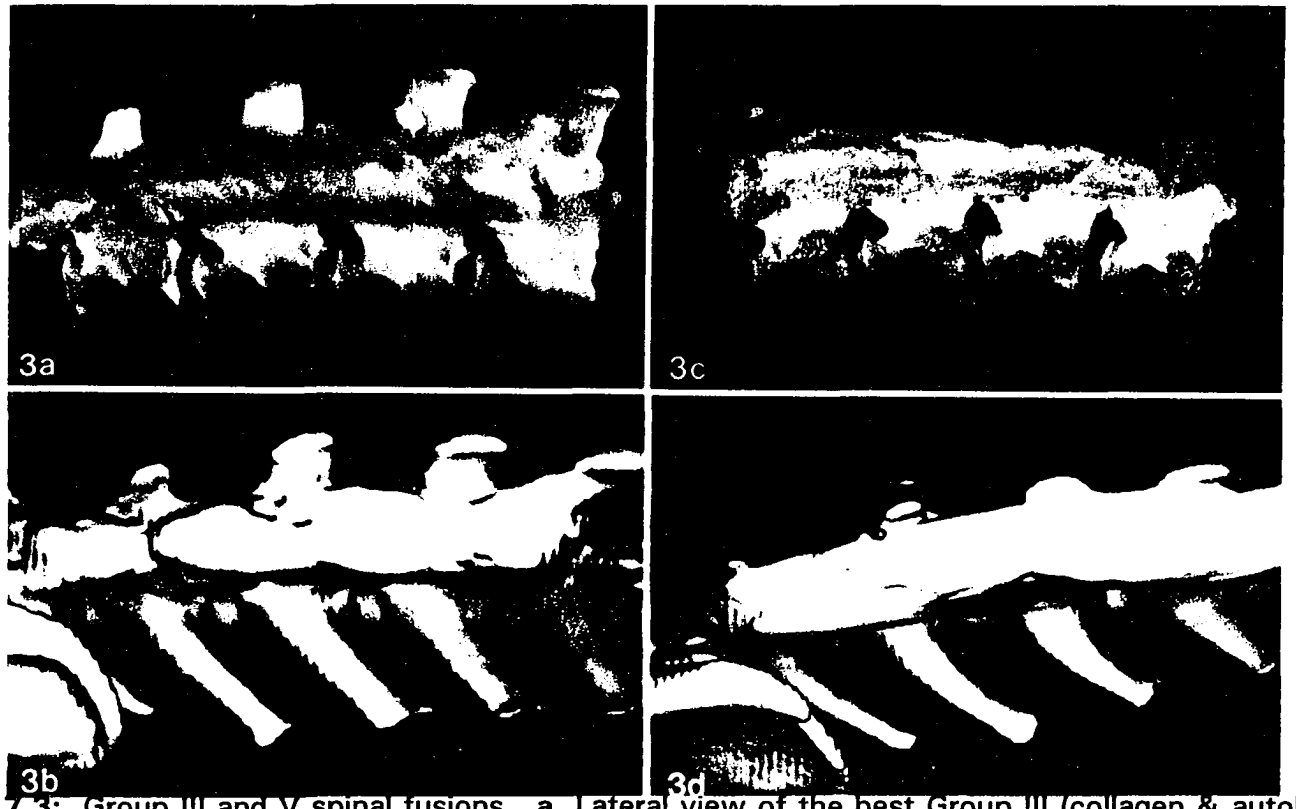

Figure 7.3: Group III and V spinal fusions. **a.** Lateral view of the best Group III (collagen & autolgous bone) spinal fusion. **b.** 3-D CT reconstruction of the spine shown in the Group III spine. **c.** Lateral view of a typical Group V (rhBMP-2 & autologous bone) spinal fusion. **d.** 3-D CT reconstruction of the spine shown in c.

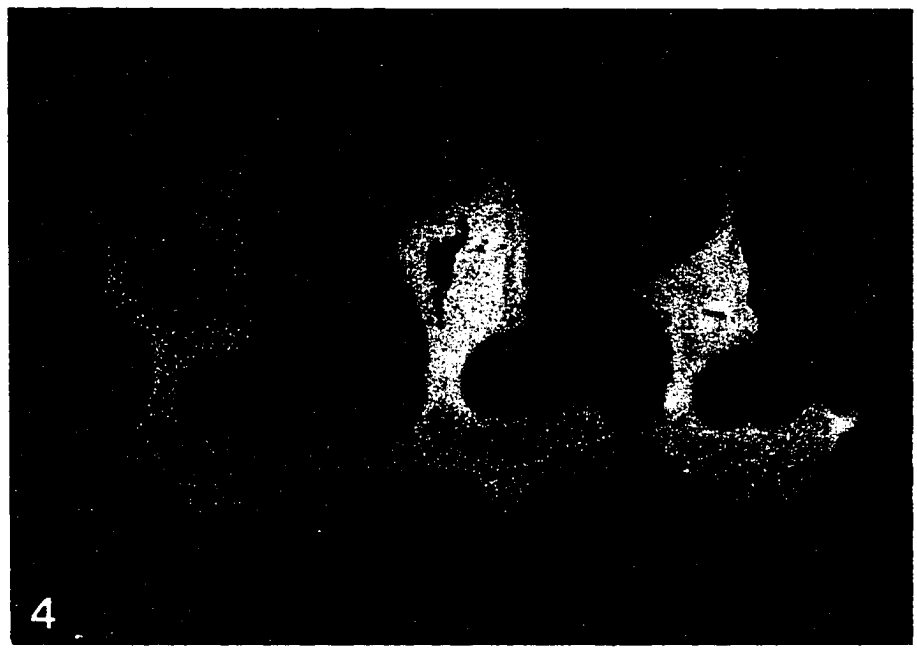

Figure 7.4: Axially cut lumbar spines demonstrating the unilateral decompressions and contralateral fusions. The spine on the left was a typical Group V spine, demonstrating a large fusion mass, actually exceeding the cross sectional area of the vertebral body. The center spine demonstrates the best fusion mass in Group III (collagen & autologous bone). The cleft in the fusion mass uses was not typically seen in this group. The spine on the right demonstrates the best fusion mass seen in Group I (autologous bone alone).

Figure 7.5: Histology of the spinal fusions. **a.** Photomicrograph of interface (arrowheads) between the fusion mass (f) and the lamina (l) in Group I spine three months post-operatively. Note the infrequent bands of bone connecting the fusion mass with the lamina. A higher magnification view of a. demonstrating the interface (arrowheads). **b.** Photomicrograph of the interface (arrowheads) between the fusion mass (f) and the spinous process (s) in a Group III spine three months post-operatively. Note the solid bony interface between the graft and host bone compared to Group I fusion. **c.** Photomicrograph of a Group II spinal fusion mass demonstrating endocondral bone formation (c) as well as fibrous tissue in the lower right hand corner.

TABLE 7.1-Fusion Analysis of the Canine Spine

Group		Intervertebral Levels Solidly Fused
I.	(autograft)	1.57±0.79
II.	(autograft, DBM)	0
III	(autograft, collagen)	1.725±0.99 ($p > 0.05$)
IV	(autograft,collagen,DBM)	0
V	(autograft, rhBMP-2)	3.00±0.63 ($p = 0.002$)

Table 7.2-Volumetric Analysis of the Spinal Fusions

Group	Change in Volume of Posterior Elements (cm^3)	
I (autograft)	0.26±0.41	
II (autograft, DBM)	3.07±1.47	($p > 0.05$)
III (autograft, collagen)	3.55±1.13	($p > 0.05$)
IV (autograft, collagen, DBM)	0.04±1.71	($p > 0.05$)
V (autograft, rhBMP-2)	10.42±2.68	($p = 0.036$)

TABLE 7.3-Biomechanical Analysis of the Spinal Fusions

Group	Extension Stiffness N.M/deg	Flexion Stiffness
N.M/deg		
I (autograft)	0.45±0.15	0.74±0.24
II (autograft, DBM))	0.12±0.06	0.15±0.05
III (autograft, collagen)	0.57±0.15	0.76±0.32
IV(autograft,collagen,DBM)	0.15±0.07	0.13±0.04
V (autograft, rhBMP-2)	0.30±0.11	0.28±0.09

References

1. Becker V., Timpl R., Kuhn K. (1972) Carboxy-terminal antigenic determinants of collagen from calf skin. Euro J Biochem 28:221-231.
2. Bolander M.E., Balian G. (1986) The use of demineralized bone matrix in the repair of segmental defects. J Bone J Surg 68:1264-1274.
3. Bowers G., Felton F., Middle C., et al (1991) Histologic comparison of regeneration in human intrabody defects when osteogenin is combined with demineralized free-dried bone allograft and with purified bovine collagen. J Periodontol 62:690-702.
4. Celeste A.J., Iannazzi J.A., Taylor R.C., Hewick R.M., Rosen V., Wang E.A., Wozney J.M. (1990) Identification of transforming growth factor-B family members present in bone-inductive protein purified from bovine bone. Proceedings of the National Academy of Sciences of the United States of America 87: 9843.
5. Cook S.D., Baffes G.C., Wolfe M.W., et al (1994) Recombinant human bone morphogenetic protein-7 induces healing in a canine long-bone segmental defect model. Clinical Orthopaedics & Related Research 302-312.
6. Cook S.D., Dalton J.E., Tan E.H., et al (1994) In vivo evaluation of recombinant human osteogenic protein (rhOP-1) implants as a bone graft substitute for spinal fusion. Spine 19:1655-1663.

7. Davison P.F., Levine L., Drake M.P., et al (1967) The serologic specificity of tropocollagen. J Exp Med 126:331-346.

8. Deporter D., Komori N., Howley T., et al (1987) Reconstituted bovine skin collagen enhances healing of bone wound in the rat calvaria. Calcif Tissue Int 42:321-325.

9. DeVore D.T. (1972) Collagen xenografts for bone replacement: the effects of aldehyde-induced cross-linking on degradation rate. Oral Surg 43:677-686.

10. Elsdale T., Bard J. (1972) Collagen substrata for studies on cell behavior. J Cell Biol 54:626-637.

11. Einhorn T.A., Lane J.M., Burstein A.H., et al (1984) The healing of segmental bone defects induced by demineralized bone matrix. J Bone J Surg 66A:274-279.

12. Frenkel S.R., Moskovich R., Spivak J., et al (1993) Demineralized bone matrix: enhancement of spinal fusion. Spine 12:1634-1639.

13. Gerhart T.N., Kirker-Head C.A., Kriz M.J., et al (1993) Healing segmental femoral defects in sheep using recombinant human bone morphogenetic protein. Clin Ortho Rel Res 293:317-326.

14. Guizzardi S., DiSilvestre M., Scandroglio R., et al (1992) Implants of heterologous demineralized bone matrix for induction of posterior spinal fusion in rats. Spine 17:701-707.

15. Guterman I.A., Boman T.E., Wang G.J., et al (1988) Bone induction in intramuscular implants by demineralized bone matrix: sequential changes of collagen synthesis. Collagen Rel Res 8:419-431.

16. Koenig B.B., Cook J.S., Wolsing D.H., et al (1994) Characterization and cloning of a receptor for BMP-2 and BMP-4 from NIH 3T3 cells. Molecular & Cellular Biology 14(9): 5961-5974.

17. Lindsley H., Mannick M., Bornstein P. (1971) The distribution of antigenic determinants in rat skin collagen. J Exp Med 133:1309-1324.

18. Lovell T.P., Dawson E.G., Nilsson O.S. (1989) Augmentation of spinal fusion with bone morphogenetic protein in dogs. Clin Orthop 243:266-274.

19. Muschler G.F., Lane J.M., Dawson E.G. (1990) The biology of spinal fusion. In Cotler D.C., Cotler H.B. (eds): Spinal Fusion: Science and Techniques. New York: Springer-Verlag pp 9-21.

20. Paralkar V.M., Nandedkar A.K., Pointer R., et al (1990) Interaction of osteogenin, a heparin binding bone morphogenetic protein, with type IV collagen. J Biol Chem 265:17281-17284.

21. Pfeilschifter J., Wolf O., Naumann A., et al (1990) Chemotactic response of osteoblastic cells to transforming growth factor B. J Bone Min Res 5:825-830.

22. Ragni P.C., Lindholm T.S. (1989) Bone formation and static changes in the thoracic spine at uni- or bilateral experimental spondylolisthesis with demineralized bone matrix. Italian J Orthop and Traumatol 15:237-252.

23. Sampath T.K., Muthukumaran N., Reddi A.H. (1987) Isolation of osteogenin, an extracellular matrix-associated, bone-inductive protein, by heparin affinity chromatography. Proc Nat Acad Sci 84:7109-7113.

24. Sasano Y., Ohtani E., Narita K., et al (1993) BMPs induce direct bone formation in ectopic sites independent of the endochondral ossification in vivo. Anat Rec 236:373-380.

25. Schmitt F.O., Levine L., Drake M.P., et al (1964) The antigenicity of tropocollagen. Proc Natl Acad Sci 51:493-497.

26. Steffen C., Timpl R., Wolff I. (1968) Immunogenicity and specificity of collagen. V. Demonstration of three different antigenic determinants on calf collagen. Immunol 15(1)135-144.

27. Summers B.N., Eisenstein S.M. (1989) Donor site pain from the ilium. J Bone J Surg 71-B:677-680.

28. Sweeney T.M., Chabra A., Brook B., et al (1994) Type I collagen gels mediate total repair of critical size bone defects through intramembranous ossification. Orthop Trans 582.

29. Toriumi D.M., Kotler H.S., Luxenberg D.P., et al (1991) Mandibular reconstruction with a recombinant bone-inducing factor. Arch Otolaryngol Head Neck Surg 117:1101-1112.

30. Urist M.R. (1965) Bone formation by autoinduction. Science 150: 893-899.

31. Urist M.R., Mikulski A., Lietz A. (1979) Solubilized and insolubilized bone morphogenetic protein. Proc Nat Acad Sci 76: 1828-1832.

32. Urist M.R., Huo Y.K., et al (1984) Purification of bovine bone morphogenetic protein by hydroxylapatite chromatography. Proc Nat Acad Sci 371-375.

33. Vukicevic S., Paralkar V.M., Cunningham N.S., et al (1990) Autoradiographic localization of osteogenin binding sites in cartilage and bone during rat embryonic development. Dev Biol 140:209-214.

34. Wang E.A., Rosen V., D'Alessandro J.S., Bauduy M., Cordes P., Harada T., Israel D.I., Hewick R.M., Kerns K.M., Lapan P., Luxenberg D.P., McQuaid D., Moutsatsos I.K., Nove J., Wozney J.M. (1990) Recombinant human bone morphogenetic protein induces bone formation. Proc Nat Acad Sci 87: 2220-2224.

35. Ward J.W. (1988) Femoral head transmits AIDS. Am Assoc Tissue Banks Newsletter 1:1.

36. Wozney J.M. (1992) The bone morphogenetic protein family and osteogenesis. Mol Rep & Dev 32(2): 160-167.

37. Wozney J.M., Rosen V., Celeste A.J., et al (1988) Novel regulators of bone formation: Molecular clones and activities. Science 242:1528-1534.

38. Yamaji N., Celeste A.J., Thies R.S., et al (1994) A mammalian serine-threonine kinase receptor specifically binds BMP-2 and BMP-4. Biochem & Biophys Res Comm 205(3): 1944-1951.

39. Yasko A.W., Lane J.M., Fellinger E.J., et al (1992) The healing of segmental bone defects, induced by rcombinant human bone morphogenetic protein (rhBMP-2). J Bone J Surgery 74-A:659-671.

40. Younger E.M., Chapman M.W. (1989) Morbidity at the donor graft site. J Orthop Trauma 3:192-195.

Conclusions to Dissertation

This dissertation clearly demonstrates that technical and scientific advances in the fields of neuroscience and bone repair will make it possible for the neurosurgeon to successfully reconstruct not only the central nervous system, but also its bony coverings. However, one problem that consistently arises when discussing issues of regeneration and reconstruction of the central nervous system is how to quantify the results.

Several recent spinal cord regeneration studies published in premiere scientific journals have been criticized because of their poor anatomical techniques. For instance, Bregman's regeneration research team has demonstrated that regeneration of the cortical spinal tract can occur if antibodies which are directed against inhibitory proteins in CNS myelin are applied to the lesioned spinal cord.[1] HRP was injected into the cerebral cortex, and axons distal to the spinal cord could be clearly identified in treated, but not control, animals. However, the experimental model was a surgical section of the dorsal half of the spinal cord, apparently including the cortical spinal tract. Unfortunately, since the cortical spinal tract is located close to the end of the cut, some of the corticospinal fibers may have actually survived lesioning. These unlesioned fibers may have been misinterpreted as fibers that had actually regenerated down the spinal cord. Although these investigators are now suggesting that the regeneration of the

cortical spinal tract actually leads to functional recovery of these rats, the results are clearly suspect. Perhaps a better system for looking at CNS regeneration would be the lesioned optic nerve. Since the optic nerve is a large, simple bundle of axons which are essentially an extension of the CNS, it may be the best pathway to study CNS regeneration. The utilization of biocytin may be quite useful in regeneration studies, since it can be used as a tract tracer at both light and electron microscopic levels. However, the technique is limited by the fact that not all of the retinal projection axons are clearly labeled. Therefore, biocytin will be useful in examining individual regenerating axons in the optic nerve, but will be of limited value in quantifying axonal regeneration.

In Chapters 3 through 6 of this dissertation, the Golgi-impregnation and immunohistochemical techniques were utilized to study fetal striatal transplants at both the light and electron microscopic levels in the rat and primate. The extension of these studies to the electron microscopic level was important to determine the ultrastructure of transplanted neurons. We clearly demonstrated, using the Golgi-impregnation technique, that grafted fetal striatal neurons in the rat can differentiate into all of the seven major cell types present in the striatum. In addition, the ultrastructure of these neurons appeared quite normal, except for some aberrant ultrastructural details in a few neuronal cell types. In addition, we clearly demonstrated

that these neurons differentiate biochemically into ChAT and substance P-like immunoreactive neurons, each of which has ultrastructural detail identical to the normal striatal. These interesting results in the rat model of Huntington's disease prompted us to extend these studies into the nonhuman primate. Although the striatal transplants demonstrated proper differentiation three months postoperatively, they demonstrated evidence of neuronal aging and degeneration after long survival periods. The instability of primate neuronal grafts is a novel finding and argues against the use of neuronal transplants in humans until the long-term viability of the transplants can be ensured.

Although one can hypothesize why the primate striatal grafts degenerated after long-term survival, further studies are needed to fully address these issues. Since only two rhesus monkeys were implanted with fetal striatal tissue in our study, it may have been a sampling error or a technical problem which arose during the transplantation procedure. However, it is more interesting to hypothesize that the neuronal transplants degenerated because they were not receiving the proper trophic support for their survival. If this is the case, it is possible that the afferent or efferent connections of the transplant were not extensive enough to acquire the proper neurotrophic factors needed to prevent degeneration. Since the distance the transplanted neurons had to project their axons to reach their

proper targets in the globus pallidus and substantia is quite small in the rat, this is not true is larger species. In the rhesus monkey, the striatal grafts were at least a centimeter away from their closest normal target, the globus pallidus. Therefore, their growing axons may not have reached this target as required for normal trophic support. In addition, in spite of there being no evidence of frank immunologic rejection in the transplant, it may have been that the monkey transplants were subacutely rejected, even though immunosuppresent therapy was initiated at the time of transplantation.

In summary, the data support the potential use of neuronal transplants in the reconstruction of the damaged or diseased central nervous system, but major issues of long-term neuronal degeneration and possibly immunologic injection of the transplants need to be fully addressed before this interesting approach is extended into the clinical setting.

The final chapter of the dissertation clearly supports the use of recombinant bone morphogenetic proteins and possibly Type I collagen gel to improve reconstruction of the bony elements of the spine. It appears that Type I collagen gel, placed between autologous bone chips, can improve the migration of osteoblasts into the collagen matrix, which not only improves the total amount of bone deposition, but improves the interface between the autograft and the host spine. It is even more convincing, however, that recombinant human BMP's can improve bone deposition and the rate of

fusion in autologous bone spinal fusions. This is the first study to clearly demonstrate that extracellular matrix or growth factors can actually have a positive effects on autologous bone grafts in the spine. Equally important, the study clearly demonstrates that these additives can improve the fusion mass without causing any compression of the delicate neural elements in the spinal canal and its foramina. Clinical studies are currently necessary in order to demonstrate the safety and efficacy of these approaches in the human spine.

In the past, neurosurgeons typically have been limited to performing operations to prevent further neurologic deficit. However, with the advent of new techniques such as neuronal transplantation, the infusion of neurotrophic factors, gene therapy, and the utilization of osteoinductive growth factors, neurosurgeons can now take a higher aim and actually improve neurologic outcome. The treatment of neurodegenerative diseases and head and spinal cord injury will certainly be amenable to novel treatments in the future and current difficulties in obtaining long-term spine stability will certainly be overcome. However, it must be stressed that proper anatomical, physiological, and functional laboratory and clinical studies need to be performed in these complex fields, since all of these advances need to be critically evaluated prior to widespread use.

References

1. Bregman, B.S., Kunkel-Bagden E., Schnell L, et al. (1995) Recovery from spinal cord injury mediated by antibodies to neurite growth inhibitors. Nature, 378:498-501.